8-10-2022

X-ray properties of early-type stars in the Tarantula Nebula from T-ReX

Paul A. Crowther

Patrick S. Broos

Leisa K. Townsley

Andy M. T. Pollock

Katie A. Tehrani

See next page for additional authors

Authors

Paul A. Crowther, Patrick S. Broos, Leisa K. Townsley, Andy M. T. Pollock, Katie A. Tehrani, and Marc Gagné

X-ray properties of early-type stars in the Tarantula Nebula from T-ReX

Paul A. Crowther[1]★, Patrick S. Broos[2], Leisa K. Townsley[2], Andy M.T. Pollock[1], Katie A. Tehrani[1], Marc Gagné[3]

1. Department of Physics and Astronomy, University of Sheffield, Sheffield, S3 7RH, UK
2. Department of Astronomy and Astrophysics, 525 Davey Laboratory, Pennsylvania State University, University Park, PA 16802, USA
3. Department of Earth and Space Sciences, West Chester University, West Chester, PA 19383, USA

Accepted 2022 July 5. Received 2022 July 5; in original form 2022 April 8

ABSTRACT

We reassess the historical L_X/L_{Bol} relation for early-type stars from a comparison between T-ReX, the *Chandra* ACIS X-ray survey of the Tarantula Nebula in the LMC, and contemporary spectroscopic analysis of massive stars obtained primarily from *VLT*/FLAMES, *VLT*/MUSE and *HST*/STIS surveys. For 107 sources in common (some host to multiple stars), the majority of which are bolometrically luminous (40% exceed $10^6 L_\odot$), we find an average $\log L_X/L_{Bol} = -6.90 \pm 0.65$. Excluding extreme systems Mk 34 (WN5h+WN5h), R140a (WC4+WN6+) and VFTS 399 (O9 IIIn+?), plus four WR sources with anomalously hard X-ray components (R130, R134, R135, Mk 53) and 10 multiple sources within the spatially crowded core of R136a, $\log L_X/L_{Bol} = -7.00 \pm 0.49$, in good agreement with Galactic OB stars. No difference is found between single and binary systems, nor between O, Of/WN and WR stars, although there does appear to be a trend towards harder X-ray emission from O dwarfs, through O (super)giants, Of/WN stars and WR stars. The majority of known OB stars in the Tarantula are not detected in the T-ReX point source catalogue, so we have derived upper limits for all undetected OB stars for which $\log L_{Bol}/L_\odot \geq 5.0$. A survival analysis using detected and upper-limit $\log L_X/L_{Bol}$ values indicates no significant difference between luminous O stars in the LMC and the Carina Nebula. This analysis suggests that metallicity does not strongly influence L_X/L_{Bol}. Plasma temperatures for single, luminous O stars in the Tarantula ($\overline{kT_m} = 1.0$ keV) are higher than counterparts in Carina ($\overline{kT_m} = 0.5$ keV).

Key words: X-rays: stars – stars: massive – stars: early-type – stars: fundamental parameters – stars: Wolf-Rayet – binaries: general

1 INTRODUCTION

It is well known that Galactic early-type stars are prominent soft (~keV) X-ray emitters (Harnden et al. 1979; Seward et al. 1979), usually attributed to shocks within their intrinsically structured outflows (Lucy & Solomon 1970; Owocki et al. 1988; Owocki & Cohen 1999). From early surveys with *Einstein*, a linear proportionality of X-ray emission to bolometric luminosity, $L_X \sim 10^{-7} L_{Bol}$, was established for O-type stars (Long & White 1980; Pallavicini et al. 1981; Chlebowski et al. 1989) which observations from successor X-ray satellites *ROSAT, XMM, Chandra* have supported (Berghöfer et al. 1997; Sana et al. 2006; Nazé 2009; Nazé et al. 2011; Rauw et al. 2015).

It is now established that a high fraction of massive stars lie in binary systems with short periods (Sana et al. 2012). A subset of binaries are known to exhibit enhanced, often harder (few keV), X-ray emission (Pollock 1987; Chlebowski & Garmany 1991; Rauw 2022) attributed to colliding stellar winds, although the majority of binaries do not exhibit excess X-ray emission (Oskinova 2005). Further, stellar atmosphere improvements to our understanding of massive stars have resulted in revisions to the properties of early-type stars including their temperatures and luminosities (Crowther et al. 2002b; Repolust et al. 2004) and a subset of early-type stars are known to possess kG-scale magnetic fields (Grunhut et al. 2017), so historical calibrations should be used with caution. In addition, γ Cas-like Oe and Be stars possess unusually bright, hard X-ray emission (Smith et al. 2016).

Very few X-ray studies of early-type stars in the Magellanic Clouds have been carried out, including *Chandra* ACIS imaging of the N66 region in the SMC, host to NGC 346 (Nazé et al. 2003), ACIS imaging of the N11 region in the LMC (Nazé et al. 2014) and the 30 Doradus or Tarantula Nebula in the LMC, host to the rich star cluster R136 (Portegies Zwart et al. 2002; Townsley et al. 2006b). However, early datasets were too shallow (20 ks for 30 Dor) to draw firm conclusions on the $L_X - L_{Bol}$ relation since only a handful of OB stars were detected, although Townsley et al. (2014) have provided an updated catalogue of X-ray sources in 30 Dor from 92 ks *Chandra* ACIS observations. Nazé et al. (2014) suggest LMC O stars possess similar X-ray properties to Milky Way counterparts, albeit based on stacked observations of undetected O stars in N11. Consequently, X-ray properties of Magellanic Cloud OB stars have historically been assumed in spectroscopic analyses (e.g. Crowther et al. 2002b), since empirical calibrations at low metallicity have not been available. Since X-rays are believed to be emitted from shocks embedded in the

★ paul.crowther@sheffield.ac.uk

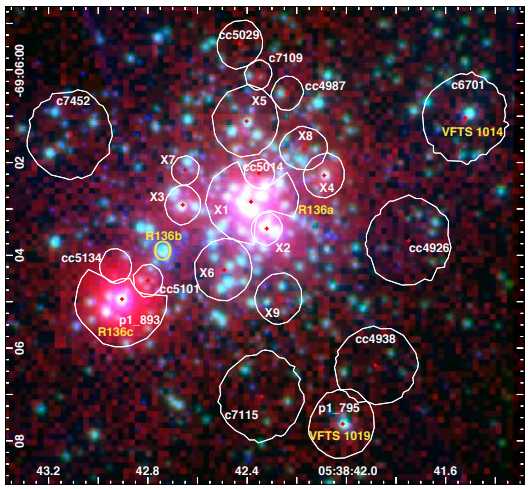

Figure 1. Three colour 10″×10″ view of R136 comprising *Chandra* ACIS 0.5–7 keV (X-ray: red, L. Townsley et al. in prep), *HST* WFC3/F555W (optical: green, De Marchi et al. 2011) and *VLT* SPHERE/K_s (near-IR: blue, Khorrami et al. 2021), with X-ray sources and selected optical counterparts labelled in white and yellow respectively, including 9 X-ray sources associated with R136a. The white polygons define X-ray event extraction apertures, and include c7452 which is host to multiple spectroscopically confirmed early-type stars. Optical counterparts to these X-ray sources are listed in Table 1. The O4 If/WN8 supergiant R136b, located at an X-ray minimum, is also indicated. North is up and East to the left.

stellar wind, one would expect $L_{\rm X}$ to depend on mass-loss, which itself dependents on luminosity as $L_{\rm Bol}^{1/\alpha'}$ with α'=0.6 (Puls et al. 2008).

The recent, much deeper (2 Ms) *Chandra* ACIS imaging survey of the Tarantula Nebula in the LMC, 'Tarantula – Revealed by X-rays' (T-ReX, PI Townsley), finally represents an opportunity to assess whether the canonical Galactic $L_{\rm X} - L_{\rm Bol}$ relation applies to LMC O-type stars, since this region is host to an exceptionally rich massive star content (Crowther 2019). The Tarantula has been extensively, spectroscopically surveyed with *Very Large Telescope (VLT)*/FLAMES (Evans et al. 2011), *VLT*/MUSE (Castro et al. 2018) and *Hubble Space Telescope (HST)*/STIS (Crowther et al. 2016). To date, Pollock et al. (2018) have utilised T-ReX to establish Melnick 34 as a colliding wind binary system, while Clark et al. (2015) have investigated the candidate high mass X-ray binary VFTS 399.

In this paper we briefly introduce the T-ReX point source catalogue in Sect. 2, present the $L_{\rm X} - L_{\rm Bol}$ relation for early-type stars in 30 Doradus in Sect. 3, and consider their X-ray hardness in Sect. 4. We investigate non-detections of some 30 Doradus luminous stars in Sect. 5, compare their X-ray properties with luminous early-type stars in the Carina Nebula in Sect. 6, and present a brief summary in Sect. 7.

2 T-REX POINT SOURCE CATALOGUE

The 2 Ms *Chandra* X-ray Visionary Program T-ReX was executed over 630 days between 2014 May 3 and 2016 Jan 22 using the ACIS instrument (Garmire et al. 2003), centred on R136a the central cluster in the heart of the Tarantula Nebula, with a 16.9′ × 16.9′ field of view for each pointing. This dataset also incorporates 92 ks ACIS observations from 2006 Jan 21–30 (Townsley et al. 2014), so represents a *hundred-fold* increase on exposure times with respect to early *Chandra* observations (Portegies Zwart et al. 2002; Townsley et al. 2006b). L. Townsley et al. (in prep) introduce T-ReX, while P. Broos & L. Townsley (in prep) have produced a T-ReX point source catalogue (PSC). In brief, data reduction, point source detection and extraction follow Townsley et al. (2018) and utilise ACIS Extract (Broos et al. 2010) tools[1].

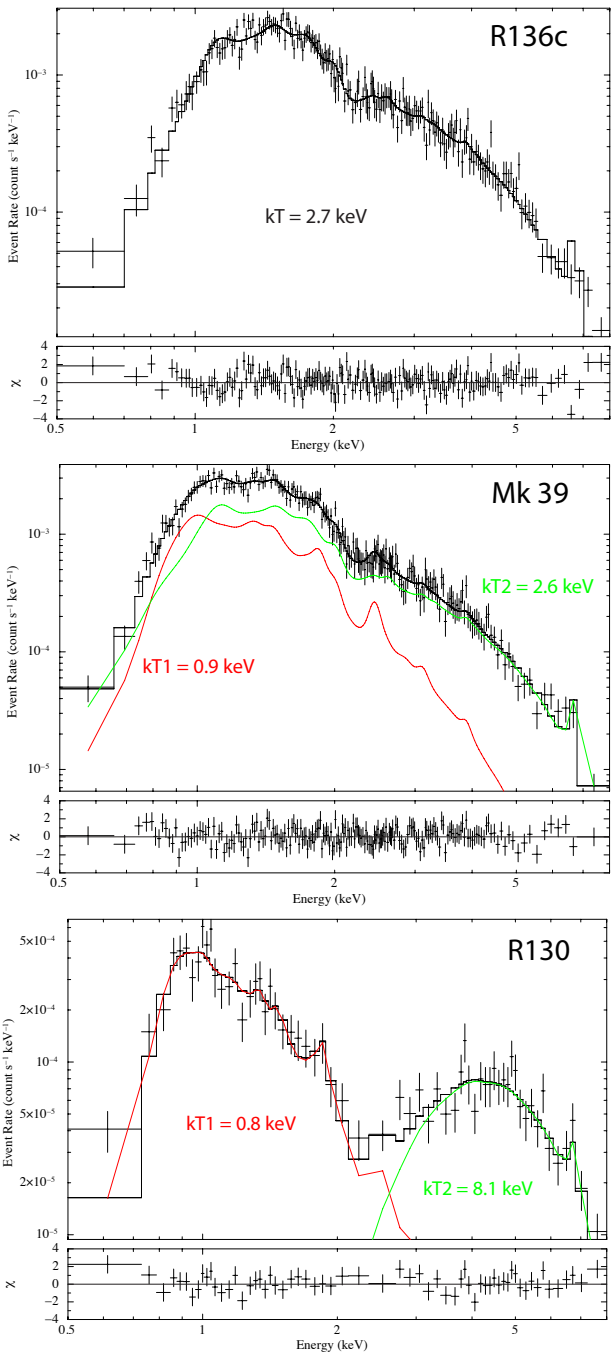

Figure 2. Representative XSPEC fits to three X-ray bright sources, involving from top to bottom: R136c (single 2.7 keV fit in black), Mk 39 (dual 0.9 keV red and 2.6 keV green fit, sum in black), and R130 (dual 0.8 keV red and 8.1 keV green fit, sum in black). R130 is one of only four early-type stars in the T-ReX sample which exhibits a very hard X-ray component. XSPEC parameters for these sources are included in Table A1.

[1] doi:10.5281/zenodo.781433

In order to identify massive star counterparts to T-ReX sources, these were cross-matched against the Doran et al. (2013) catalogue, which involved a compilation of confirmed and candidate early-type stars in the Tarantula Nebula. This was supplemented by more recent spectroscopic surveys exploiting *VLT*/MUSE (Castro et al. 2018) for the NGC 2070 region and *HST*/STIS (Crowther et al. 2016) for the R136 cluster. In addition, 4 sources inadvertently omitted from Doran et al. (2013) were common to the VLT-FLAMES Tarantula Survey (Evans et al. 2011), namely VFTS 186, 411, 564 and 640.

In total, P. Broos & L. Townsley (in prep, their table 6) identify 115 sources in common between T-ReX and optical photometric catalogues of hot, luminous stars, with a median separation of 0.15″ between X-ray and optical positions. Of these, 108 have optical spectral classifications, most of which involve a single optical source, with the exception of R140a (Moffat et al. 1987) and the rich, crowded R136 cluster, whose brightest X-ray sources are associated with multiple stars. Fig 1 shows a three colour image of R136, including *Chandra* ACIS (red, L. Townsley et al. in prep), *HST* WFC3/F555W (green, De Marchi et al. 2011) and *VLT* SPHERE/K_s (blue, Khorrami et al. 2021). The white polygons define X-ray event extraction apertures; for uncrowded sources, these represent 90% encircled energy contours of the Chandra/ACIS point spread function (extraction apertures are reduced for crowded sources). Fig 1 also highlights three X-ray counterparts to optically-bright sources elsewhere in the vicinity of R136a, namely R136c (= VFTS 1025), VFTS 1014 (=HSH 29, Hunter et al. 1995) and VFTS 1019 (= HSH 38), plus c7452, which is host to multiple early-type stars. Table 1 provides spectral types and luminosities of the primary optical counterparts to these 9 X-ray sources within R136a plus c7452.

Optical spectroscopy reveals that the majority of the sources, or primaries in binary systems, are O-type stars (71 sources), followed by Wolf-Rayet stars (14), B-type stars (7) or Of/WN stars (6). We omit cc4769 a.k.a. VFTS 1003 (= SMB 283, Selman et al. 1999) from our subsequent discussion since it is a peculiar Be star, hindering spectroscopic analysis (Evans et al. 2015), such that our final sample involves 107 sources, of which 11 are X-ray sources host to multiple populations within R136 or R140a. X-ray properties of all sources are provided in Table A1, sorted by photon flux. For each source, net counts (NetCts) and spectral fits were obtained from all observations of that source. However, in some cases a single observation was used to assess detection significance. Thus, detection significance cannot be inferred from NetCts values. For example, the detection of the last source (cc7873) was determined by a single observation from which 4.9 net counts were extracted, NetCts=4.9, and the detection p-value is 0.0018. The 2 Ms spectrum of this source has 28 total counts, but the expected background is ~27 counts.

In order to correct observed X-ray fluxes (0.5–8 keV) for absorption by interstellar gas we undertake XSPEC (Arnaud 1996) χ^2 (≥50 net counts) or Cash statistic (Cash 1979) (<50 net counts) fitting. For Mk 34 we provide an update to X-ray luminosities from Pollock et al. (2018). Clark et al. (2015) have also analysed initial T-ReX observations of VFTS 399, for which a power law fit is adopted here since high mass X-ray binaries have different X-ray emission mechanisms than OB or WR systems. VFTS 399 aside, all fits used a one-temperature or two-temperature thermal plasma model (*vapec*) with frozen metal abundances appropriate for the LMC presented in the Appendix in Table B1. Spectral fitting restricted plasma temperatures to 0.27 keV ≤ kT ≤ 9.5 keV.

Tübingen-Boulder absorption components model the Milky Way ISM (*TBabs*$^{\rm MW}$) and LMC ISM (*TBvarabs*$^{\rm LMC}$), plus we additionally consider a circumstellar absorption component (*TBvarabs*$^{\rm Circ}$), although the latter is excluded from extinction-corrected luminosities

Table 1. T-ReX sources host to multiple stellar populations within the core of R136 (X1–9, $r_{\rm d}$ ≤2.4″ or 0.6 parcsec from R136a1) plus c7452 (5″ to the east). Catalogue numbers are from WB (Weigelt & Baier 1985), MH (Malumuth & Heap 1994), HSH (Hunter et al. 1995) and BAT (Breysacher et al. 1999). Cumulative spectroscopic luminosities from alternative studies (Brands et al. 2022) agree to within ±0.1 dex.

WB	MH	HSH	BAT	Sp.Type	log $L/L_\odot$	Ref
R136a-X1 (p1_832); PhotonFlux = 1.12×10^{-5} cm^{-2} s^{-1}						
a1	498	3	108	WN5h	6.79±0.10	1
a2	511	5	109	WN5h	6.75±0.10	1
a4	474	21		O3 V((f*))	6.24±0.18	1
a5	519	20	110	O2 I(n)f*	6.29±0.10	1
a7	509	24		O3 III(f*)	6.25±0.18	1
a8	480	27		O2–3 V	6.17±0.10	2
	468	30		O6.5 Vz	5.68±0.14	1
	443	35		O3 V	5.74±0.18	1
	553	50		O3–4 V((f*))	5.71±0.11	1
	542	58		O2–3 V:	5.94±0.16	1
	518	66		O2 V–III(f*)	5.64±0.21	1
	533	70		O5 Vz	5.78±0.18	1
R136a-X2 (cc4970); PhotonFlux = 2.37×10^{-6} cm^{-2} s^{-1}						
a3	467	6	106	WN5h	6.63±0.10	1
a6	454	19,26		O2 I(n)f*p+?	6.27±0.09	1
R136a-X3 (p1_867); PhotonFlux = 1.59×10^{-6} cm^{-2} s^{-1}						
	608	36		O2 If*	6.33±0.11	1
	618	46		O2–3 III(f*)	6.16±0.18	1
	592	48		O2–3 III(f*)	6.05±0.20	1
R136a-X4 (c6981); PhotonFlux = 1.11×10^{-6} cm^{-2} s^{-1}						
	354	42		O3 V+O3 V	5.82±0.3:	3, 4
R136a-X5 (c7157); PhotonFlux = 7.67×10^{-7} cm^{-2} s^{-1}						
	508	39		O3 V+O5.5 V	5.76±0.3	3, 4
	535	40		O3 V	5.88±0.18	1
	486	49		O3 V	5.89±0.37	1
R136a-X6 (c7182); PhotonFlux = 5.86×10^{-7} cm^{-2} s^{-1}						
	537	31		O2 V((f*))	6.01±0.16	1
	517	52		O3–4 Vz	5.67±0.16	1
	551	55		O2 V((f*))z	5.76±0.15	1
	536	77		O5.5 V+O5.5 V	5.36±0.3	3, 4
	559	94		O4–5 Vz	5.52±0.23	1
	514	114		O5–6 V	5.25±0.21	1
R136a-X7 (c7257); PhotonFlux = 4.00×10^{-7} cm^{-2} s^{-1}						
	602	47		O2V((f*))	6.09±0.21	1
R136a-X8 (c7018); PhotonFlux = 2.07×10^{-7} cm^{-2} s^{-1}						
	409	75		O6 V	5.29±0.22	1
	397	108		O Vn	5.04±0.24	1
R136a-X9 (cc4968); PhotonFlux = 1.82×10^{-7} cm^{-2} s^{-1}						
	434	116		O7 V	4.84±0.16	1
	465	121		O9.5 V	4.86±0.16	1
c7452; Photon Flux = 2.08×10^{-7} cm^{-2} s^{-1}						
	744	68		O4–5 Vz	5.73±0.22	1
	741	102		O2–3 III	5.40±0.3	5
	711	129		O	4.37±0.26	1

1: Bestenlehner et al. (2020); 2: Brands et al. (2022); 3: Massey et al. (2002); 4: Doran et al. (2013); 5 Crowther et al. (2016)

Table 2. Comparison between observed atomic hydrogen column densities (from Lyman α) towards early-type stars at a range of radial distances from R136a (r_d in arcmin) and values predicted from the Galactic and LMC calibrations, $\log N(H)/E_{B-V}$ of Predehl & Schmitt (1995) and Koornneef (1982), respectively. For R136a, Brands et al. (2022) obtained a total Lyα (log) column density of 21.88±0.07 cm^{-2} from the average of the brightest 29 stars observed with HST/STIS spectroscopy, in good agreement with $21.85^{+0.10}_{-0.15}$ cm^{-2} from IUE/SWP spectroscopy (de Boer et al. 1980). A Galactic foreground of E^{MW}_{B-V}=0.07 or A^{MW}_V=0.22 mag is adopted in all cases, corresponding to $N(H)^{MW} = 3.8 \times 10^{20}$ cm^{-2} and we adopt $A^{LMC}_V = 3.5E^{LMC}_{B-V}$ (Doran et al. 2013) such that $N(H)^{Tot} = N(H)^{MW} + N(H)^{LMC}$. Overall good agreement is found between the empirical total hydrogen column density and that obtained from calibrations, $\Delta N(H) = \log N(H)^{Tot}_{Ly\alpha} - \log N(H)^{Tot}$, especially for the bulk of T-ReX sources within $r_d \leq 7$ arcmin (~ 100 pc).

Star	Aliases	r_d	A^{LMC}_V	Ref	$N(H)^{LMC}$	$\log N(H)^{Tot}$	$\log N(H)^{Tot}_{Ly\alpha}$	Ref	$\Delta N(H)$
		arcmin	mag		10^{21} cm^{-2}	cm^{-2}	cm^{-2}		dex
R136a	HD 38268, Sk –69° 243	0.00	1.58	1	9.0	21.97	21.88	2	–0.09
Mk 42	P93 922, BAT99-105	0.13	1.42	3	8.1	21.93	21.79	4	–0.14
R144	HD 38282, Sk –69° 246, P93 9037, BAT99-118	4.1	0.40	5	2.3	21.43	21.47	6	+0.05
BI 253	VFTS 72	7.78	0.65	3	3.7	21.61	21.68	6	+0.06
VFTS 696	Sk –68° 140	9.26	0.68	4	3.9	21.63	21.78	6	+0.15
HDE 269888	Sk –69° 234, VFTS 136, BAT99-90	9.84	0.83	7	4.8	21.71	21.52	4	–0.19
Average (± St. Dev.)									–0.03±0.13

1: Crowther et al. (2016) 2: Brands et al. (2022) 3: Bestenlehner et al. (2014) 4: Welty et al. (2012) 5: Shenar et al. (2021) 6: Roman-Duval et al. (2019) 7: Crowther et al. (2002a)

for consistency with other studies. For the Milky Way, we adopt a uniform atomic hydrogen column density based on

$$N_H^{MW}/E_{B-V}^{MW} = 5.3 \times 10^{21} \quad \text{cm}^{-2}\text{mag}^{-1}$$

(Predehl & Schmitt 1995) with $E^{MW}_{B-V} = 0.07$ mag adopted from Fitzpatrick & Savage (1984). For the LMC we consider a variable component, generally selected from the literature dust extinctions listed in the Appendix (Table A2) using

$$N_H^{LMC}/E_{B-V}^{LMC} = 2 \times 10^{22} \quad \text{cm}^{-2}\text{mag}^{-1}$$

(Koornneef 1982), with $A^{LMC}_V \sim 3.5E^{LMC}_{B-V}$ (Doran et al. 2013)[2]. For the total foreground column density $N(H)^{Tot}$ we sum the Milky Way and LMC components, $N(H)^{MW}$ and $N(H)^{LMC}$.

Since there is significant variation in N_H^{LMC}/E_{B-V}^{LMC} (Tumlinson et al. 2002, their fig 5) we have reassessed the Koornneef (1982) calibration for early-type stars in 30 Doradus. Table 2 compares expected hydrogen column densities to measured Lyman α column densities for six sight-lines. Overall we find excellent agreement between the observed hydrogen column densities and the total predicted from calibrations, with $\log N(H)^{Tot}_{Ly\alpha} - \log N(H)^{Tot} = -0.03\pm0.13$ dex. Frozen abundances in the *TBvarabs* components are appropriate for the LMC (Table B1). The model is implemented in XSPEC as *(TBvarabs*^{LMC}*TBabs*^{MW}*)(TBvarabs*^{Circ}**vapec)* *or* (TBvarabs^{LMC}*TBabs^{LMC})(TBvarabs^{Circ1}*vapec + TBvarabs^{Circ2}*vapec). Intrinsic X-ray luminosities assume a distance of 50 kpc to the LMC and set both N_H^{MW} and N_H^{LMC} to zero in XSPEC(which does not support the quantification of uncertainties on corrected luminosities). The average attenuation correction to observed X-ray luminosities is 0.31±0.17 dex.

Single temperature models provided satisfactory fits for the majority of X-ray sources (e.g. R136c in top panel of Fig. 2), whilst improved fits were achieved for 27 sources using two plasma temperatures. These are flagged in the Appendix (Table A1) and include Mk 39 in the central panel of Fig. 2. Four WR systems (R130, R134, R135 and Mk 53) exhibit extremely hard X-ray components, as indicated for R130 in the lower panel of Fig. 2 such that corrected X-ray luminosities represent lower limits. These sources possibly exhibit different emission mechanisms which are responsible for very hard plasmas reminiscent of γ Cas systems (Smith et al. 2016) and are therefore excluded. More detailed comparisons are deferred to subsequent studies, including K. Tehrani et al. (in prep) for WR and Of/WN stars. The X-ray faintest sources with fewer than 10 net counts were fit with a fixed kT = 0.8 keV (close to the median for other sources) so should also be treated with caution.

Table 3 compares X-ray luminosities from T-ReX for a subset of the brightest sources to literature results based on fits to historical *Chandra* shallow surveys. Luminosity estimates from early studies suffered from large uncertainties owing to short exposures (20 ks), such that T-ReX provides more reliable X-ray properties, especially for fainter sources in common. A number of bright PSC sources are known to be X-ray variable (e.g. Mk 34, Pollock et al. 2018), detailed discussion of which is deferred to K. Tehrani et al. (in prep), such that X-ray luminosities considered here are time averaged quantities (XSPEC fits have also been undertaken for Mk 33Na by Bestenlehner et al. (2022)).

Clark et al. (2019) presented a hardness colour for early-type stars in Westerlund 1, which involved $(h-s)/(h+s)$ where h is is the observed counts in the 2–8 keV range, and s is the observed counts in the 0.5–2 keV range. Here we adapt their hardness colour to calculate a hardness index, η_2, based on *intrinsic* luminosities, in the hard (2–8 keV, L^{hc}_X) versus soft (0.5–2 keV, L^{sc}_X) bands , i.e.

$$\eta_2 = \frac{(L^{hc}_X - L^{sc}_X)}{(L^{sc}_X + L^{hc}_X)},$$

such that exclusively soft emitters will have η_2 = –1 and pure hard emitters will have η_2 = +1. Our approach, involving interstellar extinction-corrected quantities, has two main advantages over observed hardness colours . First, observed event rates will evolve over time owing to the degradation of the ACIS soft energy response, whereas our XSPEC fits (on which our luminosities are based) account for these effects. Second, sources will exhibit a range of line-of sight absorptions, particularly when comparing hardness indices across different regions.

Alternatively, armed with a mix of single and dual temperature XSPEC fits we can evaluate a more physically motivated quantity,

[2] Doran et al. (2013) favour a higher ratio of $A^{LMC}_V \sim 4.2E^{LMC}_{B-V}$ in the vicinity of R136

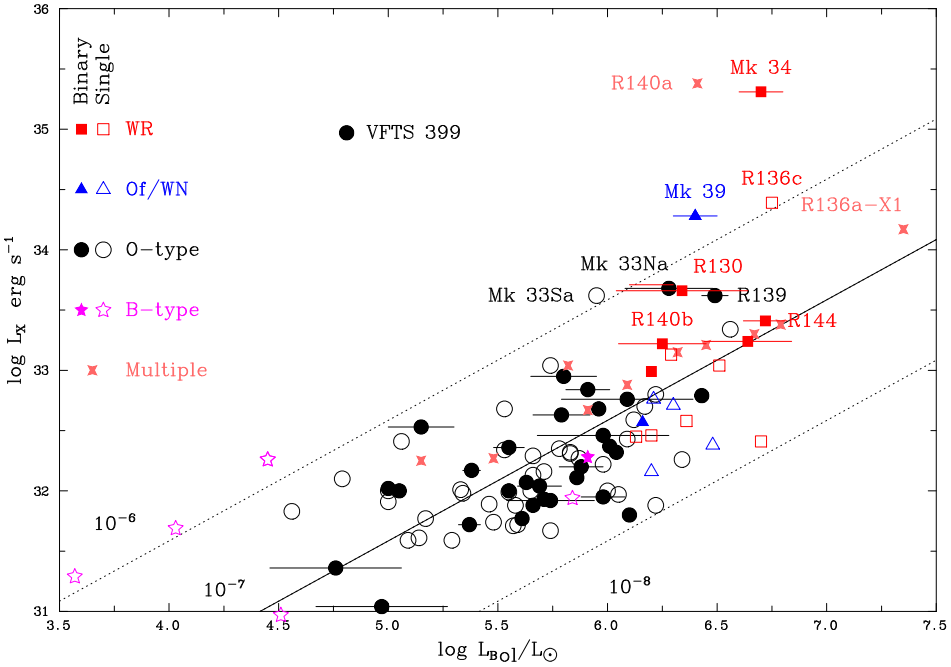

Figure 3. Comparison between X-ray and bolometric luminosities for 107 early-type sources from the T-ReX point source catalogue (P. Broos & L. Townsley, in prep). X-ray luminosities are corrected for interstellar extinction (L_X^{tc} in Table A1), while references to bolometric luminosities are provided in Tables 1 (R136) and A2 (non-R136). The solid line indicates the canonical $L_X = 10^{-7} L_{Bol}$ relation, with dotted lines offset by ±1 dex. Symbols correspond to the nature of the primary/brightest component, namely WR star (square), Of/WN star (triangle), O-type star (circle), B-type star (star). Spectroscopically confirmed binaries are shown as solid symbols and other sources (single and multiple systems lacking a known binary companion) are shown as open symbols. For clarity, uncertainties are included solely for SB2 systems.

namely a weighted mean temperature, T_m via

$$kT_m = \frac{\Sigma_i (kT_i \times EM_i)}{\Sigma_i EM_i}$$

where EM_i is the volume emission measure. η_2 and especially kT_m are sensitive to well-known degeneracies between column densities and plasma temperatures (Gayley 2014), although these are mitigated by optically-derived column densities throughout the present study (circumstellar column densities are not considered when determining X-ray luminosities). Sources for which power law slopes are adopted, such as VFTS 399, permit the determination of a hardness index, though not a plasma temperature.

Table A2 in the Appendix provides spectral type information, together with X-ray luminosities, mean plasma temperatures and hardness indices, plus identifications in 30 Doradus-specific catalogues (Melnick 1985; Parker 1993; Malumuth & Heap 1994; Hunter et al. 1995; Selman et al. 1999; Evans et al. 2011; Castro et al. 2018) plus general LMC catalogues (Feast et al. 1960; Sanduleak 1970; Brunet et al. 1975; Schild & Testor 1992; Breysacher et al. 1999).

3 NATURE OF X-RAY SOURCES AND $L_X - L_{BOL}$ RELATION

94 of the 107 T-ReX sources have been subject to spectroscopic analysis via a variety of studies, generally outlined in Crowther (2019). 50 WR, Of/WN stars and OB-type stars from VFTS have been analysed by Bestenlehner et al. (2014), McEvoy et al. (2015), Ramírez-Agudelo et al. (2017) and Sabín-Sanjulián et al. (2017). 5 OB binary systems from the TMBM survey (Almeida et al. 2017) have been spectroscopically analysed by Mahy et al. (2020). A further 18 OB stars within NGC 2070 observed with *VLT*/MUSE have been analysed by Castro et al. (2021), while Bestenlehner et al. (2020) have analysed *HST*/STIS spectroscopy of individual stars in R136a, involving 8 T-ReX sources. Rivero González et al. (2012) have analysed *HST*/STIS+FOS spectroscopy of Mk 33Sa from Massey et al. (2005) and one further candidate colliding wind binary system Mk 33Na (identified via T-ReX) has been followed up with *VLT*/UVES spectroscopic monitoring to confirm its SB2 status and has been analysed by Bestenlehner et al. (2022). The remainder include 8 single or binary Wolf-Rayet stars which have been analysed by Crowther

Table 3. Comparison between X-ray luminosities for bright early-type stars in the Tarantula Nebula from T-ReX in common with literature results (LT06 Townsley et al. (2006b); SPZ02 Portegies Zwart et al. (2002)) based on shallower *Chandra* surveys (20 ks), sorted by T-ReX photon flux. X-ray luminosities are obtained from XSPEC fits to T-ReX observations from this work ('X') or adapted from Pollock et al. (2018, P18). Variable bright X-ray sources are flagged as "var".

Photon flux cm^{-2} s^{-1}	log L_X erg s^{-1}		Ref	LT06	log L_X erg s^{-1}	SPZ02	log L_X erg s^{-1}	Source
1.48×10^{-4}	35.31	var	P18	132	35.38	CX5	35.26	Mk 34
1.46×10^{-4}	35.38	var	X	51	35.25	CX10	35.22	R140a
4.92×10^{-5}	34.79	var	X	27	34.06	—	—	VFTS 399
1.70×10^{-5}	34.39	var	X	102	35.04	CX2	34.93	R136c
1.69×10^{-5}	34.28	var	X	36	34.22	CX8	34.00	Mk 39
1.12×10^{-5}	34.17	var	X	83	34.31	CX1	34.10	R136a-X1
4.72×10^{-6}	33.62	var	X	131	34.63	CX7	33.93	Mk 33Sa
4.20×10^{-6}	33.62	var	X	82	33.39	CX11	33.34	R139
4.10×10^{-6}	33.68	var	X	133	33.99	CX9	33.44	Mk 33Na
2.97×10^{-6}	33.41	var	X	154	33.51	CX17	33.17	R144
2.81×10^{-6}	33.66	—	X	10	33.48	—	—	R130
2.37×10^{-6}	33.38	var	X	79	33.93	—	—	R136a-X2
2.05×10^{-6}	33.34	—	X	—	—	CX4	33.31	Mk 42
1.87×10^{-6}	33.24	var	X	156	33.99	CX12	33.25	R145
1.59×10^{-6}	33.30	—	X	90	33.56	—	—	R136a-X3
1.50×10^{-6}	33.22	var	X	49	33.57	—	—	R140b
1.08×10^{-6}	33.04	—	X	45	33.81	CX3	33.17	HSH 28
4.19×10^{-7}	32.68	—	X	23	—	CX14	32.55	VFTS 267
1.38×10^{-7}	32.46	—	X	—	—	CX6	32.86	R134

Table 4. Average $\log L_X/L_{Bol}$, hardness index, η_2, and mean plasma temperature, kT_m, for spectroscopically classified single/binary/multiple T-ReX point sources, including 1σ dispersions. Single and binary systems are also separated into the spectral class of the primary. We also provide average properties excluding the following outliers: 3 extreme systems Mk 34 (WN5h+WN5h, SB2), R140a (WC4+WN6+, multiple), VFTS 399 (O9 IIIn+?, SB1), plus 4 systems for which XSPEC fitting requires a discrete very hard component: R130 (WN/C+B1 I, SB2), R134 (WN6(h), single), R135 (WN5:+WN7, SB2) and Mk 53 (WN8(h), single).

Sp.Type	N	$\log \overline{L_X/L_{Bol}}$	$\overline{\eta_2}$	$\overline{kT_m}$ keV	N	$\log \overline{L_X/L_{Bol}}$	$\overline{\eta_2}$	$\overline{kT_m}$ keV	N	$\log \overline{L_X/L_{Bol}}$	$\overline{\eta_2}$	$\overline{kT_m}$ keV
		— Single —				— Binary —				— Single & Binary —		
O all	40	–7.04±0.44	–0.62±0.32	1.03±0.78	31	–6.92±0.77	–0.68±0.37	0.84±0.36	71	–6.98±0.60	–0.65±0.34	0.95±0.64
O all excl.	40	–7.04±0.44	–0.62±0.32	1.03±0.78	30	–7.03±0.42	–0.73±0.32	0.84±0.36	70	–7.04±0.43	–0.67±0.33	0.95±0.64
O V-IV	21	–7.03±0.42	–0.66±0.32	1.08±0.91	17	–7.00±0.37	–0.74±0.19	0.86±0.30	38	–7.03±0.37	–0.71±0.26	0.96±0.71
O V-IV excl.	21	–7.03±0.42	–0.66±0.32	1.08±0.91	17	–7.00±0.37	–0.74±0.19	0.86±0.30	38	–7.03±0.37	–0.71±0.26	0.96±0.71
O III–I	12	–7.02±0.51	–0.68±0.29	0.80±0.57	12	–6.75±1.18	–0.54±0.53	0.88±0.49	24	–6.88±0.88	–0.61±0.42	0.84±0.52
O III–I excl.	12	–7.02±0.51	–0.68±0.29	0.80±0.57	11	–7.06±0.56	–0.65±0.39	0.88±0.49	23	–7.06±0.56	–0.65±0.39	0.84±0.52
WR	7	–7.08±0.61	+0.26±0.46	4.12±2.80	6	–6.42±0.75	+0.33±0.32	4.36±3.04	13	–6.78±0.73	+0.29±0.38	4.23±2.79
WR excl.	5	–7.00±0.72	+0.20±0.47	2.60±1.22	3	–6.83±0.19	+0.23±0.15	2.42±1.57	8	–6.94±0.56	+0.24±0.38	2.96±1.73
Of/WN	4	–7.38±0.32	+0.50±0.18	0.86±0.24	2	–6.44±1.04	–0.33±0.07	1.25±0.55	6	–7.07±0.72	–0.44±0.17	0.99±0.37
Of/WN excl.	4	–7.38±0.32	+0.50±0.18	0.86±0.24	2	–6.44±1.04	–0.33±0.07	1.25±0.55	6	–7.07±0.72	–0.44±0.17	0.99±0.37
B	5[a]	–6.44±0.81	–0.91±0.05	0.63	1	–7.22	–0.86	0.76	6	–6.57±0.79	–0.90±0.05	0.70±0.09
All	56	–6.97±0.61	–0.50±0.45	1.44±1.62	40	–6.83±0.77	–0.51±0.51	1.43±1.76	96	–6.94±0.64	–0.50±0.47	1.44±1.76
All excl.	54	–7.00±0.53	–0.54±0.43	1.17±0.92	36	–6.99±0.45	–0.62±0.40	1.00±0.69	90	–7.00±0.49	–0.57±0.42	1.10±0.84
		— Single+SB1 —				— SB2 —				— Multiple —		
All	72	–6.97±0.70	–0.53±0.45	1.30±1.45	24	–6.74±0.59	–0.41±0.53	1.83±0.38	11	–6.56±0.67	–0.50±0.23	1.50±1.11
All excl.	69	–7.04±0.49	–0.58±0.42	1.09±0.84	21	–6.84±0.48	–0.54±0.43	1.12±0.85	10	–6.76±0.19	–0.50±0.24	1.51±1.17

(a) VFTS 186 has a measured plasma temperature while other single B stars are adopted to have a median temperature of 0.8 keV.

et al. (2010), Hainich et al. (2014), Shenar et al. (2017), Tehrani et al. (2019), Shenar et al. (2019) and Shenar et al. (2021). Spectral type calibrations are applied for the remaining 14 sources, following Doran et al. (2013), inevitably leading to higher uncertainties in bolometric luminosities. Table A2 in the Appendix provides X-ray and bolometric luminosities for the complete sample, including binary information. X-ray variables are highlighted (with "var") on the basis of Gaussian or Poissonian statistics, although inevitably these are limited to the brightest sources with unattenuated X-ray luminosities of $L_X \geq 10^{33}$ erg s^{-1}.

Oskinova (2005) concluded that, in general, binaries follow the canonical X-ray relationship for single early-type stars, although occasionally colliding wind systems exhibit enhanced, harder X-ray emission, with respect to single stars (Pittard 2011; Gagné et al. 2012; Rauw 2022). In general, establishing the single or binary nature of early-type stars is notoriously difficult. Fortunately, 76 T-ReX sources were included in VFTS, with spectroscopy across a range of cadences and whose spectroscopic binary status has been summarised in Walborn et al. (2014) and Evans et al. (2015). A subset of VFTS sources identified as spectroscopic binaries have been followed up with the Tarantula Massive Binary Monitoring (TMBM, Almeida et al. 2017, Shenar et al. in prep) and B-stars binaries characterization (BBC, Villaseñor et al. 2021) surveys in order to establish orbital properties. Excluding complex systems in R136a, 41 sources are confirmed spectroscopic binaries, of which 24 are double-lined spectroscopic binaries (SB2). One source (SMB 151) has been identified as an eclipsing binary OGLE-LMC-ECL-21413 (Graczyk et al. 2011) which we include in the statistics of (SB1) spectroscopic binaries.

Figure 3 compares X-ray to bolometric luminosities for all 107 T-ReX sources, with an average ratio of $\log L_X/L_{Bol} = -6.90 \pm 0.65$. The rich massive star population of the Tarantula Nebula provides a sample whose O-type sources alone span $4.5 \leq \log L_{Bol}/L_\odot \leq 6.5$, while all Of/WN and WR sources exceed $10^6 L_\odot$, with such high luminosity sources providing 40% of the observed T-ReX sample of early-type stars. Nine X-ray sources lie within the central 2.4″ (0.6 parsec) of the R136 star cluster (Massey & Hunter 1998; Crowther et al. 2016) so due to severe crowding the association of X-ray photons with optical counterparts is less secure than elsewhere (recall Fig 1).

The overwhelming majority of spectroscopically confirmed binaries (filled symbols) do not have higher L_X/L_{Bol} ratios than single stars. However, there are some exceptional sources with high X-ray luminosities, namely the candidate X-ray binary VFTS 399 (Clark et al. 2015), the WN5h+WN5h colliding wind binary Mk 34 (Guerrero & Chu 2008; Pollock et al. 2018; Tehrani et al. 2019), and R140a which is host to WN, WC and OB star(s). Moffat et al. (1987) have claimed that the WN star within R140a is an SB1 with a period of 2.7 days, although R140b is now favoured as host to the short period binary system (Shenar et al. 2019), while Bartzakos et al. (2001) have not found any evidence that the WC star is a member of a binary system. R140a aside, other X-ray extreme systems currently lacking a confirmed spectroscopic binary include R136c (WN5h+?, VFTS 1025) for which a tentative 8.2 day period was proposed by Schnurr et al. (2009) and Mk 33Sa (O3 III(f*), HSH 18) for which no spectroscopic evidence of binarity has been identified to date (Massey et al. 2005).

Table 4 provides a breakdown of average ratios of $\log L_X/L_{Bol}$ for single stars, spectroscopic binaries and multiple sources within

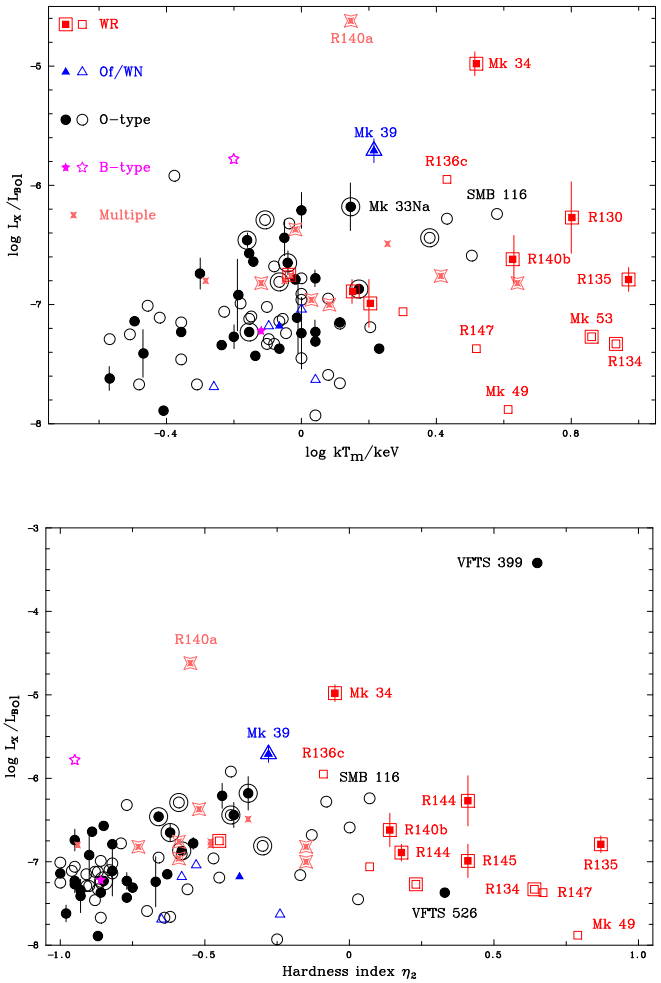

Figure 4. (*top panel*): Comparison between $\log kT_m$ and $\log L_X/L_{Bol}$ for early-type sources from the T-ReX point source catalogue (P. Broos & L. Townsley, in prep). Symbols are included in the key (filled symbols are binaries, uncertainties are included solely for SB2 systems, double concentric shapes denote sources with dual temperature plasma fits). Note that spectral fitting to T-ReX sources required $kT \gtrapprox 0.3$ keV. Several faint sources are excluded from this figure since their X-ray temperatures were adopted; (*bottom panel*): As above, except for a comparison between the hardness index η_2 and $\log L_X/L_{Bol}$ for T-ReX early-type sources. η_2 compares extinction corrected luminosities in the 2–8 keV to 0.5–2 keV energy range, such that soft emitters would possess an index of –1 and hard emitters would possess +1.

R136a and R140a, with single and binaries split by spectral type of the primary. For the entire sample, multiple systems aside, $\log L_X/L_{Bol} = -6.94 \pm 0.66$, in reasonable agreement to previous Galactic results (Chlebowski et al. 1989; Sana et al. 2006; Rauw et al. 2015). If one excludes extreme outliers (Mk 34, VFTS 399) plus four systems with extremely hard (8–10 keV) components (R130, R134, R135, Mk 53), a revised average of $\log L_X/L_{Bol} = -7.00 \pm 0.49$ is obtained.

Separating the sample into confirmed spectroscopic binaries confirms the results from previous studies (Oskinova 2005) that binary systems generally do not exhibit excess X-ray emission with respect to single stars. SB2 systems possess a modest X-ray excess which is much lower than the dispersion, i.e. $\log L_X/L_{Bol} = -6.97 \pm 0.61$ (single), $\log L_X/L_{Bol} = -6.96 \pm 0.99$ (SB1) and $\log L_X/L_{Bol} = -6.74 \pm 0.59$ (SB2). If X-ray outliers are omitted, averages are $\log L_X/L_{Bol} = -7.00 \pm 0.53$ (single), -7.19 ± 0.32 (SB1) and -6.84 ± 0.48 (SB2). For completeness, the average properties of multiple sources are $\log L_X/L_{Bol} = -6.76 \pm 0.19$, excluding R140a, although these should be treated with caution owing to the challenges of associating X-ray emission to individual sources in such a crowded environment (recall Fig. 1).

Magnetic OB stars may also be X-ray luminous. Upper limits on magnetic fields have been obtained for some luminous early-type stars in the Tarantula Nebula (Bagnulo et al. 2020). Spectroscopically, O-type stars with kG magnetic fields usually possess a peculiar O?fp spectral type, so Walborn et al. (2014) have highlighted seven Onfp stars within the Tarantula Nebula (their fig. 11). Of these, only VFTS 526 is included in the T-ReX PSC, it is also a SB1 system, in spite of which it is X-ray *faint*. Consequently we have no evidence from T-ReX that favours excess X-ray emission from potentially magnetic OB stars in the Tarantula Nebula.

We find no significant dependence of $\log L_X/L_{Bol}$ on spectral class for O, Of/WN and WR stars, especially once X-ray outliers have been omitted, although some classes suffer from low number statistics. In particular, Table 4 reveals no differences in $\log L_X/L_{Bol}$ between O dwarfs/subgiants and other luminosity classes, in contrast with the findings of Nebot Gómez-Morán & Oskinova (2018) who have investigated the dependence of X-ray properties of Galactic O stars on luminosity class. From Galactic studies, single WC stars are known to be X-ray faint, presumably because of their optically thick winds (Oskinova et al. 2003). There are no single WC stars in the T-ReX point source list, although R140a is known to host WN and WC stars, and R130 is a WN/C+B1 I binary[3].

Only six B stars are detected in T-ReX, with a significant scatter in $\log L_X/L_{Bol}$, such that we do not have sufficient statistics to comment on their X-ray properties with respect to previous studies (Berghöfer et al. 1997; Cohen et al. 1997; Nazé et al. 2011).

4 X-RAY HARDNESS OF T-REX SOURCES

Table 4 provides average hardness indices, η_2 and mean plasma temperatures, kT_m for T-ReX sources, while Fig. 4 (top panel) compares kT_m to $\log L_X/L_{Bol}$. Sources with two temperature plasma fits are indicated by two concentric shapes. The average plasma temperature for the entire sample is $kT_m = 1.44 \pm 1.61$ keV. Fig 4 (bottom panel) compares the hardness index, η_2, of T-ReX sources to $\log L_X/L_{Bol}$ with an average value of $\eta_2 = -0.50 \pm 0.45$ for the entire sample. Fig. 4 illustrates that WR systems (shown in red) are predominantly hard emitters, regardless of whether they are known binaries, with an average hardness index of $\eta_2 = +0.29 \pm 0.38$. Aside from the suspected high-mass X-ray binary VFTS 399 (Clark et al. 2015), half of the six X-ray sources with the hardest indices are apparently single: Mk 49 (WN6(h)), R134 (WN6(h)) and R147 (WN5h), while the remainder are known SB2 binaries: R135 (WN5:+WN7), R144 (WN5–6h+WN6–7h) and R145 (WN6h+O3/5If/WN7).

This suggests that high wind densities play a role in harder X-ray emission, since the corresponding hardness indices of O dwarfs/subgiants, O (super)giants, Of/WN stars are $\eta_2 = -0.71 \pm 0.26$,

[3] R130 (BAT99-92) has been assigned a variety of subtypes, ranging from WN3b + B1 Ia (Hainich et al. 2014) to WC4 + B1 Ia (Shenar et al. 2019) to WCE + WN + B1 I (Conti & Massey 1989) but WN/C is favoured (Doran et al. 2013) since the blue feature is dominated by He II λ4686 (preferring a WN or WN/C subtype) while C IV $\lambda\lambda$5801-12 is exceptionally strong (preferring a WC or WN/C subtype).

Table 5. Detection statistics of 1001 spectrally classified early-type stars (or multiple systems whose primary is an early-type star) within the T-ReX field-of-view, drawn from Crowther (2019) and references therein, excluding the spatially crowded central region of R136a.

Subtype/ Luminosity	X-ray N	X-ray %	Example	Non X-ray N	Non X-ray %	Example
O-type	71	14.2%		428	85.8%	BI 253
B-type	6	1.3%		469	98.7%	R142
Wolf-Rayet	14	70.0%		6	30.0%	Mk 33Sb
Of/WN	6	85.7%		1	14.3%	R136b
$\log(L/L_\odot) < 5$	10	1.5%	VFTS399	671	98.5%	
$5 \leq \log(L/L_\odot) < 6$	50	17.9%		229	82.1%	
$\log(L/L_\odot) \geq 6$	37	90.2%		4	9.8%	VFTS 72
Total	97	9.7%		904	90.3%	

–0.61±0.42 and –0.44±0.17, respectively. Clark et al. (2019, their fig. 2) have previously established that (single and binary) WR stars in the Galactic open cluster Westerlund 1 generally possess harder X-ray emission than OB supergiants, based on a hardness index constructed from *attenuated* fluxes, while Nebot Gómez-Morán & Oskinova (2018) found Galactic O supergiants possess harder X-ray spectra than dwarfs and giants.

A subset of OB stars are hard X-ray emitters, including SMB 116 (O3–6 V, Walborn & Blades 1997) suggesting a colliding wind binary origin. The majority of spectroscopic binaries are relatively soft, in common with previous Galactic studies. Indeed, the average hardness index of spectroscopic binaries is statistically identical to that of single stars. The average hardness index of the multiple X-ray sources associated with early-type stars in R136 is –0.50±0.24, identical to the wider sample, with 136a-X2 (host to R136a3 and an early O supergiant) and c7452 (host to two early O stars) the hardest, and R136a-X7 (host to an O2 dwarf) the softest. None possess X-ray properties which unambiguously flag the presence of a colliding wind binary.

5 T-REX PSC NON-DETECTIONS

The T-ReX point source catalogue represents an exceptionally rich dataset with which to consider X-ray emission from early-type stars in the Tarantula Nebula, yet there are over a thousand hot luminous stars in this region (Crowther 2019). In Table 5 we summarise the fraction of spectroscopically confirmed early-type stars within the T-ReX field-of-view that are detected in the PSC, according to spectral type (of the primary in a binary system) or bolometric luminosity (sum of individual components in a binary), excluding the crowded central region of R136a (recall Fig. 1). The majority of the highest luminosity stars with $\log L/L_\odot \geq 5.6$ (with overwhelmingly O, Of/WN or WR subtypes) are detected in the T-ReX PSC, though the reverse is true for moderate luminosity OB-type stars.

Consequently, we have obtained upper limits (95% probability) to photon fluxes for all luminous ($\log L/L_\odot \geq 5$) early-type stars which are undetected by T-ReX, in order for us to assess whether these are genuinely X-ray faint[4]. These are converted to attenuated luminosities from a calibration obtained from PSC detections,

$$\log L_X^t = \log(\mathrm{PhotonFlux/cm^{-2}\,s^{-1}}) + (38.81 \pm 0.16).$$

and presented in Table S1 (Supplementary Data). It was not possible to obtain upper limits for sources close to the edge of the T-ReX field of view since the background is highly variable, nor those within the vicinity of the N157B supernova remnant (Townsley et al. 2006a) since diffuse emission is highly variable, although all early-type sources are retained for completeness. Typical upper limits to attenuated luminosities lie in the range $31.6 \leq \log L_X^t/(\mathrm{erg\,s^{-1}}) \leq 32.5$. X-ray to bolometric luminosity ratios follow, based on average attenuation corrections of 0.31±0.17 dex. Star-by-star corrections based on measured optical extinctions cannot be determined since intrinsic X-ray spectral energy distributions are unknown.

By way of example, VFTS 419 (O9: V(n)) has a luminosity of $\log L/L_\odot = 5.07$ (Sabín-Sanjulián et al. 2017), close to the average of all 499 visually classified O-type stars in the Tarantula. We find an upper limit of $\log L_X^t/(\mathrm{erg\,s^{-1}}) \leq 31.71$ for VFTS 419, such that $\log L_X^{tc}/L_{\rm Bol} \leq -6.64$. Consequently we are not able to assess whether low luminosity O stars are X-ray 'normal' or faint. This is further illustrated in Fig. 5 where we compare *attenuated* X-ray luminosities, or limits, to bolometric luminosities for the full sample.

The absence of 4 very high luminosity stars with $\log L/L_\odot \geq 6$ from the T-ReX PSC (Table 5) merits further discussion. Of these, one lies at the edge of the survey field (VFTS 3), two lie in regions of very high background (R136b, HSH 59) though one, BI 253, does permit a useful upper limit of $\log L_X^t/(\mathrm{erg\,s^{-1}}) \leq 32.18$, indicating $\log L_X/L_{\rm Bol} \leq -7.16$. R136b represents the only non-detected

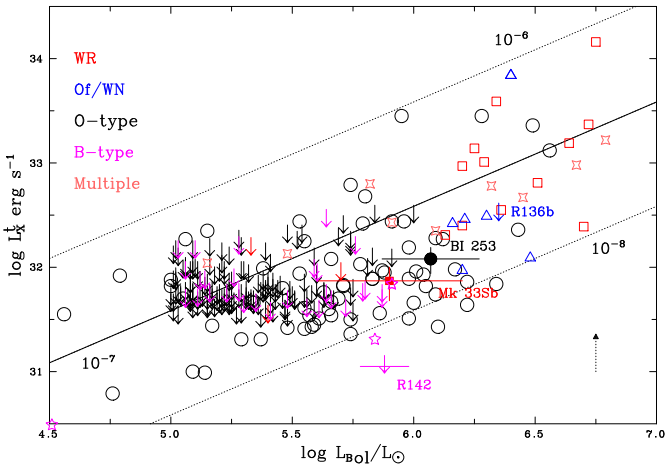

Figure 5. Comparison between *observed* X-ray luminosities and bolometric luminosities for 107 early-type sources from the T-ReX point source catalogue, additionally including limits for non-detected luminous ($\log L/L_\odot \geq 5$) early-type stars plus inferred X-ray luminosities from count rate analysis (Sect. 5) of BI 253 (O2 V–III, solid black circle), R142 (B1.5 Ia$^+$, purple arrow) and Mk 33Sb (WC5, solid red square). R136b (O4 If/WN8, blue arrow) is also indicated. Symbols correspond to the nature of the primary/brightest component, namely WR star (square), Of/WN star (triangle), O-type star (circle), B-type star (star). The solid line indicates the canonical $L_X = 10^{-7} L_{\rm Bol}$ relation, with dotted lines offset by ±1 dex, and the vertical dotted arrow indicates average X-ray attenuation corrections (star-by-star corrections cannot be determined since intrinsic X-ray spectral energy distributions are unknown).

type stars. Those within 1–2″ of luminous stars are noted in Table S1 in the Supplementary Data

[4] It is important to emphasise that optical counterparts are excluded if they are offset from X-ray PSC centroids by $\gtrapprox 1''$. P. Broos & L. Townsley (in prep, their table 5) identify PSC sources in close proximity to known early-

Table 6. Count rates (CR) and inferred observed X-ray luminosities L_X^t for a selection of luminous early-type stars absent from the T-ReX point source catalogue, based on the maximum-likelihood solution (MLS) approach. Intrinsic X-ray luminosities, L_X^{tc} are estimated from typical attenuation corrections of 0.31±0.17 dex. Catalogues include R (Feast et al. 1960), BI (Brunet et al. 1975), Mk (Melnick 1985), VFTS (Evans et al. 2011), MH (Malumuth & Heap 1994) HSH (Hunter et al. 1995), SMB (Selman et al. 1999), P (Parker 1993), CCE (Castro et al. 2018), BAT (Breysacher et al. 1999)

R	BI	Mk	VFTS	MH	HSH	SMB	P	CCE	BAT	Spect. Type	Ref	log L_{Bol} $L_\odot$	Ref	CR ksec^{-1}	log L_X^t erg s^{-1}	log L_X^{tc}/L_{Bol}	Nature	Ref
···	253	···	72	···	···	···	···	···	···	O2 V–III	1	6.07±0.2	2	0.043±0.012	$32.08^{+0.11}_{-0.14}$	$-7.26^{+0.10}_{-0.14}$	Single	1
142	···	···	533	···	···	3	987	2912	···	B1.5 Ia$^+$	3	5.88±0.10	4	0.000±0.004	<31.05	<−8.1	Single	3
···	···	33Sb	···	859	34	···	1111	···	115	WC5	5	5.9 ±0.3	6	0.026±0.009	$31.87^{+0.13}_{-0.19}$	$-7.31^{+0.13}_{-0.18}$	V.Comp	7

1: Walborn et al. (2014); 2: Sabín-Sanjulián et al. (2017); 3: Evans et al. (2015); 4: McEvoy et al. (2015); 5: Massey & Hunter (1998); 6: Doran et al. (2013); 7: Bartzakos et al. (2001)

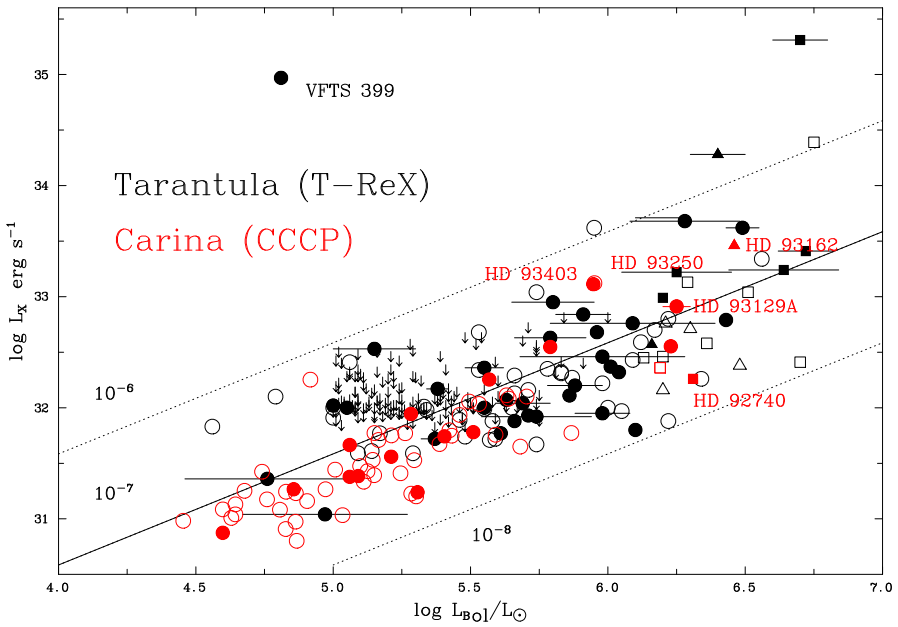

Figure 6. Comparison between X-ray and bolometric luminosities for single (open) and binary (filled) O stars (circles), Of/WN stars (triangles) and WN stars (squares) in the Tarantula Nebula from XSPEC fits to T-ReX observations (black) with those in the Carina Nebula from CCCP (red). Overall there are no systematic differences between LMC and Galactic early-type stars, although T-ReX statistics are poor below log $L/L_\odot$ ~ 5.0. According to Owocki et al. (2013) one would anticipate lower L_X/L_{Bol} ratios for stars with dense stellar winds, which is not apparent from observations. The solid line indicates the canonical $L_X = 10^{-7} L_{Bol}$ relation, with dotted lines offset by ±1 dex. Upper limits to attenuation corrected X-ray luminosities of O stars in the Tarantula have been included (arrows). CCCP results for O stars are drawn from Nazé et al. (2011) and Gagné et al. (2011), with the bolometric luminosity of HD 93129A updated according to Gruner et al. (2019) while CCCP results for Of/WN (HD 93162) and WN stars (HD 92740, HD 93131) are newly presented here.

Of/WN supergiant in T-ReX, though it lies in a complex region (Fig. 1).

We have employed one other technique to estimate X-ray luminosities for a subset of very luminous stars excluded from the T-ReX PSC. We have constructed spatial models incorporating weak target stars and any survey neighbours into multiple overlapping PSFs and a background term and seeking the maximum-likelihood solution (MLS) with respect to all the count rates (CRs) simultaneously. Count rates map into observed luminosities via $\log(L_X^t/\mathrm{erg\,s^{-1}}) = \log(\mathrm{CR} \times T_{Exp}) + (30.15 \pm 0.18)$, where T_{Exp} is the total exposure time, obtained from a comparison with 16 *Chandra* Source Catalog Release 2.0[5] sources within the T-ReX field. By way of a sanity check, for 6 sources in common with the T-ReX point source catalogue (Table A1) we find log L_X^t(MLS) – log L_X^t(PSC) = +0.09 ± 0.06 dex.

For the MLS technique we have considered the luminous O star BI 253 (O2 V–III), the early B supergiant R142 (B1.5 Ia$^+$) and the WR star Mk 33Sb (WC5), none of which are included in the T-ReX PSC (Table 5). Results of our analysis are presented in Table 6, and reveal *unattenuated* X-ray to bolometric luminosity ratios, L_X^{tc}/L_{Bol}, for the early O star and WC star which are consistent with early-type stars detected in the T-ReX PSC after folding in typical attenuation corrections. Consequently, it is currently not possible to conclude whether typical OB stars in 30 Dor are subluminous in X-rays.

We have highlighted these systems in Fig. 5, which further illustrates that the B hypergiant R142 is also X-ray faint. Galactic B stars are known to exhibit a larger dispersion in L_X/L_{Bol} than O stars, with a tendency towards a lower value for high luminosity sources (Nazé et al. 2011). Still, R142 does appear to be anomalously X-ray faint, in common with Mk 54 (B0.5 Ia), the latest luminous B supergiant detected in the T-ReX PSC with log L_X/L_{Bol} = −7.49. Of these three sources one would expect that the WC star Mk 33Sb would be X-ray faint rather than the B hypergiant, since single Galactic WC stars have not been detected in X-rays (Oskinova et al. 2003). Perhaps Mk 33Sb is an unidentified binary system (see Bartzakos et al. 2001).

6 METALLICITY DEPENDENCE OF L_X/L_{BOL}

X-rays originate in shocks embedded within stellar winds due to instabilities arising from the line driven phenomenon, so one would expect a mass-loss dependence, either $L_X \sim \dot{M}$ if the shocks are radiative, or $L_X \sim \dot{M}^2$ if they are adiabatic (Owocki et al. 2013). To date, Nazé et al. (2014) have suggested LMC O stars possess comparable X-ray emission to Milky Way O stars from stacked (300 ks)

[5] https://cxc.cfa.harvard.edu/csc

Table 7. Comparison between average log L_X/L_{Bol}, hardness indices, η, and mean plasma temperature kT_m for *luminous* (log $L_{Bol}/L_\odot \geq 5$) OB, Of/WN and WN stars in the Carina Nebula (Nazé et al. 2011; Gagné et al. 2011) versus the Tarantula Nebula from this study. The hardness index for Galactic OB stars, $\eta_{2.5}$ is defined relative to a 2.5 keV threshold instead of 2 keV for LMC stars, so will produce systematically softer indices. Average properties for Carina OB stars are also presented excluding O-type outliers HD 93250 (single), HD 93403 (binary). We include previously unpublished Carina CCCP X-ray results for HD 92740 (WN7ha+O), HD 93131 (WN6ha) and HD 93162 (O2.5 If*/WN6+O) for completeness (including η_2), adjusting spectroscopic results (Hamann et al. 2019) to Gaia eDR3 distances following the approach of Rate & Crowther (2020).

Subtype	N	$\log \overline{L_{Bol}/L_\odot}$	$\log \overline{L_X/L_{Bol}}$	$\overline{\eta_{2.5}}$	$\overline{kT_m}$	N	$\log \overline{L_{Bol}/L_\odot}$	$\log \overline{L_X/L_{Bol}}$	$\overline{\eta_2}$	$\overline{kT_m}$
		— Carina (Milky Way) —					— Tarantula (LMC) —			
O single	28	5.37±0.25	–7.25±0.27	–0.94±0.10	0.47±0.39	38	5.68±0.39	–7.08±0.41	–0.63±0.31	0.99±0.75
(excl.)	27	5.38±0.28	–7.28±0.21	–0.96±0.06	0.40±0.15	38	5.68±0.39	–7.08±0.41	–0.63±0.31	0.99±0.75
O binary[a]	13	5.52±0.42	–7.10±0.31	–0.89±0.13	0.77±0.76	28	5.77±0.37	–7.02±0.42	–0.73±0.28	0.84±0.36
(excl.)	12	5.48±0.42	–7.15±0.24	–0.90±0.13	0.75±0.79	28	5.77±0.37	–7.02±0.42	–0.73±0.28	0.84±0.36
B single	2	5.28±0.16	–7.74±0.15	–0.66±0.45	1.46±1.27	1	5.84	–7.49	–0.87	···
B binary	0	···	···	···	···	1	5.91	–7.22	–0.86	0.76
Subtype	N	$\log L_{Bol}/L_\odot$	$\log L_X/L_{Bol}$	η_2	kT_m keV	N	$\log \overline{L_{Bol}/L_\odot}$	$\log \overline{L_X/L_{Bol}}$	$\overline{\eta_2}$	$\overline{kT_m}$ keV
		— Carina (Milky Way) —					— Tarantula (LMC) —			
Of/WN single	0	···	···	···	···	4	6.30±0.13	–7.38±0.32	–0.50±0.18	0.86±0.24
Of/WN binary[b]	1	6.46	–6.58	–0.44	1.86	2	6.28±0.17	–6.44±1.04	–0.33±0.07	1.25±0.55
WN single[b]	1	6.19	–7.42	–0.38	1.94	8	6.42±0.22	–6.77±1.04	+0.16±0.51	4.12±2.80
WN binary[b]	1	6.31	–7.63	–0.40	1.70	5	6.50±0.25	–6.45±0.84	+0.31±0.35	3.97±3.22

(a): Updated luminosity for HD 93129A from Gruner et al. (2019); (b): X-ray properties of Carina Of/WN and WN stars are based on CCCP observations, with luminosities resulting from Gaia eDR3 distances of 2.48, 2.62 and 2.19 kpc for HD 92740, HD 93131 and HD 93162, respectively.

Chandra observations of undetected O stars in N11. At face value our results favour reduced X-ray output from single O stars in the LMC (log $L_X/L_{Bol} = -7.04 \pm 0.44$) versus the Milky Way based on log $L_X/L_{Bol} = -6.72 \pm 0.49$ obtained by Nazé (2009) for a large sample of single O stars. However, the latter are a heterogenous sample while the former are strongly biased to high luminosity O stars which possess strong winds.

In order to quantitatively compare X-ray properties of LMC O stars with realistic Galactic O-type counterparts, we focus on the Carina Nebula, which is the closest Galactic analogue to 30 Doradus[6], comprising a rich population of massive stars spanning a range of ages in a large star-forming complex. The Carina Nebula has been surveyed in X-rays with the *Chandra* Carina Complex Project (CCCP, Townsley et al. 2011). Nazé et al. (2011) and Gagné et al. (2011) have studied the X-ray properties of OB stars in the Carina Nebula. We have supplemented these results with CCCP X-ray results for HD HD92740 (WN7ha+O), HD 93131 (WN6ha) and HD 93162 (O2.5 If*/WN6+O) based on Gaia eDR3 distances of 2.48, 2.62 and 2.19 kpc, respectively, following the approach of Rate & Crowther (2020). Bolometric luminosities for these stars from Hamann et al. (2019) have been adjusted to the eDR3 distances.

Fig. 6 compares the X-ray luminosities to bolometric luminosities of O stars, Of/WN stars and WN stars in the Tarantula (T-ReX, black) and Carina (CCCP, red). Very few members of Carina significantly exceed the 10^{-7} X-ray to bolometric ratio relation, two single stars HD 93250 (O4 III(fc)), Tr14 MJ 496 (O8.5 V) plus two known binaries HD 93403 (O5.5 I+O7 V) and HD 93162 (O2.5 If/WN6+O). From inspection, Galactic and LMC O stars reveal comparable X-ray luminosities, contrary to expectations that weaker winds at reduced metallicity would lead to lower X-ray luminosities (Owocki et al. 2013). A couple of comments are necessary regarding Fig. 6. Firstly, CCCP is sensitive to weak X-ray emission from relatively low luminosity O stars, whereas T-ReX has detected exclusively the most extreme X-ray sources in the Tarantula. Indeed only two O stars in Carina exceed log $L_{Bol}/L_\odot = 6$ (both binaries)[7] versus 18 sources in 30 Doradus, such that the bulk of the Carina O star sample are lower luminosity, late subtypes (log $\overline{L_{Bol}/L_\odot} = 5.20 \pm 0.40$) while there are large numbers of high luminosity, early O subtypes in the T-ReX sample (log $\overline{L_{Bol}/L_\odot} = 5.65 \pm 0.45$).

In view of the differences between Carina and Tarantula O star samples, we compare the X-ray properties of *luminous* OB stars, Of/WN stars and WN stars in these star-forming regions with log $L/L_\odot \geq 5$ in Table 7. For luminous O stars in Carina log $L_X/L_{Bol} = -7.25 \pm 0.27$ for 28 single stars (vs -7.08 ± 0.42 for 37 single O stars in the Tarantula) and log $L_X/L_{Bol} = -7.10 \pm 0.31$ for 13 binaries (vs -7.02 ± 0.42 for 28 O-type binaries in the Tarantula), confirming results for the full datasets. Detailed comparisons between the Of/WN and WN stars are severely constrained by their scarcity, although their bolometric luminosities are comparable, and Carina WN stars are relatively X-ray faint. The well known colliding wind binary HD 93162 (Pollock & Corcoran 2006; Gamen et al. 2006) is conspicuous in Carina for its exceptional L_X/L_{Bol}, yet in comparison with the Tarantula its properties are intermediate between those of Of/WN binaries Mk 39 and Mk 30 (Fig. 6).

Table 7 also provides mean plasma temperatures for luminous O stars in Carina and the Tarantula Nebula, and reveals softer X-ray emission in the Milky Way ($\overline{kT_m} = 0.5$ keV) than the LMC ($\overline{kT_m} =$

[6] Moffat et al. (2002), Townsley et al. (2014) and Huenemoerder et al. (2019) have investigated the X-ray properties of luminous stars in NGC 3603, which is the closest Galactic analogue to the R136 cluster (Moffat et al. 1994)

[7] The most extreme O-type system in Carina is HD 93129A (Gruner et al. 2019) which exhibits normal X-ray properties despite being a spectroscopic binary (O2 If* + O3 III(f*)), presumably due to the large physical separation between the two components, diluting any wind-wind collision contribution.

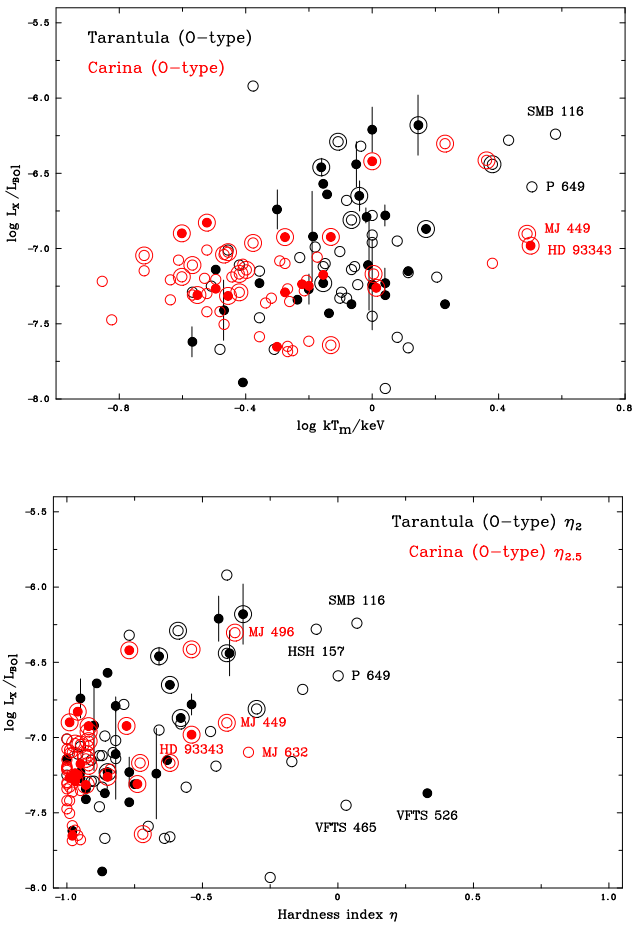

Figure 7. (*Top panel*): Comparison between $\log kT_{\rm m}$ and $\log L_{\rm X}/L_{\rm Bol}$ for single (open) and binary (filled) O stars in the Tarantula Nebula (black) with those in the Carina Nebula (red) from Nazé et al. (2011) and Gagné et al. (2011), in which two plasma temperature components are indicated with two concentric circles. Single O stars in the LMC possess higher plasma temperatures than their counterparts in Carina. Note that spectral fitting to T-ReX sources *required* $kT \gtrapprox 0.3$ keV. Sources with $kT_m \geq 3$ keV are labelled. (*Bottom panel*): As above, except for a comparison between hardness index, η, and $\log L_{\rm X}/L_{\rm Bol}$. A modified index $\eta_{2.5}$ is adopted for Carina O stars since Nazé et al. (2011) provided soft, medium and hard luminosities, such that the Galactic $\eta_{2.5}$ index will be systematically softer than the LMC index η_2.

1.0 keV). The upper panel of Fig. 7 compares kT_m and $L_{\rm X}/L_{\rm Bol}$ ratios of Carina O stars to those in the Tarantula. Sources with $kT_m \geq 3$ keV are labelled and include HD 93343 (O8 V+O7–8.5 V, binary) and MJ 449 (O8.5 V((f)), single) in Carina, plus SMB 116 (O3–6 V, single) and P 649 (O8–9 V, single) in the Tarantula.

Nazé et al. (2011) provide extinction-corrected luminosities of Carina stars in the soft (≤ 1 keV), medium (1–2.5 keV, $L_{\rm X}^{mc}$) and hard (≥ 2.5 keV, $L_{\rm X}^{hc}$) bands, it is necessary to use a modified hardness index, $\eta_{2.5}$,

$$\eta_{2.5} = \frac{L_{\rm X}^{hc} - (L_{\rm X}^{sc} + L_{\rm X}^{mc})}{(L_{\rm X}^{sc} + L_{\rm X}^{mc} + L_{\rm X}^{hc})}.$$

The lower panel of Fig. 7 compares the hardness indices of Carina and Tarantula O stars, although these are more difficult to directly compare than plasma temperatures. Nevertheless, the average $\eta_{2.5}$ = –0.94±0.10 for single O stars in Carina is *significantly* softer than the average η_2 = –0.64±0.32 for single O stars in the Tarantula, too large a difference to be explained solely by their different definitions.

Overall, there does not appear to be a significant difference between the X-ray luminosities of luminous single O-type stars in the LMC and Galaxy, aside from higher temperatures/harder X-ray emission for single stars at lower metallicity. Table 7 also reinforces higher plasma temperatures and harder η_2 indices for WN stars in the Tarantula than their Carina counterparts.

In Fig. 8 we present an estimate of the cumulative distribution function (CDF) for $\log L_{\rm X}/L_{\rm Bol}$, for three samples of luminous O stars: the T-ReX sample presented here (224 stars, comprising 66 detections from Table A2, BI 253 from Table 6, plus 157 attenuation-corrected upper limits from Table S1), the Carina sample (41 stars from Gagné et al. (2011), no upper limits, excluding the X-ray subluminous supergiant HDE 305619) and the combined T-ReX-Carina sample (263 stars). Since these samples contain upper limits, the CDF is calculated using the Kaplan-Meier estimator.

We compare the Tarantula and Carina CDFs using the common method–statistical hypothesis testing, which computes the probability ("p-value") that the Tarantula and Carina samples would produce CDFs less similar than we observed, under the null hypothesis that Tarantula and Carina have the same $L_{\rm X}/L_{\rm Bol}$ relationship. The measure similarity of our CDFs, we used three two-sample statistical tests (Gehan-Breslow, Prentice, Peto) that are designed for Kaplan-Meier distributions (Babu & Feigelson 1996, see p.173). Since these three hypothesis tests produced large p-values (0.682, 0.831, and 0.827, respectively), we find that these data do not provide enough evidence to support the alternative hypothesis – that Tarantula and Carina have different $L_{\rm X}/L_{\rm Bol}$ relationships.

Theoretically Owocki & Cohen (1999) have argued $L_{\rm X} \sim (\dot{M}/v_\infty)^2$ for optically thin winds, so for $\dot{M} \propto Z^{0.83}$ (Mokiem et al. 2007) and $v_\infty \propto Z^{0.13}$ (Leitherer et al. 1992), one would expect $L_{\rm X} \propto (Z^{0.7})^2$ i.e. $\log L_{\rm X} \propto 1.4 \log Z$, so X-ray luminosities of LMC O stars would be expected to be 0.4 dex lower than Galactic counterparts owing to a half-solar metallicity (Table B1). Therefore, contrary to Owocki & Cohen (1999), we find no evidence supporting lower X-ray luminosities in LMC O stars than Galactic counterparts. Owocki et al. (2013) provided an alternative parameterisation in which $L_{\rm X} \propto \dot{M}^{1-m} \propto L_{\rm Bol}^{(1-m)/\alpha'}$, where a mixing exponent $m = 1 - \alpha' \sim 0.4$ is required to reproduce the empirical Galactic $L_{\rm X} \sim 10^{-7} L_{\rm Bol}$ relationship. This scaling suggests $L_{\rm X} \propto (Z^{0.83})^{0.6}$ or $\log L_{\rm X} \propto 0.5 \log Z$ based on the empirical mass-loss dependence on Z (Mokiem et al. 2007), such that LMC O stars are expected to be offset by only 0.15 dex from Milky Way counterparts, which is much more challenging to observationally verify. Owocki et al. (2013) also propose that X-ray luminosities should decrease for optically thick winds with very high mass-loss rates. Since we find no systematic difference between $L_{\rm X}/L_{\rm Bol}$ for single O, Of/WN and WR stars, this result does challenge predictions given our sample includes very luminous stars with dense stellar winds.

In summary, the null hypothesis is that the T-ReX and Carina $\log L_{\rm X}/L_{\rm Bol}$ values for luminous O stars are drawn from the same parent population. Since these three hypothesis tests produce relatively large p-values, we conclude that there is *no* evidence in these data that the Carina and T-ReX samples are drawn from different underlying $\log L_{\rm X}/L_{\rm Bol}$ distributions. This result confirms a similar result for the LMC star forming region N11 (Nazé et al. 2014). Further work on low-Z O star wind acceleration may be needed to explain this result.

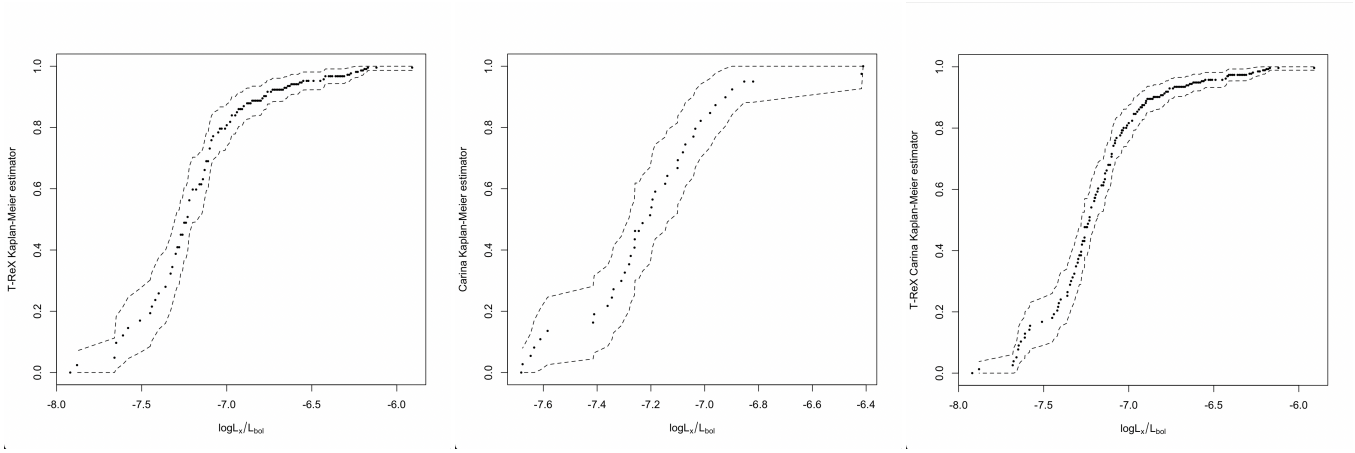

Figure 8. (*left panel*): Cumulative distribution function (CDF) of log L_X/L_{Bol} for luminous O stars in the T-ReX sample (N=224, 67 detections ncluding BI 253 plus 157 upper limits), with 95% confidence limits, calculated using the Kaplan-Meier estimator since sample includes upper limits; (*centre panel*): CDF for luminous O stars in Carina (N=41, Nazé et al. 2011; Gagné et al. 2011, excl. HDE 305619); (*right panel*): CDF for the joint T-ReX and Carina O star samples (N=265).

7 SUMMARY

From a comparison between the rich X-ray point source catalogue from T-ReX (P. Broos & L. Townsley, in prep.) to optical photometric and spectroscopic surveys of the Tarantula Nebula we have obtained the X-ray properties of a rich population of luminous early-type stars at a sub-solar metallicity for the first time, building on previous analyses of shallow X-ray observations (Portegies Zwart et al. 2002; Townsley et al. 2006b, 2014). Overall, excluding extreme outliers and multiple systems we find $\log L_X/L_{Bol} = -7.00 \pm 0.49$, in good agreement with studies of Galactic early-type stars.

Armed with extensive binary properties of early-type stars in the Tarantula from VFTS (Sana et al. 2013; Walborn et al. 2014), TMBM (Almeida et al. 2017, Shenar et al, in prep) and BBC (Villaseñor et al. 2021) we have been able to separate T-ReX sources into single, SB1 and SB2. In general, we confirm previous X-ray studies of Galactic OB stars that binaries possess similar X-ray properties to single stars (Oskinova 2005). Exceptional X-ray properties are observed in some systems (Mk 34, R140a and VFTS 399) and some WR systems are unusually hard X-ray emitters (R130, R134, R135, Mk 53). Indeed, the hardness index increases from O dwarfs, through O (super)giants, Of/WN stars and WN stars, in common with recent Galactic results for OB stars (Nebot Gómez-Morán & Oskinova 2018).

We find no statistical evidence supporting reduced X-ray luminosities for O stars in the LMC than high luminosity counterparts in the Carina Nebula (Nazé et al. 2011; Gagné et al. 2011), folding in upper X-ray limits to hundreds of luminous early-type stars undetected by T-ReX. Consistent results for O, Of/WN and WN stars challenges predictions for X-ray emission from single stars at high luminosity with strong winds (Owocki et al. 2013).

We advocate $L_X \sim 10^{-7} L_{Bol}$ and (median) $kT_m \sim 0.8$ keV for UV spectroscopic analysis of single LMC O stars from the ULLYSES[8] programme since it is well established that X-ray production influences the predicted strength of high ionization metallic resonance lines (Lucy & White 1980; Pauldrach et al. 1994; Crowther et al. 2002b). Further analysis is deferred to future T-ReX studies, including a detailed discussion of X-ray properties of WR and Of/WN stars (K. Tehrani et al, in prep).

[8] https://ullyses.stsci.edu/

ACKNOWLEDGEMENTS

We would like to thank Lidia Oskinova and the anonymous referee for useful comments which helped to clarify a number of topics in the submitted manuscript, and Tomer Shenar for sharing TMBM results prior to publication.

This work was supported by the *Chandra X-ray Observatory* General Observer grants GO5-6080X (PI: L. Townsley) and by GO4-15131X (PI: L. Townsley) and by the Penn State ACIS Instrument Team Contract SV4-74108. All of these were issued by the *Chandra* X-ray Centre, which is operated by the Smithsonian Astrophysical Observatory for and on behalf of NASA under contract NAS8-03060. PAC is supported by the Science and Technology Facilities Council research grant ST/V000853/1 (PI. V. Dhillon). We would like to thank Leigh Parrott's contribution to the statistical tests comparing T-ReX and Carina samples.

This research has made extensive use of NASA's Astrophysics Data System Bibliographic Services, and the SIMBAD database, operated at CDS, Strasbourg, France. For the purpose of open access, the author has applied a Creative Commons Attribution (CC BY) license to any Author Accepted Manuscript version arising.

DATA AVAILABILITY

T-ReX data products are archived in Zenodo collection 10.5281/zenodo.6808367. For every T-ReX point source in this paper we include spectral fitting products and a region file, together with a FITS table and a separate FITS table for upper-limits summarised in the supplementary data. The full T-ReX point source catalog will be added to the Zenodo collection upon publication. Individual T-ReX datasets may also be accessed via the Chandra Data Archive.

REFERENCES

Almeida L. A., et al., 2017, A&A, 598, A84
Andrievsky S. M., Kovtyukh V. V., Korotin S. A., Spite M., Spite F., 2001, A&A, 367, 605
Arnaud K. A., 1996, in Jacoby G. H., Barnes J., eds, ASP Conf. Ser. Vol. 101, Astronomical Data Analysis Software and Systems V. p. 17
Asplund M., Grevesse N., Sauval A. J., Scott P., 2009, ARA&A, 47, 481
Babu G. J., Feigelson E. D., 1996, Astrostatistics
Bagnulo S., et al., 2020, A&A, 635, A163
Bartzakos P., Moffat A. F. J., Niemela V. S., 2001, MNRAS, 324, 18
Berghöfer T. W., Schmitt J. H. M. M., Danner R., Cassinelli J. P., 1997, A&A, 322, 167
Bestenlehner J. M., et al., 2011, A&A, 530, L14
Bestenlehner J. M., et al., 2014, A&A, 570, A38
Bestenlehner J. M., et al., 2020, MNRAS, 499, 1918
Bestenlehner J. M., Crowther P. A., Broos P. S., Pollock A. M. T., Townsley L. K., 2022, MNRAS, 510, 6133
Bosch G., Terlevich R., Melnick J., Selman F., 1999, A&AS, 137, 21
Bosch G., Terlevich E., Terlevich R., 2009, AJ, 137, 3437
Brands S. A., et al., 2022, arXiv e-prints, p. arXiv:2202.11080
Breysacher J., Azzopardi M., Testor G., 1999, A&AS, 137, 117
Broos P. S., Townsley L. K., Feigelson E. D., Getman K. V., Bauer F. E., Garmire G. P., 2010, ApJ, 714, 1582
Broos P. S., et al., 2011, ApJS, 194, 2
Brunet J. P., Imbert M., Martin N., Mianes P., Prévot L., Rebeirot E., Rousseau J., 1975, A&AS, 21, 109
Cash W., 1979, ApJ, 228, 939
Castro N., Crowther P. A., Evans C. J., Mackey J., Castro-Rodriguez N., Vink J. S., Melnick J., Selman F., 2018, A&A, 614, A147
Castro N., et al., 2021, A&A, 648, A65
Chlebowski T., Garmany C. D., 1991, ApJ, 368, 241
Chlebowski T., Harnden F. R. J., Sciortino S., 1989, ApJ, 341, 427
Clark J. S., et al., 2015, A&A, 579, A131
Clark J. S., Ritchie B. W., Negueruela I., 2019, A&A, 626, A59
Cohen D. H., Cassinelli J. P., MacFarlane J. J., 1997, ApJ, 487, 867
Conti P. S., Massey P., 1989, ApJ, 337, 251
Crowther P. A., 2019, Galaxies, 7, 88
Crowther P. A., Smith L. J., 1997, A&A, 320, 500
Crowther P. A., Walborn N. R., 2011, MNRAS, 416, 1311
Crowther P. A., Dessart L., Hillier D. J., Abbott J. B., Fullerton A. W., 2002a, A&A, 392, 653
Crowther P. A., Hillier D. J., Evans C. J., Fullerton A. W., De Marco O., Willis A. J., 2002b, ApJ, 579, 774
Crowther P. A., Schnurr O., Hirschi R., Yusof N., Parker R. J., Goodwin S. P., Kassim H. A., 2010, MNRAS, 408, 731
Crowther P. A., et al., 2016, MNRAS, 458, 624
de Boer K. S., Koornneef J., Savage B. D., 1980, ApJ, 236, 769
De Marchi G., et al., 2011, ApJ, 739, 27
Dopita M. A., Seitenzahl I. R., Sutherland R. S., Nicholls D. C., Vogt F. P. A., Ghavamian P., Ruiter A. J., 2019, AJ, 157, 50
Doran E. I., et al., 2013, A&A, 558, A134
Dufton P. L., et al., 2018, A&A, 615, A101
Dunstall P. R., et al., 2012, A&A, 542, A50
Evans C. J., et al., 2011, A&A, 530, A108
Evans C. J., et al., 2015, A&A, 574, A13
Feast M. W., Thackeray A. D., Wesselink A. J., 1960, MNRAS, 121, 337
Fitzpatrick E. L., Savage B. D., 1984, ApJ, 279, 578
Foellmi C., Moffat A. F. J., Guerrero M. A., 2003, MNRAS, 338, 1025
Gagné M., et al., 2011, ApJS, 194, 5
Gagné M., Fehon G., Savoy M. R., Cartagena C. A., Cohen D. H., Owocki S. P., 2012, in Drissen L., Robert C., St-Louis N., Moffat A. F. J., eds, ASP Conf. Ser. Vol. 465, Proceedings of a Scientific Meeting in Honor of Anthony F. J. Moffat. p. 301 (arXiv:1205.3510)
Gamen R., et al., 2006, A&A, 460, 777
Garmire G. P., Bautz M. W., Ford P. G., Nousek J. A., Ricker George R. J., 2003, in Truemper J. E., Tananbaum H. D., eds, Society of Photo-Optical Instrumentation Engineers (SPIE) Conference Series Vol. 4851, X-Ray and Gamma-Ray Telescopes and Instruments for Astronomy.. pp 28–44, doi:10.1117/12.461599
Garnett D. R., 1999, in Chu Y. H., Suntzeff N., Hesser J., Bohlender D., eds, Vol. 190, New Views of the Magellanic Clouds. p. 266
Gayley K. G., 2014, ApJ, 788, 90
Graczyk D., et al., 2011, Acta Astron., 61, 103
Gruner D., et al., 2019, A&A, 621, A63
Grunhut J. H., et al., 2017, MNRAS, 465, 2432
Guerrero M. A., Chu Y.-H., 2008, ApJS, 177, 216
Hainich R., et al., 2014, A&A, 565, A27
Hamann W. R., et al., 2019, A&A, 625, A57
Harnden F. R. J., et al., 1979, ApJ, 234, L51
Hénault-Brunet V., et al., 2012, A&A, 546, A73
Hill V., Andrievsky S., Spite M., 1995, A&A, 293, 347
Huenemoerder D. P., Schulz N. S., Nichols J. S., 2019, AJ, 157, 29
Hunter D. A., Shaya E. J., Holtzman J. A., Light R. M., O'Neil Earl J. J., Lynds R., 1995, ApJ, 448, 179
Hunter I., et al., 2007, A&A, 466, 277
Khorrami Z., et al., 2021, MNRAS, 503, 292
Koornneef J., 1982, A&A, 107, 247
Korn A. J., Becker S. R., Gummersbach C. A., Wolf B., 2000, A&A, 353, 655
Lebouteiller V., Bernard-Salas J., Brandl B., Whelan D. G., Wu Y., Charmandaris V., Devost D., Houck J. R., 2008, ApJ, 680, 398
Leitherer C., Robert C., Drissen L., 1992, ApJ, 401, 596
Long K. S., White R. L., 1980, ApJ, 239, L65
Lucy L. B., Solomon P. M., 1970, ApJ, 159, 879
Lucy L. B., White R. L., 1980, ApJ, 241, 300
Mahy L., et al., 2020, A&A, 634, A118
Malumuth E. M., Heap S. R., 1994, AJ, 107, 1054
Massey P., Hunter D. A., 1998, ApJ, 493, 180
Massey P., Penny L. R., Vukovich J., 2002, ApJ, 565, 982
Massey P., Puls J., Pauldrach A. W. A., Bresolin F., Kudritzki R. P., Simon T., 2005, ApJ, 627, 477
Massey P., Morrell N. I., Neugent K. F., Penny L. R., DeGioia-Eastwood K., Gies D. R., 2012, ApJ, 748, 96
McEvoy C. M., et al., 2015, A&A, 575, A70
Melnick J., 1985, A&A, 153, 235
Moffat A. F. J., Niemela V. S., Phillips M. M., Chu Y.-H., Seggewiss W., 1987, ApJ, 312, 612
Moffat A. F. J., Drissen L., Shara M. M., 1994, ApJ, 436, 183
Moffat A. F. J., et al., 2002, ApJ, 573, 191
Mokiem M. R., et al., 2007, A&A, 473, 603
Nazé Y., 2009, A&A, 506, 1055
Nazé Y., Hartwell J. M., Stevens I. R., Manfroid J., Marchenko S., Corcoran M. F., Moffat A. F. J., Skalkowski G., 2003, ApJ, 586, 983
Nazé Y., et al., 2011, ApJS, 194, 7
Nazé Y., Wang Q. D., Chu Y.-H., Gruendl R., Oskinova L., 2014, ApJS, 213, 23
Nebot Gómez-Morán A., Oskinova L. M., 2018, A&A, 620, A89
Oskinova L. M., 2005, MNRAS, 361, 679
Oskinova L. M., Ignace R., Hamann W. R., Pollock A. M. T., Brown J. C., 2003, A&A, 402, 755
Owocki S. P., Cohen D. H., 1999, ApJ, 520, 833
Owocki S. P., Castor J. I., Rybicki G. B., 1988, ApJ, 335, 914
Owocki S. P., Sundqvist J. O., Cohen D. H., Gayley K. G., 2013, MNRAS, 429, 3379
Pallavicini R., Golub L., Rosner R., Vaiana G. S., Ayres T., Linsky J. L., 1981, ApJ, 248, 279
Parker J. W., 1993, AJ, 106, 560
Pauldrach A. W. A., Kudritzki R. P., Puls J., Butler K., Hunsinger J., 1994, A&A, 283, 525
Pawlak M., et al., 2016, Acta Astron., 66, 421
Pittard J., 2011, Bulletin de la Societe Royale des Sciences de Liege, 80, 555
Pollock A. M. T., 1987, ApJ, 320, 283
Pollock A. M. T., Corcoran M. F., 2006, A&A, 445, 1093
Pollock A. M. T., Crowther P. A., Tehrani K., Broos P. S., Townsley L. K., 2018, MNRAS, 474, 3228

Portegies Zwart S. F., Pooley D., Lewin W. H. G., 2002, ApJ, 574, 762
Predehl P., Schmitt J. H. M. M., 1995, A&A, 500, 459
Puls J., Vink J. S., Najarro F., 2008, A&ARv, 16, 209
Ramírez-Agudelo O. H., et al., 2017, A&A, 600, A81
Rate G., Crowther P. A., 2020, MNRAS, 493, 1512
Rauw G., 2022, arXiv e-prints, p. arXiv:2203.16842
Rauw G., et al., 2015, ApJS, 221, 1
Repolust T., Puls J., Herrero A., 2004, A&A, 415, 349
Rivero González J. G., Puls J., Massey P., Najarro F., 2012, A&A, 543, A95
Roman-Duval J., et al., 2019, ApJ, 871, 151
Sabín-Sanjulián C., et al., 2017, A&A, 601, A79
Sana H., Rauw G., Nazé Y., Gosset E., Vreux J. M., 2006, MNRAS, 372, 661
Sana H., et al., 2012, Science, 337, 444
Sana H., et al., 2013, A&A, 550, A107
Sanduleak N., 1970, Contributions from the Cerro Tololo Inter-American Observatory, 89
Schild H., Testor G., 1992, A&AS, 92, 729
Schneider F. R. N., et al., 2018, Science, 359, 69
Schnurr O., Moffat A. F. J., St-Louis N., Morrell N. I., Guerrero M. A., 2008, MNRAS, 389, 806
Schnurr O., Chené A. N., Casoli J., Moffat A. F. J., St-Louis N., 2009, MNRAS, 397, 2049
Selman F., Melnick J., Bosch G., Terlevich R., 1999, A&A, 341, 98
Seward F. D., Forman W. R., Giacconi R., Griffiths R. E., Harnden F. R. J., Jones C., Pye J. P., 1979, ApJ, 234, L55
Shenar T., et al., 2017, A&A, 598, A85
Shenar T., et al., 2019, A&A, 627, A151
Shenar T., et al., 2021, A&A, 650, A147
Shenar T., et al., 2022, Nature Astronomy
Smith L. F., Shara M. M., Moffat A. F. J., 1990, ApJ, 348, 471
Smith L. J., Nota A., Pasquali A., Leitherer C., Clampin M., Crowther P. A., 1998, ApJ, 503, 278
Smith M. A., Lopes de Oliveira R., Motch C., 2016, Advances in Space Research, 58, 782
Tehrani K. A., Crowther P. A., Bestenlehner J. M., Littlefair S. P., Pollock A. M. T., Parker R. J., Schnurr O., 2019, MNRAS, 484, 2692
Toribio San Cipriano L., Domínguez-Guzmán G., Esteban C., García-Rojas J., Mesa-Delgado A., Bresolin F., Rodríguez M., Simón-Díaz S., 2017, MNRAS, 467, 3759
Townsley L. K., Broos P. S., Feigelson E. D., Brandl B. R., Chu Y.-H., Garmire G. P., Pavlov G. G., 2006a, AJ, 131, 2140
Townsley L. K., Broos P. S., Feigelson E. D., Garmire G. P., Getman K. V., 2006b, AJ, 131, 2164
Townsley L. K., et al., 2011, ApJS, 194, 1
Townsley L. K., Broos P. S., Garmire G. P., Bouwman J., Povich M. S., Feigelson E. D., Getman K. V., Kuhn M. A., 2014, ApJS, 213, 1
Townsley L. K., Broos P. S., Garmire G. P., Anderson G. E., Feigelson E. D., Naylor T., Povich M. S., 2018, ApJS, 235, 43
Trundle C., Dufton P. L., Hunter I., Evans C. J., Lennon D. J., Smartt S. J., Ryans R. S. I., 2007, A&A, 471, 625
Tsamis Y. G., Barlow M. J., Liu X. W., Danziger I. J., Storey P. J., 2003, MNRAS, 338, 687
Tumlinson J., et al., 2002, ApJ, 566, 857
Villaseñor J. I., et al., 2021, MNRAS, 507, 5348
Walborn N. R., Blades J. C., 1997, ApJS, 112, 457
Walborn N. R., et al., 2014, A&A, 564, A40
Weigelt G., Baier G., 1985, A&A, 150, L18
Welty D. E., Xue R., Wong T., 2012, ApJ, 745, 173

SUPPLEMENTARY MATERIAL

Supplementary Material are available at MNRAS online.

Table S1. Upper limits to observed X-ray luminosities L_X^t for luminous ($\log L/L_\odot \geq 5$) early-type stars excluded from the T-ReX point source catalogue, in RA order.

APPENDIX A: THERMAL PLASMA FITS AND PROPERTIES OF EARLY-TYPE STARS OF T-REX SOURCES

Table A1. Thermal plasma fits to X-ray spectroscopy for T-ReX sources, sorted by decreasing photon flux. Notes: Quantities marked with an asterisk (∗) were frozen in the fit. Quantities marked with ‡ are at the upper (9.5 keV) or lower (0.27 keV) limit chosen for the model; uncertainties are not computed when fit parameters are at such limits. Uncertainties represent 90% confidence intervals. X-ray luminosities in the soft (s) band (0.5–2 keV), hard (h) band (2–8 keV), total (t) band (0.5–8 keV) are derived from the model spectrum. Absorption-corrected luminosities, superscripted with a c, are calculated with *only* the Galactic and LMC ISM absorption components removed, no correction is made for any circumstellar absorption ($N(H)^1$, $N(H)^2$). For two-temperature fits, luminosities are shown for each thermal plasma component so that their relative contribution can be assessed.

T-ReX Source					Spectral Fit							X-ray Luminosities							
Label	CXOU J	Photon Flux	NetCts	χ^2_ν	$N(H)^{\rm LMC}$	$N(H)^1$	kT^1	EM^1	$N(H)^2$	kT^2	EM^2	$L_{\rm X}^{1,t}$	$L_{\rm X}^{1,tc}$	$L_{\rm X}^{2,t}$	$L_{\rm X}^{2,tc}$	$L_{\rm X}^{sc}$	$L_{\rm X}^{hc}$	$L_{\rm X}^{t}$	$L_{\rm X}^{tc}$
		$\rm cm^{-2}\,s^{-1}$	count		$10^{22}\rm cm^{-2}$	$10^{22}\rm cm^{-2}$	keV	log $\rm cm^{-3}$	$10^{22}\rm cm^{-2}$	keV	log $\rm cm^{-3}$	log erg $\rm s^{-1}$							
p1_995[a]	053844.25−690605.9	1.48×10^{-4}	74445	1.05	$1.05^{+0.04}_{-0.04}$	0.0∗	$1.05^{+0.03}_{-0.03}$	$57.62^{+0.14}_{-0.14}$	0.0∗	$3.92^{+0.12}_{-0.12}$	$58.15^{+0.03}_{-0.03}$	34.17	34.55	35.07	35.23	35.03	34.99	35.12	35.31
p1_752[a]	053841.59−690513.4	1.46×10^{-4}	54076	1.13	$1.15^{+0.07}_{-0.07}$	0.0∗	$0.63^{+0.02}_{-0.02}$	$58.15^{+0.18}_{-0.18}$	0.0∗	$2.19^{+0.06}_{-0.06}$	$58.14^{+0.04}_{-0.04}$	34.46	35.06	34.86	35.10	35.27	34.73	35.01	35.38
p1_610	053833.43−691159.0	4.92×10^{-5}	22077	1.01	Power law fit to entire dataset vs Clark et al. (2015) fit to partial dataset							···	···	···	···	34.22	34.89	···	34.98
p1_893	053842.90−690604.9	1.70×10^{-5}	6955	1.04	1.4∗	0.0∗	$2.7^{+0.1}_{-0.1}$	$57.4^{+0.01}_{-0.01}$	···	···	···	···	···	···	···	34.13	34.05	34.16	34.39
p1_698	053840.22−690559.8	1.69×10^{-5}	7988	0.86	0.83∗	$1.0^{+0.2}_{-0.2}$	$0.88^{+0.08}_{-0.10}$	$57.2^{+0.1}_{-0.2}$	0.0∗	$2.6^{+0.3}_{-0.2}$	$57.1^{+0.06}_{-0.07}$	33.55	33.80	33.93	34.11	34.09	33.84	34.08	34.28
p1_832	053842.38−690602.8	1.12×10^{-5}	4453	1.10	0.92∗	$0.67^{\cdots}_{-0.03}$	$0.47^{+0.1}_{\cdots}$	$57.4^{\cdots}_{-0.3}$	$0.80^{+1.1}_{\cdots}$	$2.1^{+0.6}_{-0.3}$	$57.0^{+0.2}_{-0.1}$	33.44	33.93	33.69	33.80	34.04	33.58	33.88	34.17
p1_979	053844.12−690556.6	4.72×10^{-6}	2181	1.18	0.62∗	$1.7^{+0.2}_{-0.3}$	0.3∗	$57.7^{+0.2}_{-0.2}$	$1.4^{+1.2}_{-0.8}$	$1.6^{+0.2}_{-0.2}$	$56.7^{+0.09}_{-0.10}$	33.00	33.30	33.26	33.34	33.47	33.09	33.45	33.62
p1_830	053842.34−690458.1	4.20×10^{-6}	1681	0.94	0.76∗	$1.0^{+0.7}_{-0.3}$	$0.49^{+0.1}_{-0.3}$	$57.0^{+0.4}_{-0.3}$	$1.4^{+0.9}_{-0.6}$	$1.1^{+0.2}_{-0.2}$	$56.7^{+0.2}_{-0.3}$	33.01	33.36	33.11	33.27	33.54	32.86	33.36	33.62
p1_1000	053844.33−690554.7	4.10×10^{-6}	1866	0.92	0.90∗	$1.1^{+0.2}_{-0.3}$	$0.73^{+0.08}_{-0.08}$	$56.8^{+0.2}_{-0.2}$	0.0∗	$3.5^{+3.7}_{-0.9}$	$56.3^{+0.1}_{-0.2}$	33.07	33.38	33.22	33.38	33.51	33.19	33.45	33.68
p1_1194	053853.36−690200.9	2.97×10^{-6}	1233	0.86	0.23∗	$1.1^{+0.4}_{-0.6}$	$0.66^{+0.1}_{-0.2}$	$56.5^{+0.2}_{-0.4}$	$5.1^{+2.3}_{-1.8}$	$1.8^{+0.4}_{-0.3}$	$56.8^{+0.2}_{-0.1}$	32.83	32.95	33.22	33.23	33.02	33.18	33.37	33.41
p1_296	053749.06−690508.1	2.81×10^{-6}	1174	0.97	0.53∗	$0.55^{+0.2}_{-0.2}$	$0.78^{+0.09}_{-0.11}$	$56.4^{+0.1}_{-0.1}$	$34^{+8.5}_{-6.2}$	$8.1^{\cdots}_{-3.6}$	$56.9^{+0.20}_{-0.09}$	32.93	33.19	33.48	33.49	33.14	33.51	33.59	33.66
cc4970	053842.32−690603.4	2.37×10^{-6}	496	1.02	0.93∗	$1.6^{+0.7}_{-0.9}$	$0.86^{+0.3}_{-0.5}$	$56.8^{+0.2}_{-0.5}$	$10^{\cdots}_{\cdots}$	$2.3^{\cdots}_{\cdots}$	$56.3^{+0.9}_{-6.9}$	33.05	33.26	32.73	32.76	33.14	33.01	33.22	33.38
p1_812	053842.11−690555.2	2.05×10^{-6}	934	0.87	0.81∗	$1.2^{+0.5}_{-0.2}$	$0.51^{+0.2}_{-0.2}$	$56.8^{+0.3}_{-0.4}$	$0.72^{+3.7}_{\cdots}$	$2.6^{+2.4}_{-0.9}$	$56.1^{+0.3}_{-0.3}$	32.76	33.09	32.88	32.97	33.18	32.82	33.12	33.34
p1_1256	053857.06−690605.6	1.87×10^{-6}	784	1.23	0.67∗	$3.1^{+0.6}_{-0.6}$	$1.6^{+0.3}_{-0.2}$	$56.8^{+0.10}_{-0.10}$	···	···	···	···	···	···	···	32.71	33.09	33.19	33.24
p1_1088	053847.48−690025.1	1.74×10^{-6}	694	1.24	0.42∗	$1.3^{+0.3}_{-0.4}$	$0.77^{+0.08}_{-0.11}$	$56.6^{+0.2}_{-0.9}$	$5.6^{\cdots}_{\cdots}$	$1.5^{\cdots}_{\cdots}$	$56.0^{+0.6}_{-6.5}$	32.92	33.06	32.29	32.31	32.99	32.57	33.01	33.13
p1_867	053842.65−690602.9	1.59×10^{-6}	522	1.67	1.0∗	$0.97^{+0.4}_{-0.2}$	$0.65^{+0.1}_{-0.1}$	$56.7^{+0.10}_{-0.17}$	0.0∗	9.5‡	$55.4^{+0.4}_{-5.9}$	32.82	33.21	32.47	32.58	33.20	32.62	32.98	33.30
p1_754	053841.62−690515.1	1.50×10^{-6}	397	1.12	0.41∗	0.0∗	$0.78^{+0.1}_{-0.5}$	$55.5^{+0.2}_{-1.6}$	$0.94^{+2.2}_{\cdots}$	$5.1^{\cdots}_{-2.4}$	$56.1^{+0.2}_{-0.2}$	32.37	32.65	33.06	33.09	32.86	32.98	33.14	33.22
c6981	053842.08−690602.2	1.11×10^{-6}	337	0.95	0.70∗	0.0∗	$0.63^{+0.4}_{\cdots}$	$55.5^{\cdots}_{-0.5}$	$1.9^{+2.1}_{-1.1}$	$1.0^{+0.6}_{-0.3}$	$56.4^{+0.2}_{-0.3}$	32.16	32.64	32.70	32.83	32.92	32.42	32.81	33.04
p1_745	053841.49−690556.9	1.08×10^{-6}	474	0.36	0.79∗	$1.3^{+0.6}_{-0.3}$	$0.58^{+0.2}_{-0.4}$	$56.7^{+0.4}_{-0.2}$	$21^{\cdots}_{\cdots}$	$1.1^{+6.4}_{\cdots}$	$56.5^{\cdots}_{-7.0}$	32.70	32.99	32.08	32.10	32.94	32.35	32.79	33.04
c7157	053842.40−690601.1	7.67×10^{-7}	345	0.65	0.86∗	0.0∗	$0.69^{+0.1}_{-0.5}$	$55.9^{\cdots}_{-0.1}$	0.0∗	$8.6^{\cdots}_{-6.5}$	$55.4^{+0.3}_{-0.2}$	32.48	33.01	32.50	32.60	33.05	32.47	32.79	33.15
p1_1234	053855.52−690426.7	7.14×10^{-7}	303	0.61	2.4∗	$0.78^{+1.0}_{\cdots}$	$2.0^{+0.6}_{-0.4}$	$56.2^{+0.2}_{-0.1}$	···	···	···	···	···	···	···	32.70	32.76	32.81	33.04
p1_663	053838.02−690543.3	6.90×10^{-7}	216	1.10	0.96∗	$0.89^{+1.2}_{\cdots}$	$0.49^{+0.4}_{-0.3}$	$56.3^{+0.4}_{-0.8}$	$3.0^{+30.5}_{\cdots}$	$1.9^{\cdots}_{-0.9}$	$55.9^{+0.5}_{-1.5}$	32.31	32.76	32.44	32.50	32.79	32.42	32.68	32.95
p1_924	053843.20−690614.4	6.01×10^{-7}	261	1.24	0.79∗	$1.4^{+0.5}_{-0.4}$	$0.80^{+0.2}_{-0.1}$	$56.3^{+0.2}_{-0.2}$	···	···	···	···	···	···	···	32.61	32.04	32.49	32.71
c7182	053842.49−690604.3	5.86×10^{-7}	259	1.65	0.96∗	0.0∗	0.27‡	$56.3^{+0.1}_{-0.2}$	0.0∗	$2.7^{+1.8}_{-0.9}$	$55.7^{+0.1}_{-0.1}$	32.15	33.06	32.51	32.70	33.15	32.36	32.67	33.21
p1_786	053841.87−690614.4	4.97×10^{-7}	194	0.65	1.2∗	$0.95^{+0.7}_{-0.7}$	$1.0^{+0.3}_{-0.4}$	$56.1^{+0.4}_{-0.2}$	···	···	···	···	···	···	···	33.64	32.12	32.46	32.76
p1_911	053843.09−690546.9	4.66×10^{-7}	204	1.20	0.74∗	$2.0^{+0.6}_{-0.4}$	$0.86^{+0.2}_{-0.2}$	$56.2^{+0.2}_{-0.2}$	···	···	···	···	···	···	···	32.41	32.06	32.42	32.57
p1_441	053759.53−690901.5	4.58×10^{-7}	182	1.05	0.30∗	$0.51^{\cdots}_{-0.4}$	$0.50^{+0.2}_{-0.2}$	$56.0^{+0.7}_{-0.4}$	···	···	···	···	···	···	···	32.62	31.13	32.42	32.63
p1_480	053813.97−690747.7	4.19×10^{-7}	169	0.85	0.54∗	0.0∗	$0.7^{+0.2}_{\cdots}$	$55.3^{+0.2}_{-0.3}$	$0.055^{+4.3}_{\cdots}$	$2.1^{+2.1}_{-0.9}$	$55.4^{+0.4}_{-0.2}$	32.01	32.38	32.24	32.38	32.58	32.02	32.44	32.68
c7257	053842.65−690602.1	4.00×10^{-7}	93	0.44	1.1∗	$0.53^{+1.4}_{\cdots}$	$0.52^{+0.3}_{\cdots}$	$56.2^{\cdots}_{-0.4}$	···	···	···	···	···	···	···	32.87	31.43	32.32	32.88
p1_1186	053852.72−690643.2	4.00×10^{-7}	153	1.16	0.79∗	0.0∗	$1.1^{+0.3}_{\cdots}$	$55.4^{+0.1}_{-0.5}$	0.0∗	$5.0^{\cdots}_{\cdots}$	$55.1^{+0.5}_{-0.5}$	32.15	32.48	32.13	32.25	32.53	32.16	32.44	32.68
c5349	053833.82−690957.1	3.98×10^{-7}	147	1.75	0.77∗	0.0∗	0.27‡	$55.8^{+0.2}_{-6.3}$	0.0∗	$2.2^{+1.1}_{-0.5}$	$55.5^{+0.1}_{-0.2}$	31.78	32.55	32.33	32.52	32.75	32.12	32.44	32.84
p1_795	053842.01−690607.6	3.94×10^{-7}	158	0.85	0.95∗	$0.42^{+0.5}_{-0.4}$	$0.65^{+0.2}_{-0.2}$	$55.9^{+0.4}_{-0.2}$	···	···	···	···	···	···	···	32.74	31.49	32.28	32.76
c6974	053842.09−690545.5	3.82×10^{-7}	161	0.52	0.79∗	$1.3^{+0.6}_{\cdots}$	$1.0^{+0.9}_{-0.3}$	$56.0^{+0.2}_{-0.3}$	···	···	···	···	···	···	···	32.39	31.99	32.35	32.53
p1_611	053833.62−690450.4	3.72×10^{-7}	140	2.05	0.44∗	0.0∗	$0.70^{\cdots}_{\cdots}$	$54.7^{+1.8}_{-0.4}$	49‡	9.5‡	$56.4^{+0.2}_{-0.1}$	31.52	31.83	32.96	32.96	31.81	32.96	32.97	32.99
p1_749	053841.55−690519.4	3.46×10^{-7}	113	1.50	0.67∗	0.0∗	$0.41^{+0.2}_{\cdots}$	$55.7^{+0.3}_{-1.0}$	0.0∗	$1.6^{\cdots}_{-0.6}$	$55.2^{+0.3}_{-0.4}$	32.10	32.66	32.00	32.22	32.76	31.70	32.36	32.79

a: Most observations of p1_995 and p1_752 suffer from an instrumental problem known as photon pile-up. Those piled spectra were corrected using a model of the ACIS detectors (see Appendix of Broos et al. 2011)

Table A1. (continued)

T-ReX Source					Spectral Fit							X-ray Luminosities							
Label	CXOU J	Photon Flux $cm^{-2}\ s^{-1}$	NetCts count	χ^2_ν	$N(H)^{LMC}$ $10^{22}cm^{-2}$	$N(H)^1$ $10^{22}cm^{-2}$	kT^1 keV	EM^1 log cm^{-3}	$N(H)^2$ $10^{22}cm^{-2}$	kT^2 keV	EM^2 log cm^{-3}	$L_X^{1,t}$	$L_X^{1,tc}$	$L_X^{2,t}$	$L_X^{2,tc}$	L_X^{sc} log erg s^{-1}	L_X^{hc}	L_X^t	L_X^{tc}
p1_722	053841.21−690258.3	3.44×10^{-7}	93	0.64	0.35∗	$0.84^{+0.9}_{...}$	$1.1^{+0.5}_{-0.5}$	$55.6^{+0.4}_{-0.2}$	···	···	···	···	···	···	···	32.25	31.74	32.25	32.36
c10289	053911.27−690201.2	3.23×10^{-7}	100	0.66	0.76∗	$2.9^{+3.3}_{-2.2}$	$3.3^{...}_{-1.4}$	$55.8^{+0.3}_{-0.3}$	···	···	···	···	···	···	···	31.79	32.50	32.55	32.58
p1_955	053843.67−690547.8	2.77×10^{-7}	116	0.74	0.51∗	0.0∗	$0.97^{+0.1}_{-0.1}$	$55.4^{+0.07}_{-0.09}$	···	···	···	···	···	···	···	32.42	31.42	32.19	32.46
c893	053708.89−690720.9	2.47×10^{-7}	74	0.55	0.55∗	$0.31^{+0.9}_{...}$	$0.70^{+0.5}_{...}$	$55.7^{+1.6}_{-0.4}$	···	···	···	···	···	···	···	32.56	31.35	32.27	32.59
c7131	053842.37−690615.1	2.45×10^{-7}	90	0.46	1.3∗	$2.2^{+1.7}_{-1.0}$	$0.55^{+0.3}_{-0.2}$	$56.4^{+0.5}_{-0.5}$	···	···	···	···	···	···	···	32.30	31.63	32.09	32.38
p1_1033	053844.93−690554.1	2.18×10^{-7}	96	1.44	0.90∗	$1.2^{+0.9}_{-1.2}$	$1.0^{+0.6}_{-0.5}$	$55.7^{+0.5}_{-0.3}$	···	···	···	···	···	···	···	32.16	31.73	32.08	32.29
p1_1035	053845.11−690508.4	2.08×10^{-7}	50	1.02	0.79∗	0.0∗	$3.8^{...}_{-1.6}$	$55.3^{+0.1}_{-0.1}$	···	···	···	···	···	···	···	32.08	32.14	32.27	32.41
c7452	053843.11−690601.3	2.08×10^{-7}	124	1.01	1.1∗	$0.062^{+4.3}_{...}$	$0.63^{...}_{...}$	$55.3^{+1.1}_{-5.8}$	0.49...	8.1...	$55.3^{+0.4}_{-5.8}$	31.67	32.32	32.34	32.42	32.43	32.30	32.43	32.67
c7018	053842.17−690601.6	2.07×10^{-7}	45	0.95	0.82∗	$1.5^{+1.2}_{-0.6}$	$0.89^{+0.8}_{-0.3}$	$55.8^{+0.2}_{-0.3}$	···	···	···	···	···	···	···	32.14	31.68	32.07	32.27
c6701	053841.52−690601.0	2.03×10^{-7}	61	0.90	1.2∗	0.0∗	$0.35^{+0.6}_{...}$	$55.9^{+0.7}_{-0.6}$	···	···	···	···	···	···	···	32.80	30.43	31.86	32.80
p1_987	053844.23−690547.1	1.99×10^{-7}	84	0.40	0.67∗	$0.41^{+0.6}_{...}$	$0.79^{+0.4}_{-0.5}$	$55.5^{+1.0}_{-0.3}$	···	···	···	···	···	···	···	32.31	31.29	32.03	32.35
c6062	053839.15−690621.2	1.92×10^{-7}	66	1.08	0.67∗	$4.2^{+6.4}_{-2.8}$	$4.1^{...}_{-2.6}$	$55.6^{+0.5}_{-0.3}$	···	···	···	···	···	···	···	31.41	32.36	32.39	32.41
c4876	053828.43−691119.4	1.90×10^{-7}	69	1.02	0.31∗	$0.045^{+2.9}_{...}$	$0.96^{+0.3}_{...}$	$55.1^{...}_{-0.2}$	···	···	···	···	···	···	···	32.13	31.14	31.99	32.17
p1_682	053839.36−690606.5	1.88×10^{-7}	67	1.39	1.2∗	0.0∗	$0.59^{+0.3}_{-0.3}$	$55.6^{+0.6}_{-0.2}$	···	···	···	···	···	···	···	32.69	31.06	31.98	32.70
cc4968	053842.27−690604.9	1.82×10^{-7}	66	0.62	0.76∗	0.0∗	$1.8^{+4.5}_{-0.7}$	$55.3^{+0.2}_{-0.3}$	···	···	···	···	···	···	···	32.08	31.76	32.03	32.25
p1_760	053841.74−690625.0	1.77×10^{-7}	72	1.55	0.94∗	0.0∗	$1.1^{+0.3}_{-0.4}$	$55.3^{+0.10}_{-0.13}$	···	···	···	···	···	···	···	32.26	31.39	31.93	32.32
p1_866	053842.63−690556.2	1.72×10^{-7}	62	1.30	1.4∗	$1.4^{...}_{...}$	$0.83^{+0.8}_{-0.6}$	$55.7^{+1.5}_{-0.5}$	···	···	···	···	···	···	···	32.11	31.55	31.89	32.22
c8160	053846.17−690617.2	1.70×10^{-7}	64	0.16	0.67∗	$0.63^{+1.1}_{...}$	$0.44^{+0.5}_{...}$	$55.8^{...}_{-0.7}$	···	···	···	···	···	···	···	32.36	30.79	31.96	32.37
p1_637	053836.40−690657.5	1.70×10^{-7}	67	1.16	1.1∗	0.0∗	$1.6^{+1.0}_{-0.4}$	$55.2^{+0.1}_{-0.2}$	49‡	9.5‡	$55.6^{+0.4}_{-6.1}$	31.89	32.19	32.10	32.11	32.04	32.24	32.31	32.45
c6030	053838.82−690649.6	1.60×10^{-7}	50	1.27	1.2∗	$1.6^{+1.4}_{...}$	$1.1^{+1.0}_{-0.5}$	$55.6^{+0.4}_{-0.4}$	···	···	···	···	···	···	···	31.95	31.74	31.97	32.16
c7410	053843.04−690611.2	1.55×10^{-7}	69	0.55	0.97∗	$0.56^{+1.0}_{...}$	$0.71^{...}_{-0.4}$	$55.5^{+1.0}_{-0.4}$	···	···	···	···	···	···	···	32.28	31.22	31.89	32.32
p1_695	053840.17−690551.2	1.55×10^{-7}	63	0.29	1.1∗	0.0∗	$1.6^{+0.9}_{-0.4}$	$55.3^{+0.1}_{-0.1}$	···	···	···	···	···	···	···	32.13	31.71	31.97	32.27
c6973	053842.05−6906	1.51×10^{-7}	39	0.74	1.1∗	$1.2^{+0.7}_{-0.7}$	$0.49^{+0.2}_{-0.1}$	$56.0^{+0.4}_{-0.5}$	···	···	···	···	···	···	···	32.23	31.01	31.84	32.26
c6443	053840.79−690525.1	1.48×10^{-7}	46	0.89	0.90∗	0.0∗	$1.0^{+0.2}_{-0.2}$	$55.3^{+0.1}_{-0.1}$	···	···	···	···	···	···	···	32.29	31.36	31.94	32.34
c8112	053845.69−690622.5	1.42×10^{-7}	55	1.31	0.90∗	$0.31^{+0.9}_{...}$	$0.76^{+0.3}_{-0.4}$	$55.3^{+0.6}_{-0.3}$	···	···	···	···	···	···	···	32.25	31.12	31.84	32.28
c7859	053844.41−690536.2	1.40×10^{-7}	28	0.64	0.79∗	$4.4^{...}_{-2.3}$	$0.33^{+0.3}_{...}$	$57.0^{+1.7}_{-7.6}$	···	···	···	···	···	···	···	31.88	31.21	31.82	31.97
c6370	053840.54−690557.1	1.38×10^{-7}	35	0.96	0.75∗	0.0∗	$1.1^{...}_{-0.6}$	$54.7^{+0.3}_{-0.4}$	$25^{...}_{-14.2}$	9.5‡	$55.6^{+0.7}_{...}$	31.45	31.76	32.35	32.36	31.70	32.37	32.40	32.46
p1_553	053823.69−690503.4	1.37×10^{-7}	60	0.49	0.30∗	0.0∗	$0.63^{+0.2}_{-0.2}$	$55.1^{+0.3}_{-0.2}$	···	···	···	···	···	···	···	32.19	30.63	31.95	32.20
c7907	053844.55−690451.1	1.31×10^{-7}	49	0.87	0.63∗	$0.59^{+1.0}_{...}$	$0.38^{+0.2}_{-0.2}$	$55.8^{+1.2}_{-0.5}$	···	···	···	···	···	···	···	32.30	30.50	31.89	32.31
p1_718	053840.97−690556.0	1.22×10^{-7}	45	0.83	0.71∗	$0.27^{+0.6}_{...}$	$0.86^{+0.3}_{-0.3}$	$55.2^{+0.3}_{-0.3}$	···	···	···	···	···	···	···	32.12	31.12	31.83	32.16
p1_766	053841.80−690532.2	1.09×10^{-7}	31	1.02	0.62∗	$3.2^{+1.1}_{-2.0}$	$0.83^{+0.2}_{-0.2}$	$55.8^{+0.1}_{-0.2}$	···	···	···	···	···	···	···	31.66	31.55	31.82	31.91
p1_672	053838.76−690613.0	1.03×10^{-7}	29	1.20	0.87∗	$0.0^{...}_{...}$	$1.3^{...}_{...}$	$55.1^{...}_{...}$	···	···	···	···	···	···	···	31.98	31.34	31.76	32.07
p1_937	053843.29−690616.4	1.00×10^{-7}	39	1.07	0.75∗	0.0∗	$0.31^{+0.06}_{-0.05}$	$55.6^{+0.2}_{-0.2}$	···	···	···	···	···	···	···	32.43	29.83	31.74	32.43
cc5383	053844.97−690507.8	9.87×10^{-8}	20	0.76	0.50∗	$1.2^{+1.9}_{...}$	$1.3^{+1.9}_{-0.5}$	$55.2^{+0.4}_{-0.4}$	···	···	···	···	···	···	···	31.66	31.51	31.80	31.89
p1_1062	053846.26−690559.3	8.68×10^{-8}	32	1.45	0.79∗	$1.0^{+2.3}_{...}$	$0.44^{+0.5}_{...}$	$55.7^{...}_{-0.8}$	···	···	···	···	···	···	···	31.97	30.62	31.61	31.99

Table A1. (continued)

T-ReX Source					Spectral Fit							X-ray Luminosities							
Label	CXOU J	Photon Flux	NetCts	χ^2_ν	$N(H)^{\rm LMC}$	$N(H)^1$	kT^1	EM^1	$N(H)^2$	kT^2	EM^2	$L_{\rm X}^{1,t}$	$L_{\rm X}^{1,tc}$	$L_{\rm X}^{2,t}$	$L_{\rm X}^{2,tc}$	$L_{\rm X}^{sc}$	$L_{\rm X}^{hc}$	$L_{\rm X}^{t}$	$L_{\rm X}^{tc}$
		$\rm cm^{-2}\ s^{-1}$	count		$10^{22}\rm cm^{-2}$	$10^{22}\rm cm^{-2}$	keV	log $\rm cm^{-3}$	$10^{22}\rm cm^{-2}$	keV	log $\rm cm^{-3}$	log erg $\rm s^{-1}$							
c5984	053838.40−690418.2	8.67×10^{-8}	38	1.10	0.54∗	$0.012^{+2.8}$	3.2	$54.9^{+0.7}_{-0.2}$	···	···	···	···	···	···	···	31.70	31.70	31.88	32.00
c5572	053835.56−690606.5	8.67×10^{-8}	18	0.67	0.90∗	0.0∗	$0.88^{+0.3}_{-0.3}$	$55.0^{+0.2}_{-0.2}$	···	···	···	···	···	···	···	32.10	30.96	31.67	32.13
c5987	053838.51−690621.8	8.47×10^{-8}	28	1.02	0.79∗	0.0∗	$1.1^{+0.3}_{-0.2}$	$55.0^{+0.1}_{-0.2}$	···	···	···	···	···	···	···	31.99	31.11	31.70	32.04
c6213	053839.84−690609.4	8.31×10^{-8}	24	0.93	0.79∗	$0.66^{+0.9}$	$0.70^{+0.3}_{-0.3}$	$55.3^{+0.5}_{-0.4}$	···	···	···	···	···	···	···	31.99	30.96	31.67	32.02
c3084	053752.08−690439.5	7.96×10^{-8}	43	1.15	0.62∗	0.0∗	$0.63^{+0.2}_{-0.2}$	$55.2^{+0.2}_{-0.2}$	···	···	···	···	···	···	···	32.25	30.70	31.82	32.26
c6472	053840.92−690554.9	7.93×10^{-8}	22	0.82	0.90∗	0.0∗	$1.2^{+0.5}_{-0.4}$	$55.0^{+0.2}_{-0.2}$	···	···	···	···	···	···	···	31.93	31.18	31.66	32.00
p1_1021	053844.57−690512.4	7.89×10^{-8}	25	1.32	1.4∗	$0.84^{+1.0}_{-0.6}$	$1.0^{+0.4}_{-0.3}$	$55.3^{+0.2}_{-0.2}$	···	···	···	···	···	···	···	31.91	31.34	31.67	32.01
c10271	053910.87−690613.7	7.55×10^{-8}	31	1.12	0.79∗	0.0∗	$0.90^{+0.3}_{-0.3}$	$54.9^{+0.2}_{-0.2}$	···	···	···	···	···	···	···	31.97	30.87	31.60	32.00
cc4651	053839.59−690559.3	7.50×10^{-8}	42	1.09	0.90∗	0.0∗	$2.7^{+5.0}_{-1.1}$	$55.1^{+0.2}_{-0.2}$	···	···	···	···	···	···	···	31.83	31.76	31.92	32.10
c8320	053848.07−690442.4	7.32×10^{-8}	18	1.10	1.6∗	$1.6^{+4.2}$	$1.1^{+1.2}_{-0.6}$	$55.4^{+1.0}_{-0.4}$	···	···	···	···	···	···	···	31.68	31.46	31.64	31.88
c7031	053842.21−690832.5	7.19×10^{-8}	28	1.02	1.5∗	$2.2^{+3.9}$	$1.7^{}_{-1.0}$	$55.3^{+0.7}_{-0.6}$	···	···	···	···	···	···	···	31.45	31.75	31.82	31.93
c6170	053839.70−690608.6	7.10×10^{-8}	22	0.95	0.90∗	0.0∗	$1.2^{+0.5}_{-0.3}$	$55.0^{+0.2}_{-0.2}$	···	···	···	···	···	···	···	31.90	31.21	31.66	31.98
c7552	053843.42−690542.1	6.63×10^{-8}	27	1.04	0.67∗	$0.39^{+0.8}$	$0.92^{+1.0}_{-0.3}$	$54.9^{+0.2}_{-0.3}$	···	···	···	···	···	···	···	31.78	30.91	31.55	31.83
p1_1530	053939.79−690430.5	6.57×10^{-8}	27	0.99	0.46∗	$0.13^{+1.5}$	$0.72^{+0.3}$	$55.0^{+1.7}_{-0.3}$	···	···	···	···	···	···	···	31.97	30.67	31.70	32.00
c8591	053850.32−690538.3	6.16×10^{-8}	24	0.99	0.63∗	$0.085^{+0.4}$	$0.86^{+0.3}_{-0.3}$	$54.8^{+0.2}_{-0.2}$	···	···	···	···	···	···	···	31.85	30.74	31.54	31.88
c8052	053845.24−690546.3	6.15×10^{-8}	22	1.07	0.67∗	$0.93^{+1.6}$	$0.73^{+1.0}_{-0.4}$	$55.2^{+0.9}_{-0.5}$	···	···	···	···	···	···	···	31.72	30.86	31.51	31.77
c7254	053842.67−690635.9	6.02×10^{-8}	22	1.01	0.87∗	$1.3^{+1.7}$	$0.34^{+0.3}$	$56.0^{+0.6}_{-0.9}$	···	···	···	···	···	···	···	31.90	30.36	31.50	31.92
c8204	053846.82−690603.0	5.69×10^{-8}	25	1.21	0.85∗	$0.10^{+1.3}$	$0.58^{+0.3}$	$55.1^{+1.7}_{-0.4}$	···	···	···	···	···	···	···	32.09	30.50	31.56	32.11
c3981	053812.09−690634.0	5.57×10^{-8}	23	1.15	1.1∗	$1.8^{+3.6}_{-0.9}$	$0.39^{+0.3}$	$56.0^{+1.3}_{-0.9}$	···	···	···	···	···	···	···	31.77	30.63	31.43	31.80
c8180	053846.49−690428.0	5.32×10^{-8}	23	0.67	0.88∗	$1.5^{+0.9}_{-0.7}$	0.27‡	$56.4^{+0.3}_{-0.2}$	···	···	···	···	···	···	···	31.95	30.14	31.51	31.95
c5374	053834.08−690421.4	4.68×10^{-8}	21	0.97	0.57∗	$0.19^{+0.6}$	$0.79^{+0.4}_{-0.4}$	$54.7^{+0.2}_{-0.3}$	···	···	···	···	···	···	···	31.71	30.56	31.42	31.74
c7235[b]	053842.64−690536.7	4.64×10^{-8}	7	0.86	0.79∗	0.0∗	0.8∗	54.8	···	···	···	···	···	···	···	31.86	30.60	31.43	31.88
c7528	053843.37−690547.9	4.62×10^{-8}	22	0.90	0.56∗	$1.2^{+2.1}_{-1.0}$	$0.44^{+0.6}$	$55.5^{}_{-0.9}$	···	···	···	···	···	···	···	31.69	30.44	31.45	31.72
cc4601	053839.04−690659.0	4.61×10^{-8}	16	1.06	1.4∗	0.50	1.0	54.9	···	···	···	···	···	···	···	31.64	30.93	31.31	31.72
c6094	053839.32−690639.4	4.54×10^{-7}	13	1.07	1.7∗	$3.1^{+2.9}_{-1.6}$	$1.0^{+0.6}_{-0.3}$	$55.4^{+0.3}_{-0.3}$	···	···	···	···	···	···	···	31.39	31.42	31.54	31.71
c6164	053839.72−690623.7	4.40×10^{-8}	11	1.30	0.90∗	$0.0^{+5.1}$	$1.3^{+5.7}$	$54.7^{+0.3}_{-0.4}$	···	···	···	···	···	···	···	31.58	30.96	31.36	31.67
c5695	053836.31−690608.1	4.17×10^{-8}	13	0.68	0.67∗	$0.61^{+1.2}$	$0.66^{+0.4}_{-0.3}$	$55.0^{+0.4}_{-0.5}$	···	···	···	···	···	···	···	31.74	30.62	31.44	31.77
c10098	053907.21−690745.9	4.08×10^{-8}	18	0.93	0.82∗	$2.6^{+3.5}_{-1.6}$	0.27‡	$56.5^{+0.6}_{-7.0}$	···	···	···	···	···	···	···	31.57	30.23	31.31	31.59
c5200	053832.33−690523.6	3.55×10^{-8}	13	0.96	0.63∗	0.0∗	$0.32^{+0.8}$	$55.1^{+0.8}_{-0.8}$	···	···	···	···	···	···	···	32.00	29.46	31.41	32.00
c5633[b]	053835.94−690609.2	3.25×10^{-8}	12	0.80	1.4∗	0.097	0.80∗	54.9∗	···	···	···	···	···	···	···	31.91	30.72	31.31	31.94
cc7769[b]	053916.35−690120.4	2.51×10^{-8}	6	0.97	1.2∗	0.0∗	0.80∗	54.5	···	···	···	···	···	···	···	31.57	30.31	31.00	31.59
cc4200[b]	053834.76−690500.7	2.27×10^{-8}	8	1.18	0.15∗	0.0∗	0.80∗	54.2∗	···	···	···	···	···	···	···	31.27	30.02	31.16	31.29
cc4181[b]	053834.58−690605.7	2.16×10^{-8}	7	1.00	1.2∗	0.0∗	0.80∗	54.5	···	···	···	···	···	···	···	31.58	30.33	30.99	31.61
p1_1274[b]	053858.66−690752.3	1.23×10^{-8}	4	1.38	1.1∗	0.0∗	0.80∗	54.2∗	···	···	···	···	···	···	···	31.33	30.08	30.79	31.36
cc4294[b]	053835.68−690617.6	8.27×10^{-9}	3	1.19	0.87∗	0.0∗	0.80∗	53.9	···	···	···	···	···	···	···	30.95	29.69	30.49	30.97
cc5800[b]	053849.65−690855.2	6.50×10^{-9}	7	0.97	0.67∗	0.0∗	0.80∗	54.6	···	···	···	···	···	···	···	31.66	30.41	31.29	31.69
cc7873[b]	053918.60−690748.3	3.91×10^{-9}	1	0.90	1.5∗	0.0∗	0.80∗	53.9	···	···	···	···	···	···	···	31.01	29.76	30.35	31.04

b: For these sources, no reasonable fit could be obtained without assuming a plasma temperature.We chose a median value of 0.8 keV.

More significant digits are used for uncertainties <0.1 in order to avoid large rounding errors; for consistency, the same number of significant digits is used for both lower and upper uncertainties. Uncertainties are missing when XSPEC was unable to compute them or when their values were so large that the parameter is effectively unconstrained. Fits lacking uncertainties, fits with large uncertainties, and fits with frozen parameters should be viewed merely as splines to the data to obtain rough estimates of luminosities; the listed parameter values are not robust.

Table A2. Properties of early-type stars in the T-ReX point source catalogue for which spectroscopic observations are available. Bright X-ray variables are flagged with "var". Visual extinctions, A_V represent total extinctions, with an adopted Galactic foreground of A_V^{MW} = 0.22 mag. Catalogues include R (Feast et al. 1960), Sk (Sanduleak 1970), Mk (Melnick 1985), VFTS (Evans et al. 2011), MH (Malumuth & Heap 1994) HSH (Hunter et al. 1995), SMB (Selman et al. 1999), P (Parker 1993), ST (Schild & Testor 1992), CCE (Castro et al. 2018), BAT (Breysacher et al. 1999). Spectral type calibrations have been applied in some instances following Doran et al. (2013), noted with ":".

T-ReX Label	HD	R	Sk	Mk	VFTS	MH	HSH	SMB	P	ST	CCE	BAT	Spectral Type	Ref	A_V mag	Ref	log L_{Bol} $L_\odot$	Ref	log L_X erg s^{-1}	Var?	log L_X/L_{Bol}	kT_m keV	Hardness η_2	Nature	Ref
p1_995	···	···	···	34	···	880	8	17	1134	···	1766	116	WN5h+WN5h	1	2.0	1	6.70±0.1	1	35.31	var	–4.98±0.1	3.3	–0.05	SB2	1
p1_752	269919a	140a	···	···	507	···	···	···	6	877	···	3191	101–2	WC4+WN6+?	2	1.6	2	6.41±0.3:	2	35.38	var	–4.62±0.3:	1.4	–0.55	···	···
p1_610	···	···	···	···	399	···	···	···	···	···	···	···	···	O9 IIIn	3	1.7	4	4.81±0.04	5	34.97	var	–3.42±0.04	···	+0.65	SB1	4
p1_893	···	136c	···	···	1025	681	10	···	998	···	···	112	WN5h+?	6	2.7	7	6.75±0.15	6	34.39	var	–5.95±0.15	2.7	–0.09	SB?	8
p1_698	···	···	···	39	482	57	7	14	767	···	2003	99	O2.5 If*/WN6+O3	9, 10	1.7	7	6.4 ±0.1	7	34.28	var	–5.71±0.1	1.6	–0.28	SB2	10-12
p1_832	———	R136a-X1: see Table 1 for details	———												1.8	13	7.35±0.1	14	34.17	var	–6.76±0.1	0.93	–0.48	···	···
p1_979	···	···	···	33Sa	870	···	18	44	1120	···	2177		O3 III(f*)	11	1.3	11	5.95±0.2	15	33.62	var	–5.92±0.2	0.42	–0.41	Single	11
p1_830	···	139	···	···	527	···	···	2	952	···	···	107	O6.5 Iafc+O7 Iaf	3	1.6	16	6.49±0.06	17	33.62	var	–6.46±0.06	0.69	–0.66	SB2	17-18
p1_1000	···	···	···	33Na	···	887	16	33	1140	···	1943	···	OC2.5 If+O4 V	19	1.8	19	6.28±0.2	19	33.68	var	–6.18±0.2	1.4	–0.35	SB2	19
p1_1194	38282	144	–69° 246	···	···	···	···	···	9037	···	···	118	WN5-6h+WN6-7h	20	0.6	20	6.72±0.1	20	33.41	var	–6.89±0.1	1.4	+0.18	SB2	20
p1_296	269891	130	–69° 235	···	···	···	···	···	···	···	···	92	WN/C+B1 I	2	1.1	16	6.34±0.3	16	33.66	···	–6.27±0.3	6.3	+0.41	SB2	16
cc4970	———	R136a-X2: see Table 1 for details	———												1.8	13	6.79±0.1	14	33.38	var	–7.00±0.1	1.2	–0.15	···	···
p1_812	···	···	···	42	···	374	2	···	922	···	2102	105	O2 If	9	1.6	7	6.56±0.1	7	33.34	···	–6.81±0.1	0.86	–0.30	···	···
p1_1256	269928	145	–69° 248		695	···	···	···	1788	···	···	119	WN6h+O3.5 If/WN7	21	1.4	21	6.64±0.2	21	33.24	var	–6.81±0.2	0.86	–0.30	SB2	12,21
p1_1088	269926	146	–69° 245		617	···	···	···	9033	···	···	117	WN5ha	22	1.0	7	6.29±0.1	7	33.13	···	–6.75±0.1	0.92	–0.45	Single	23
p1_867	———	R136a-X3: see Table 1 for details	———												2.0	13	6.67±0.1	14	33.30	···	–6.96±0.1	1.07	–0.59	···	···
p1_754	269919b	140b	···	···	509	···	···	8	880	···	3174	103	WN5h+O4 V	16	0.9	16	6.25±0.2	16	33.22	var	–6.62±0.2	4.2	+0.14	SB2	12,16
c6981	———	R136a-X4: see Table 1 for details	———												1.5	13	5.82±0.3:	2,24	33.04	···	–6.37±0.3:	0.96	–0.52	SB2	24
p1_745	···	···	···	···	···	201	28	53	860	···	1912	···	O3 V	25	1.6	26	5.74±0.12	26	33.04	···	–6.29±0.12	0.78	–0.59	···	···
c7157	———	R136a-X5: see Table 1 for details	———												1.7	13	6.32±0.1	7	33.15	···	–6.76±0.1	2.6	–0.59	···	···
p1_1234	···	···	···	···	682	···	···	···	1732	···	···	···	WN5h	27	4.5	7	6.51±0.1	7	33.04	···	–7.06±0.1	2.0	+0.07	Single	27
p1_663	···	···	···	···	445	···	···	97	621	···	2981	···	O3–4 V+O4–7 V	3	1.9	7	5.80±0.15	26	32.95	···	–6.44±0.15	0.89	–0.40	SB2	3,18
p1_924	···	···	···	35	545	742	12	23	1029	···	1474	114	O2 If/WN5	9	1.6	7	6.30±0.1	7	32.71	···	–7.18±0.1	0.80	–0.58	···	···
c7182	———	R136a-X6: see Table 1 for details	———												1.9	13	6.45±0.1	14	33.21	···	–6.82±0.1	0.76	–0.73	···	···
p1_786	···	···	···	37Wb	1017	283	44	88	897	···	1374	104	O2 If/WN5	9	2.3	7	6.21±0.1	7	32.76	···	–7.04±0.1	1.0	–0.53	SB?	28
p1_911	···	···	···	30	542	728	15	24	1018	···	2999	113	O2 If/WN5	9	1.5	7	6.16±0.1	7	32.57	···	–7.18±0.1	0.86	–0.38	SB	12
p1_441	···	···	···	···	217	···	···	···	···	1–98	···	···	O4 V+O5 V	3	0.7	2	5.79±0.13	17	32.63	···	–6.74±0.13	0.50	–0.95	SB2	3,17
p1_480	···	···	···	···	267	···	···	···	···	···	···	···	O3 III-I(n)f*	3	1.2	7	5.96±0.1	7	32.68	···	–6.87±0.1	1.5	–0.58	SB1	3,18
c7257	———	R136a-X7: see Table 1 for details	———												2.1	13	6.09±0.2	14	32.88	···	–6.80±0.2	0.52	–0.94	···	···
p1_1186	···	···	···	4	664	···	···	65	1607	···	774	···	O7 II(f)	3	1.6	7	5.53±0.1	5	32.68	···	–6.44±0.1	2.4	–0.41	SB?	3
c5349	···	···	···	···	404	···	···	···	···	···	···	···	O3.5: V:+O5V:	3, 42	1.6	7	5.91±0.1	7	32.84	···	–6.65±0.1	0.91	–0.62	SB2	3,42
p1_795	···	···	···	···	1019	320	38	70	912	···	1608	···	O3 V+O6 V	24	1.9	2	6.09±0.3:	2	32.76	···	–6.92±0.3:	0.65	–0.90	SB2	24
c6974	···	···	···	···	522	···	82	134	921	···	3030	···	O6 II–Iab+O5.5 V	3	1.6	26	5.15±0.15	26	32.53	···	–6.21±0.15	1.0	–0.44	SB2	3,29
p1_611	···	135	···	···	402	···	···	12	355	···	···	95	WN5:+WN7	16	1.0	16	6.20±0.1	16	32.99	···	–6.79±0.1	9.3	+0.87	SB2	12,16
p1_749	···	···	···	25	506	···	···	19	871	···	2395	···	ON2 V	3	1.4	7	6.43±0.2	30	32.79	···	–7.23±0.2	0.70	–0.85	SB1	3

Table A2. continued

T-ReX Label	HD	R	Sk	Mk	VFTS	MH	HSH	SMB	P	ST	CCE	BAT	Spectral Type	Ref	A_V mag	Ref	log L_{Bol} $L_\odot$	Ref	log L_X erg s^{-1}	Var?	log L_X/L_{Bol}	kT_m keV	Hardness η_2	Nature	Ref
p1_722	···	···	···	···	500	···	···	···	···	···	···	···	O6.5 IV+O6.5 V	3	0.8	2	5.55±0.07	17	32.36	···	–6.78±0.07	1.1	–0.54	SB2	3,17
c10289	38344	147	–69° 251	···	758	···	···	···	···	···	···	122	WN5h	22	1.6	7	6.36±0.1	7	32.58	···	–7.37±0.1	3.3	+0.67	Single	23
p1_955	···	···	···	···	1031	815	25	39	1080	···	2186	···	O3 V	25	1.1	2	5.98±0.3:	2	32.46	···	–7.11±0.3:	0.97	–0.82	SB2	18,28
c893	···	···	···	···	16	···	···	···	···	···	···	···	O2 III-If*	3	1.2	7	6.12±0.1	5	32.59	···	–7.11±0.1	0.97	–0.82	Single	3
c7131	···	···	···	37	1022	493	14	28	949	···	1442	···	O3.5 If/WN7	9	2.5	7	6.48±0.1	7	32.38	···	–7.69±0.1	0.55	–0.65	Single	28
p1_1033	···	···	···	···	···	926	43	83	1195	···	2112	···	O3 V	25	1.8	26	5.66±0.07	26	32.29	···	–6.96±0.25	1.0	–0.47	···	···
p1_1035	···	···	···	···	···	···	···	116	1222	···	3180	···	O3–6 V	31	1.6	26	5.06±0.05	26	32.41	···	–6.24±0.25	3.8	+0.07	···	···
c7452	——— R136: see Table 1 for details ———														2.2	13	5.91±0.2	14	32.67	···	–6.82±0.2	4.4	–0.15	···	···
c7018	——— R136a-X8: see Table 1 for details ———														1.7	13	5.48±0.2	14	32.27	···	–6.80±0.2	0.89	–0.48	Single?	14
c6701	···	···	···	···	1014	203	29	56	863	···	1956:	···	O3 V+	25	2.4	7	6.22±0.2	7	32.80	···	–7.01±0.2	0.35	–1.00	Single	18
p1_987	···	···	···	32	1034	878	13	21	1130	···	3043	···	O7.5 II	31	1.4	26	5.78±0.10	26	32.35	···	–7.02±0.25	0.79	–0.82	Single	28
c6062	···	···	···	49	···	···	···	30	691	···	1261	98	WN6(h)	32	1.4	2	6.7 ±0.2	33	32.41	···	–7.88±0.2	4.1	+0.79	Single	12
c4876	···	···	···	···	352	···	···	···	···	···	···	···	O4.5 Vz:+O5.5 Vz:	3	0.8	2	5.38±0.04	17	32.17	···	–6.79±0.04	0.96	–0.82	SB2	3,17-18
p1_682	···	···	···	36	468	17	···	86	706	···	1749	···	O2 V((f*))+?	3	2.2	7	6.17±0.2	30	32.70	···	–7.06±0.2	0.59	–0.95	Single	3
cc4968	——— R136a-X9: see Table 1 for details ———														1.5	13	5.15±0.2	14	32.25	···	–6.49±0.2	1.8	–0.35	Single	14
p1_760	···	···	···	···	512	···	···	68	885	···	1199	···	O2 V–III	3	1.9	7	6.04±0.2	7	32.32	···	–7.31±0.2	1.1	–0.75	SB1	3
p1_866	···	···	···	···	···	620	54	109	978	···	1963	···	O4:	26	2.6	26	5.96±0.11	26	32.22	···	–7.33±0.11	0.83	–0.56	···	···
c8160	···	···	···	13	599	···	···	40	1311	···	1433	···	O3 III(f*)	3	1.4	7	6.01±0.10	5	32.37	···	–7.23±0.10	0.44	–0.95	SB1	3
p1_637	···	···	···	53	427	···	···	51	···	···	389	96	WN8(h)	22	2.2	7	6.13±0.1	7	32.45	···	–7.27±0.1	7.2	+0.23	Single	12
c6030	···	···	···	51	457	···	···	50	666	···	603	97	O3.5 If/WN7	9	2.3	7	6.2 ±0.1	7	32.16	···	–7.63±0.1	1.1	–0.24	Single	12
c7410	···	···	···	35N	1026	716	41	76	1013	···	1494	···	O3 III+	25	1.9	7	5.83±0.2	7	32.32	···	–7.10±0.2	0.71	–0.83	Single	28
p1_695	···	···	···	···	···	53	63	105	761	···	2077	···	O3–6 V	31	2.2	26	5.87±0.15	26	32.27	···	–7.19±0.15	1.6	–0.45	···	···
c6973	···	···	···	37Wa	1021	339	11	25	917	···	1349	···	O4 If$^+$	25	2.2	7	6.34±0.1	7	32.26	···	–7.67±0.1	0.49	–0.86	Single	28
c6443	···	···	···	28a	···	···	···	80	805	···	2447	···	O5–6 V	34	1.8	26	5.53±0.05	26	32.34	···	–6.78±0.05	1.0	–0.79	SB?	35
c8112	···	···	···	12	591	···	···	11	1257	···	1279	···	B0.2 Ia	36	1.8	26	5.91±0.15	37	32.28	···	–7.22±0.15	0.76	–0.86	SB:	36,38
c7859	···	···	···	26	562	···	···	32	1150	···	2819	···	O4 V	39	1.6	7	6.05±0.2	7	31.97	···	–7.67±0.2	0.33	–0.64	···	···
c6370	···	134	···	···	1001	71	···	···	786	···	1978	100	WN6(h)	32	1.5	7	6.2 ±0.1	7	32.46	···	–7.33±0.1	8.6	+0.64	Single	12
p1_553	···	133	···	···	333	···	···	···	42	···	···	···	O9 II+O9.2 V	3,42	0.8	7	5.88±0.1	5	32.20	···	–7.27±0.1	0.63	–0.95	SB2	3,42
c7907	···	···	···	23	566	···	···	42	1163	···	···	···	O3 III(f*)	3	1.3	7	5.83±0.1	5	32.31	···	–7.11±0.1	0.38	–0.96	Single	3
p1_718	···	···	···	···	···	108	51	89	812	···	···	···	O3 V	25	1.5	2	5.71±0.3:	2	32.16	···	–7.14±0.3:	0.86	–0.82	···	···
p1_766	···.	···	···	···	513	···	···	266	···	···	2799	···	O6–7 II	3	1.3	2	5.00±0.1	5	31.91	···	–6.68±0.1	0.83	–0.13	Single	3
p1_672	···	···	···	···	455	···	···	108	661	···	1572	···	O5:V	3	1.7	7	5.63±0.2	7	32.07	···	–7.15±0.2	1.3	–0.63	SB1	3
p1_937	···	···	···	35Sa	1028	749	23	37	1036	···	1423	···	O3 III(f*)	25	1.5	7	6.09±0.2	7	32.43	···	–7.25±0.2	0.31	–1.00	Single	28
cc5383	···	···	···	···	579	···	···	171	1201	···	3116	···	O9:((n))	3	1.1	2	5.46±0.02	5	31.89	···	–7.16±0.02	1.3	–0.17	SB?	3
p1_1062	···	···	···	14N	601	986	···	91	1317	···	1890	···	O5–6 V	3	1.6	30	5.55±0.18	30	31.99	···	–7.15±0.18	0.44	–0.91	Single	3

Table A2. (continued)

T-ReX Label	HD	R	Sk	Mk	VFTS	MH	HSH	SMB	P	ST	CCE	BAT	Spectral Type	Ref	A_V mag	Ref	log L_{Bol} $L_\odot$	Ref	log L_X erg s^{-1}	Var?	log L_X/L_{Bol}	kT_m keV	Hardness η_2	Nature	Ref
c5984	···	···	···	···	···	···	···	···	649	···	···	···	O8–9 V	34	1.2	2	5.00±0.3:	2	32.00	···	–6.59±0.3:	3.2	+0.00	···	···
c5572	···	···	···	···	416	···	···	93	467	···	1700	···	O8.5 V	29	1.8	26	5.66±0.05	26	32.13	···	–7.12±0.05	0.88	–0.87	···	···
c5987	···	···	···	50	450	···	···	34	643	···	1293	···	O9.7 III:+O7::	3	1.6	26	5.69±0.1	17	32.04	···	–7.23±0.1	1.1	–0.77	SB2	3,17
c6213	···	···	···	···	···	···	···	151	743	···	1523	···	O6:	26	1.6	26	5.00±0.29	26	32.02	···	–6.57±0.29	0.70	–0.85	EB	40
c3084	···	···	···	···	186	···	···	···	···	···	···	···	B1 IV	36	1.3	26	4.45±0.3:	2	32.26	···	–5.78±0.3:	0.63	–0.95	Single	36
c6472	···	···	···	···	···	116	95	155	···	···	1920	···	O4:	26	1.8	26	6.00±0.15	26	32.00	···	–7.59±0.15	1.2	–0.70	···	···
p1_1021	···	···	···	···	564	···	···	253	···	···	3200	···	O6–8 V	3	2.6	30	5.33±0.13	30	32.01	···	–6.91±0.13	1.0	–0.58	Single	3
c10271	···	···	···	···	755	···	···	···	2041	···	···	···	O3 Vn((f*))	3	1.6	7	5.65±0.2	30	32.00	···	–7.24±0.2	0.90	–0.86	Single	3
cc4651	···	···	···	···	···	25	157	255	···	···	1858	···	O7:	26	1.8	26	4.79±0.06	26	32.10	···	–6.28±0.06	2.7	–0.08	···	···
c8320	···	···	···	···	621	···	···	···	1429	···	···	···	O2 V((f)*)z	3	3.0	7	6.22±0.2	30	31.88	···	–7.93±0.2	1.1	–0.25	V. Comp	3
c7031	···	···	···	···	526	···	···	···	925	···	···	···	O8.5 I(n)fp+?	3	2.9	2	5.71±0.3:	2	31.93	···	–7.37±0.3:	1.7	+0.33	SB1	3
c6170	···	···	···	···	···	28	138	144	729	···	1535	···	O6–7	24	1.8	26	5.34±0.07	26	31.98	···	–6.95±0.07	1.2	–0.66	···	···
c7552	···	···	···	···	1030	···	···	335	1043	···	···	···.	O9 V	41	1.4	2	4.56±0.3:	2	31.83	···	–6.32±0.3:	0.92	–0.77	···	···
p1_1530	···	···	···	···	830	···	···	···	2270	···	···	···	O5–6 V	3	1.0	2	5.05±0.3:	2	32.00	···	–6.64±0.3:	0.72	–0.89	SB	3
c8591	···	···	···	8	648	···	···	58	1531	···	2780	···	O5.5 IV(f)	3	1.3	30	5.66±0.13	30	31.88	···	–7.37±0.13	0.86	–0.86	SB	3
c8052	···	···	···	···	585	943	···	31	1231	···	2193	···	O7 V(n)	3	1.4	26	5.61±0.25	26	31.77	···	–7.43±0.25	0.73	–0.77	SB1	3
c7254	···	···	···	···	532	···	···	104	974	···	963	···	O3.5: V(n)+B III-I	3,42	1.8	7	5.74±0.2	7	31.92	···	–7.41±0.2	0.34	–0.93	SB2	3,42
c8204	···	···	···	14	608	999	···	64	1350	···	1827	···	O4 III(f)	3	1.7	7	5.86±0.1	7	32.11	···	–7.34±0.1	0.58	–0.93	SB1	3
c3981	···	···	···	···	259	···	···	···	···	···	···	···	O6 Iaf	3	2.1	7	6.1 ±0.1	7	31.80	···	–7.89±0.1	0.39	–0.87	SB1	3
c8180	···	···	···	10	603	···	···	···	1341	···	···	···	O4 III:+OB:	3,42	1.8	7	5.98±0.1	7	31.95	···	–7.62±0.1	0.27	–0.98	SB2	3,42
c5374	···	···	···	55	406	···	···	···	370	···	···	···	O6 Vnn	3	1.2	7	5.48±0.2	7	31.74	···	–7.33±0.2	0.79	–0.87	Single	3
c7235	···	···	···	···	···	···	···	71	975	···	2748	···	O6–7 V	34	1.6	26	5.58±0.25	26	31.88	···	–7.29±0.25	···	···	Single	35
c7528	···	···	···	···	1029	764	56	87	1042	···	2128	···	O3.5 I+OB	41	1.2	26	5.59±0.3:	2	31.72	···	–7.46±0.3:	0.44	–0.88	SB?	28
cc4601	···	···	···	···	460	···	···	278	674	···	290	···	O7.5 V+O7.5 V	3	2.6	26	5.37±0.05	26	31.72	···	–7.24±0.05	1.0	–0.67	SB2	3,35
c6094	···	···	···	···	465	···	···	365	700	···	830	···	On	3	3.2	26	5.57±0.10	5	31.71	···	–7.45±0.10	1.0	+0.03	Single	3
c6164	···	···	···	···	···	···	···	75	724	···	1274	···	O7 III	34	1.8	26	5.74±0.25	26	31.67	···	–7.66±0.25	1.3	–0.62	···	···
c5695	···	···	···	···	···	···	···	82	···	···	1632	···	O8:	26	1.4	26	5.17±0.05	26	31.77	···	–6.99±0.05	0.66	–0.86	···	···
c10098	···	···	···	···	746	···	···	···	···	···	···	···	O6 Vnn	3	1.7	30	5.29±0.24	30	31.59	···	–7.29±0.24	0.27	–0.91	Single	3
c5200	···	···	···	···	385	···	···	84	288	···	2451	···	O4–5 V	3	1.3	30	5.55±0.29	30	32.00	···	–7.14±0.29	0.32	–1.00	SB	3
c5633	···	···	···	54	420	···	···	16	488	···	1689	···	B0.5 Ia	36	2.6	26	5.84±0.15	37	31.94	···	–7.49±0.15	···	···	Single	36
cc7769	···	···	···	···	768	···	···	···	···	···	···	···	O8 Vn	3	2.3	30	5.09±0.22	30	31.59	···	–7.09±0.22	···	···	SB2?	3
cc4200	···	···	···	···	411	···	···	409	···	···	···	···	B1–3 V–III	36	0.5	2	3.57±0.4:	2	31.29	···	–5.87±0.4:	···	···	Single	36
cc4181	···	···	···	···	410	···	···	288	409	···	1864	···	O7–8 V	3	2.4	30	5.14±0.13	30	31.61	···	–7.12±0.13	···	···	V. Comp	3
p1_1274	···	···	···	···	703	···	···	···	1828	···	···	···	O7: V+O8: V	3	2.1	2	4.76±0.3:	2	31.36	···	–6.99±0.3:	···	···	SB2	3
cc4294	···	···	···	···	417	···	···	204	···	···	1399	···	B2 Ib	36	1.7	2	4.51±0.15	37	30.97	···	–7.13±0.15	···	···	Single	36
cc5800	···	···	···	···	640	···	···	···	1489	···	···	···	B2 V	36	1.4	2	4.03±0.3:	2	31.69	···	–5.93±0.3:	···	···	Single	36
cc7873	···	···	···	···	774	···	···	···	···	···	···	···	O7.5 IVp+O9.5:V	3	2.8	2	4.97±0.3:	2	31.04	···	–7.52±0.3:	···	···	SB2	3

1: Tehrani et al. (2019) 2: Doran et al. (2013) 3: Walborn et al. (2014) 4: Clark et al. (2015) 5: Ramírez-Agudelo et al. (2017) 6: Crowther et al. (2010) 7: Bestenlehner et al. (2014) 8: Schnurr et al. (2009) 9: Crowther & Walborn (2011) 10: A.M.T. Pollock et al. (in prep) 11: Massey et al. (2005) 12: Schnurr et al. (2008) 13: Crowther et al. (2016) 14: Bestenlehner et al. (2020) 15: Rivero González et al. (2012) 16: Shenar et al. (2019) 17: Mahy et al. (2020) 18: Almeida et al. (2017) 19: Bestenlehner et al. (2022) 20: Shenar et al. (2021) 21: Shenar et al. (2017) 22: Evans et al. (2011) 23: Foellmi et al. (2003) 24: Massey et al. (2002) 25: Massey & Hunter (1998) 26: Castro et al. (2021) 27: Bestenlehner et al. (2011) 28: Hénault-Brunet et al. (2012) 29: Massey et al. (2012) 30: Sabín-Sanjulián et al. (2017) 31: Walborn & Blades (1997) 32: Crowther & Smith (1997) 33: Hainich et al. (2014) 34: Bosch et al. (1999) 35: Bosch et al. (2009) 36: Evans et al. (2015) 37: McEvoy et al. (2015) 38 :Villaseñor et al. (2021) 39: Melnick (1985) 40: Graczyk et al. (2011) 41: D.J. Lennon (priv. comm.), 42: T. Shenar et al. submitted

APPENDIX B: LMC BASELINE ABUNDANCES

Table B1. LMC abundances (X/H by number) adopted for XSPEC fitting with respect to $Z_\odot$ from Asplund et al. (2009, AGS09). Values shown in parentheses are excluded from the average, due to issues with enhancements owing to mixing (e.g. N), depletion on dust grains (Fe) or other concerns. 0.5 $Z_\odot$ is adopted for Co

Element	SNR	——— H II regions ———				—— B stars ——			— F supergiants —		<LMC>		Solar	<LMC>
	D19	G99	P03/SCT17	T03	L08	K00/K05	T07/H07	D18	HAS95	A01	X/H	logX/H+12	AGS09	$Z_\odot$
He	···	···	8.5×10^{-2}	···	···	8.1×10^{-2}	···	···	···	···	8.3×10^{-2}	10.92	8.5×10^{-2}	1.0
C	1.2×10^{-4}	7.9×10^{-5}	1.0×10^{-4}	···	···	9.5×10^{-5}	···	···	1.2×10^{-4}	8.9×10^{-5}	1.0×10^{-4}	8.01	2.7×10^{-4}	0.38
N	(1.6×10^{-5})	7.9×10^{-6}	1.6×10^{-5}	···	···	1.0×10^{-5}	7.9×10^{-6}	···	···	···	1.1×10^{-5}	7.03	6.8×10^{-5}	0.16
O	2.2×10^{-4}	2.5×10^{-5}	3.2×10^{-4}	2.2×10^{-4}	···	2.5×10^{-4}	2.3×10^{-4}	···	(2.8×10^{-4})	(3.2×10^{-4})	2.5×10^{-4}	8.40	4.9×10^{-4}	0.51
Ne	4.0×10^{-5}	4.0×10^{-5}	6.8×10^{-5}	4.6×10^{-5}	5.8×10^{-5}	···	···	···	···	···	5.0×10^{-5}	7.70	8.5×10^{-5}	0.59
Na	···	···	···	···	···	···	···	···	1.5×10^{-6}	7.9×10^{-7}	1.2×10^{-6}	6.1	1.7×10^{-6}	0.7
Mg	1.5×10^{-5}	···	···	···	···	1.4×10^{-5}	1.2×10^{-5}	1.0×10^{-5}	1.6×10^{-5}	···	1.3×10^{-5}	7.13	4.0×10^{-5}	0.34
Al	···	···	···	···	···	7.2×10^{-7}	···	···	2.2×10^{-6}	···	1.5×10^{-6}	6.2	2.8×10^{-6}	0.5
Si	1.3×10^{-5}	5.0×10^{-6}	···	···	···	1.2×10^{-5}	1.6×10^{-5}	···	(3.7×10^{-5})	···	1.1×10^{-5}	7.06	3.2×10^{-5}	0.35
S	9.5×10^{-6}	5.0×10^{-6}	9.8×10^{-6}	5.9×10^{-6}	5.9×10^{-6}	···	···	···	9.9×10^{-6}	···	7.7×10^{-6}	6.88	1.3×10^{-5}	0.58
Cl	9.1×10^{-8}	···	6.6×10^{-8}	···	···	···	···	···	···	···	7.9×10^{-8}	4.9	3.2×10^{-7}	0.2
Ar	6.2×10^{-7}	1.6×10^{-6}	1.8×10^{-6}	1.4×10^{-6}	2.1×10^{-6}	···	···	···	···	···	1.5×10^{-6}	6.2	2.5×10^{-6}	0.6
Ca	1.0×10^{-6}	···	···	···	···	···	···	···	1.6×10^{-6}	···	1.3×10^{-6}	6.1	2.2×10^{-6}	0.6
Cr	2.2×10^{-7}	···	···	···	···	···	···	···	2.6×10^{-7}	···	2.4×10^{-7}	5.4	4.4×10^{-7}	0.6
Fe	2.1×10^{-5}	···	(2.5×10^{-6})	···	(1.7×10^{-6})	1.2×10^{-5}	1.7×10^{-5}	···	1.7×10^{-5}	···	1.7×10^{-5}	7.23	3.2×10^{-5}	0.54
Ni	7.9×10^{-7}	···	···	···	···	···	···	···	9.2×10^{-7}	···	8.6×10^{-7}	5.9	1.7×10^{-6}	0.5

HAS95: Hill et al. (1995); G99: Garnett (1999); K00: Korn et al. (2000) (He/Al/Fe only); K05: ; (excl He/Al/Fe) A01: Andrievsky et al. (2001); P03: **?** (excl. C/O);T03: Tsamis et al. (2003); T07: Trundle et al. (2007); H07: Hunter et al. (2007); L08: Lebouteiller et al. (2008); SCT17: Toribio San Cipriano et al. (2017) (C/O recomb lines for 30 Dor); D18: Dufton et al. (2018); D19: Dopita et al. (2019)

Table S1. Upper limits to observed X-ray luminosities L_X^t for luminous ($\log L/L_\odot \geq 5$) early-type stars excluded from the T-ReX point source catalogue, in RA order. Conversions from photon flux to attenuated luminosity are obtained from early-type stars in the T-ReX PSC, namely $\log L_X^t = \log(\text{PhotonFlux/cm}^{-2}\,\text{s}^{-1}) + (38.81\pm0.16)$. Spectral type calibrations have been applied in some instances following Doran et al. (2013), noted with ":". Limits on intrinsic X-ray luminosities are estimated from average attenuation corrections of 0.31±0.17 dex. Catalogues include R (Feast et al. 1960), Sk (Sanduleak 1970), BI (Brunet et al. 1975), Mk (Melnick 1985), VFTS (Evans et al. 2011), MH (Malumuth & Heap 1994), HSH (Hunter et al. 1995), SMB (Selman et al. 1999), P (Parker 1993), ST (Schild & Testor 1992), CCE (Castro et al. 2018), BAT (Breysacher et al. 1999). T-ReX PSC sources in close proximity (~1-2″) to the star ‡.

RA h m s	Dec deg m s	R	Sk	BI	Mk	VFTS	MH	HSH	SMB	P	ST	CCE	BAT	Spect. Type	Ref	$\log L_{Bol}/L_\odot$	Ref	Photon Flux cm^{-2} s^{-1}	$\log L_X^t$ erg s^{-1}	$\log L_X^{tc}/L_{Bol}$	Nature	Ref	PSC source‡
05 36 55.24	–69 11 37.6	···	–69° 224	···	···	3	···	···	···	···	···	···	···	B1 Ia+	1	6.03±0.10	2-3	Variable background (survey field edge)			···	···	···
05 37 07.51	–69 05 06.9	···	···	···	···	14	···	···	···	···	···	···	···	O8.5 Vz	4	5.16±0.16	3,5	$<2.41\times10^{-7}$	<32.19	<–6.25±0.28	SB	4	···
05 37 11.48	–69 07 38.2	···	···	···	···	19	···	···	···	···	···	···	86	WN3(h)	6	5.33±0.20	7	$<2.47\times10^{-7}$	<32.20	<–6.40±0.30	Single	8	···
05 37 17.85	–69 09 46.2	···	···	250	···	28	···	···	···	···	···	···	···	B0.7 Ia Nwk	1	5.76±0.10	2-3	$<2.50\times10^{-7}$	<32.21	<–6.83±0.25	···	···	···
05 37 24.64	–69 09 52.9	···	···	···	···	39	···	···	···	···	1–01	···	···	B0:e	1	5.28±0.3:	6	$<2.50\times10^{-7}$	<32.21	<–6.35±0.38	···	···	···
05 37 26.18	–69 08 56.5	···	···	···	···	45	···	···	···	···	1–04	···	···	O9.7 Ib–II Nwk	4	5.24±0.15	2	$<1.99\times10^{-7}$	<32.11	<–6.41±0.27	SB1	4	···
05 37 26.18	–69 09 53.0	···	···	···	···	46	···	···	···	···	1–05	···	···	O9.7 II((n))	4	5.09±0.1	3,9	$<2.31\times10^{-7}$	<32.17	<–6.19±0.25	SB?	4	···
05 37 27.82	–69 08 02.8	···	···	···	···	51	···	···	···	···	1–06	···	···	OBpe	4	5.03±0.13	9	$<1.93\times10^{-7}$	<32.10	<–6.21±0.26	···	···	···
05 37 29.15	–69 08 41.4	···	···	···	···	56	···	···	···	···	1–07	···	···	O6.5 V+O6.5 V	4	5.09±0.3:	6	$<1.68\times10^{-7}$	<32.03	<–6.33±0.38	SB2	4	···
05 37 30.09	–69 09 50.9	···	···	···	···	58	···	···	···	···	1–09	···	···	O8.5: V+B	4	5.02±0.3:	6	$<2.31\times10^{-7}$	<32.17	<–6.12±0.38	SB2	4	···
05 37 30.75	–69 05 17.5	···	···	···	···	61	···	···	···	···	···	···	···	O8.5 III:+O9.7 V:	4	5.06±0.05	10	$<1.59\times10^{-7}$	<32.01	<–6.33±0.24	SB2	10	···
05 37 30.87	–69 11 48.5	···	···	···	···	63	···	···	···	···	1–11	···	···	O5 III(n)(fc)+	4	5.74±0.08	10	$<2.80\times10^{-7}$	<32.26	<–6.76±0.24	SB2	4	c1186
05 37 30.92	–69 11 07.0	···	···	···	···	64	···	···	···	···	1–12	···	···	O8 II(f)+O6 V+O6 V	4,37	5.74±0.03	9	$<2.46\times10^{-7}$	<32.20	<–6.82±0.23	SB2	4,37	···
05 37 33.02	–69 08 35.8	···	···	···	···	···	···	···	···	···	1–15	···	···	O4 III	11	5.41±0.3:	6	$<1.67\times10^{-7}$	<32.04	<–6.65±0.38	···	···	···
05 37 33.57	–69 11 12.5	···	···	···	···	···	···	···	···	···	1–18	···	···	O5 V((f))	11	5.29±0.3:	6	$<2.46\times10^{-7}$	<32.20	<–6.37±0.38	···	···	···
05 37 33.75	–69 08 13.2	···	···	···	···	69	···	···	···	···	1–17	···	···	B0.7 Ib–Iab	1	5.59±0.10	2-3	$<1.53\times10^{-7}$	<31.99	<–6.87±0.25	···	···	c1216
05 37 34.46	–69 01 10.2	···	···	253	···	72	···	···	···	···	···	···	···	O2 V–III(n)((f*))	4	6.07±0.13	3,5	$<2.37\times10^{-7}$	<32.18	<–7.16±0.26	···	···	c1245
05 37 34.80	–69 08 01.3	···	···	···	···	76	···	···	···	···	1–21	···	···	O9.2 III	4	5.10±0.1	3,9	$<1.53\times10^{-7}$	<31.99	<–6.38±0.25	···	···	···
05 37 35.73	–69 08 40.0	···	···	···	···	79	···	···	···	···	···	···	88	WN4b/CE	8	5.80±0.20	3,7	$<1.46\times10^{-7}$	<31.97	<–7.10±0.30	Single	8	···
05 37 36.08	–69 06 44.9	···	···	···	···	82	···	···	···	···	···	···	···	B0.5 Ib–Iab	4	5.26±0.10	2-3	$<1.23\times10^{-7}$	<31.90	<–6.64±0.25	···	···	···
05 37 36.54	–69 10 32.5	···	···	···	···	86	···	···	···	···	1–24	···	···	O9.5 III+O8 IV:	4,37	5.31±0.3:	6	Variable background (N157B SNR)			SB2	4,37	···
05 37 36.66	–69 07 31.9	···	···	···	···	87	···	···	···	···	···	···	···	O9.7 Ib-II	4	5.29±0.1	3,9	$<1.46\times10^{-7}$	<31.97	<–6.59±0.25	SB	4	···
05 37 36.87	–69 08 22.8	···	···	···	···	89	···	···	···	···	1–25	···	···	O6.5 V((f))z Nstr	4	5.09±0.18	3,5	$<1.46\times10^{-7}$	<31.97	<–6.39±0.29	···	···	···
05 37 37.81	–69 05 45.5	···	···	···	···	93	···	···	···	···	···	···	···	O8.5 V+B0.2: V	4,37	5.02±0.03	9	$<1.26\times10^{-7}$	<31.91	<–6.39±0.23	SB2	4,37	···
05 37 37.91	–69 10 14.8	···	···	···	···	94	···	···	···	···	1–28	···	···	O3.5 Inf*p+O6:	4	5.68±0.11	10	Variable background (N157B SNR)			SB2	4,10	···
05 37 38.51	–69 10 19.9	···	···	···	···	96	···	···	···	···	1–29	···	···	O6 V((n))((fc))z	4	5.67±0.26	5	Variable background (N157B SNR)			SB	4	···
05 37 38.80	–69 08 08.5	···	···	···	···	98	···	···	···	···	1–30	···	···	O9 III(n)	4	5.11±0.3:	6	$<1.43\times10^{-7}$	<31.97	<–6.42±0.38	SB1	4	···
05 37 39.23	–69 09 51.0	···	···	···	···	102	···	···	···	···	1–32	···	···	O9: Vnnne+	4	5.37±0.10	3	Variable background (N157B SNR)			···	···	···
05 37 39.25	–69 11 34.3	···	···	···	···	103	···	···	···	···	···	···	···	O8.5 III((f))	4	5.21±0.1	3,9	$<2.19\times10^{-7}$	<32.15	<–6.34±0.25	···	···	···
05 37 39.44	–69 10 49.9	···	···	···	···	···	···	···	···	···	1–34	···	···	O7 V	11	5.09±0.3:	6	Variable background (N157B SNR)			···	···	···
05 37 40.25	–69 10 46.3	···	···	···	···	105	···	···	···	···	1–37	···	···	O8: Vz+O9–B0	4	5.06±0.3:	6	Variable background (N157B SNR)			EB, SB2	4,12	···
05 37 40.50	–69 07 57.7	···	–69° 233	···	···	108	···	···	···	···	···	···	89	WN7h	13	5.70±0.1	3,14	$<1.41\times10^{-7}$	<31.96	<–7.02±0.25	Single	15	···
05 37 40.87	–69 10 48.4	···	···	···	···	110	···	···	···	···	1–40	···	···	O6 V((n))z	4	5.40±0.20	5	Variable background (N157B SNR)			···	···	···
05 37 41.47	–69 10 47.0	···	···	···	···	117	···	···	···	···	···	···	···	O6: Vz	4	5.02±0.26	5	Variable background (N157B SNR)			SB?	4	···
05 37 41.96	–69 08 33.5	···	···	···	···	120	···	···	···	···	1–43	···	···	O9.2 IV+B+O+O	4,37	5.08±0.3:	6	$<1.46\times10^{-7}$	<31.97	<–6.38±0.38	EB, 2×SB2	4,37	···
05 37 42.95	–69 10 35.1	···	···	···	···	125	···	···	···	···	1–47	···	···	Ope	4	5.90±0.19	3,9	Variable background (N157B SNR)			SB2?	4	···
05 37 43.68	–69 10 50.5	···	···	···	···	130	···	···	···	···	···	···	···	O8.5 V((n))	4	5.06±0.12	3,5	Variable background (N157B SNR)			···	···	···
05 37 44.63	–69 14 25.7	···	–69° 234	···	···	136	···	···	···	···	···	···	90	WC4	17	5.44±0.2	18	Variable background (survey field edge)			Single	19	···
05 37 45.25	–69 10 13.7	···	···	···	···	140	···	···	···	···	1–56	···	···	O7.5 +O7.5 V	10	5.05±0.06	10	Variable background (N157B SNR)			SB2	4,10	···
05 37 45.91	–69 11 09.3	···	···	···	···	143	···	···	···	···	1–60	···	···	O3.5 V((fc))	4	5.53±0.3:	6	Variable background (N157B SNR)			SB1	4	···

Table S1. (continued)

RA h m s	Dec deg m s	R	Sk	BI	Mk	VFTS	MH	HSH	SMB	P	ST	CCE	BAT	Spect. Type	Ref	log L_{Bol} $L_\odot$	Ref	Photon Flux cm^{-2} s^{-1}	log L_X^t erg s^{-1}	log L_X^{tc}/L_{Bol}	Nature	Ref	PSC source‡
05 37 46.08	–69 09 08.8	···	···	···	···	145	···	···	···	···	···	···	···	O8fp	4	5.63±0.03	10	Variable background (N157B SNR)			SB1	4	···
05 37 46.19	–69 09 10.4	···	···	···	···	147	···	···	···	···	···	···	91	WN6(h)	20	5.83±0.2	14	Variable background (N157B SNR)			Single	15	···
05 37 46.41	–69 09 12.1	···	···	···	···	150	···	···	···	···	···	···	···	O9.5 III	4	5.02±0.3:	6	Variable background (N157B SNR)			SB2	4	···
05 37 46.52	–69 09 08.8	···	···	···	···	151	···	···	···	···	···	···	···	O6.5 II(f)p	4	5.87±0.02	9	Variable background (N157B SNR)			SB	4	···
05 37 46.50	–69 10 08.5	···	···	···	···	···	···	···	···	···	1–62	···	···	O3–4 V	11	5.02±0.3:	6	Variable background (N157B SNR)			···	···	···
05 37 46.70	–69 06 19.6	···	···	···	···	152	···	···	···	···	···	···	···	B2 IIIe	1	5.12±0.10	3	<1.15×10^{-7}	<31.87	<–6.53±0.25	···	···	···
05 37 46.71	–69 09 11.3	···	···	···	···	153	···	···	···	···	···	···	···	O9 III((n))	4	5.22±0.03	9	Variable background (N157B SNR)			···	···	···
05 37 47.09	–69 09 07.7	···	···	···	···	154	···	···	···	···	···	···	···	O8.5 V	4	5.30±0.12	3,5	Variable background (N157B SNR)			SB	4	···
05 37 47.43	–69 04 12.7	···	···	···	···	158	···	···	···	···	···	···	···	B1–1.5 Ve+	1	5.06±0.10	3	<1.46×10^{-7}	<31.97	<–6.36±0.25	···	···	···
05 37 47.80	–69 09 14.9	···	···	···	···	160	···	···	···	···	1–65	···	···	O9.5 III(n)	4	5.36±0.1	3,9	Variable background (N157B SNR)			SB1	4	···
05 37 48.06	–69 09 26.4	···	···	···	···	163	···	···	···	···	···	···	···	O8.,5 IV	4	5.20±0.10	3	Variable background (N157B SNR)			···	···	···
05 37 48.33	–69 09 15.2	···	···	···	···	165	···	···	···	···	1–68	···	···	O9.7 Iab	4	5.49±0.10	3	Variable background (N157B SNR)			···	···	···
05 37 49.91	–69 10 28.0	···	···	···	···	169	···	···	···	···	1–71	···	···	O2.5 V(n)((f*))	4	5.91±0.13	3,5	Variable background (N157B SNR)			SB?	4	···
05 37 50.02	–69 09 59.9	···	···	···	···	171	···	···	···	···	1–72	···	···	O8.5 III:+B1.5: V	4,37	5.43±0.02	9	Variable background (N157B SNR)			SB2:	4,37	···
05 37 50.66	–69 08 48.4	···	···	···	···	174	···	···	···	···	1–75	···	···	O7.5 V+O9.7: V:	10	5.07±0.04	10	Variable background (N157B SNR)			SB2	4,10	···
05 37 50.97	–69 11 00.3	···	···	···	···	176	···	···	···	···	1–77	···	···	O6 I:+B0.2: V:	10	5.27±0.02	10	Variable background (N157B SNR)			EB, SB2	4,12	···
05 37 51.03	–69 06 10.6	···	···	···	···	177	···	···	···	···	···	···	···	O7n(f)p	4	5.40±0.1	3,9	<1.13×10^{-7}	<31.86	<–6.81±0.25	···	···	···
05 37 51.05	–69 09 34.0	···	···	···	···	178	···	···	···	···	1–76	···	···	O9.7 Iab	4	5.60±0.03	9	Variable background (N157B SNR)			SB	4	···
05 37 51.34	–69 09 46.7	···	···	···	···	180	···	···	···	···	1–78	···	···	O3 If*	4	5.85±0.02	9	Variable background (N157B SNR)			SB	4	···
05 37 51.92	–69 09 20.9	···	···	···	···	185	···	···	···	···	1–80	···	···	O7.5 III((f))	4	5.28±0.1	3,9	Variable background (N157B SNR)			···	···	···
05 37 53.30	–69 12 57.3	···	···	···	···	190	···	···	···	···	···	···	···	O7 Vnn((f))p	4	5.28±0.10	3	<2.86×10^{-7}	<32.27	<–6.29±0.25	SB?	4	···
05 37 54.45	–69 09 41.5	···	···	···	···	197	···	···	···	···	1–87	···	···	O9.,5 V+O8.5 III	10	5.51±0.03	10	Variable background (N157B SNR)			SB2	10	···
05 37 54.95	–69 10 12.6	···	···	···	···	200	···	···	···	···	1–89	···	···	B1–1.5 IIIe+	1	5.06±0.10	3	Variable background (N157B SNR)			···	···	···
05 37 56.22	–69 11 50.8	···	···	···	···	208	···	···	···	···	1–93	···	···	O6(n)fp	4	5.59±0.04	10	<1.96×10^{-7}	<32.10	<–6.77±0.24	SB	4	···
05 37 59.06	–69 11 56.8	···	···	···	···	216	···	···	···	···	1–97	···	···	O4 V((fc))	4	5.83±0.13	3,5	<1.96×10^{-7}	<32.10	<–7.01±0.26	SB?	4	cc1675
05 38 00.61	–69 08 41.9	···	···	···	···	223	···	···	···	···	1–101	···	···	O9.5 IV	4	5.05±0.13	3,5	Variable background (N157B SNR)			SB	4	···
05 38 08.40	–69 09 19.0	···	···	···	···	243	···	···	···	···	···	···	···	O7 V(n)((f))	4	5.20±0.04	36	<1.06×10^{-7}	<31.84	<–6.64±0.24	SB1	4,36	···
05 38 08.42	–69 05 44.6	···	···	···	···	244	···	···	···	···	···	···	···	O5 III(n)(fc)	4	5.58±0.10	3,9	<8.56×10^{-8}	<31.74	<–7.11±0.25	SB	4	···
05 38 12.34	–69 00 57.3	···	···	···	···	261	···	···	···	···	···	···	···	B5 Ia	1	5.14±0.20	2,3	<1.17×10^{-7}	<31.88	<–6.54±0.30	···	···	···
05 38 13.30	–69 11 19.0	···	···	···	···	266	···	···	···	···	···	···	···	O8 V((f))z	4	5.05±0.12	3,5	<1.47×10^{-7}	<31.98	<–6.35±0.26	···	···	···
05 38 16.10	–69 09 16.7	···	···	···	···	277	···	···	···	···	···	···	···	O9 V+B4–5 V	4,37	5.00±0.3:	6	<8.04×10^{-8}	<31.72	<–6.56±0.38	SB2	4,37	···
05 38 19.05	–69 06 34.5	···	···	···	···	303	···	···	···	···	···	···	···	O9.5 IV	4	5.00±0.11	5	<7.01×10^{-8}	<31.66	<–6.62±0.25	···	···	···
05 38 19.25	–69 06 00.5	···	···	···	80	306	···	···	···	···	···	···	···	O8.5 II((f))	4	5.36±0.1	3,9	<6.55×10^{-8}	<31.63	<–7.01±0.25	SB?	4	···
05 38 19.30	–68 57 15.7	···	–68°	136	···	307	···	···	···	···	···	···	···	B1 II-Ib	1	5.09±0.20	2,3	Variable background (survey field edge)			···	···	···
05 38 23.31	–69 07 16.1	···	···	···	70	332	···	···	···	32	···	···	···	O9 III+O9.2 V	4,37	5.32±0.03	9	<7.38×10^{-8}	<31.68	<–6.92±0.23	SB2	4,37	···
05 38 28.06	–69 06 29.1	···	···	···	···	350	···	···	···	124	···	···	···	O8.5 V+O9.5 V	4,37	5.29±0.3:	6	<5.50×10^{-8}	<31.55	<–7.02±0.38	SB2	4,37	···
05 38 29.15	–68 57 39.3	···	···	···	···	355	···	···	···	···	···	···	···	O4 V((n))((fc))z	4	5.52±0.19	3,5	<2.85×10^{-7}	<32.26	<–6.53±0.30	SB2	4	···
05 38 29.21	–69 09 13.8	···	···	···	···	356	···	···	···	153	···	···	···	O6: V(n)z	4	5.14±0.20	3,5	<1.02×10^{-7}	<31.82	<–6.60±0.30	SB?	4	···
05 38 29.43	–69 05 21.2	···	···	···	···	360	···	···	107	169	···	···	···	O9.7	4	5.37±0.08	9	<5.02×10^{-8}	<31.51	<–7.14±0.24	···	···	···
05 38 29.52	–69 06 20.6	···	···	···	···	361	···	···	216	171	···	···	···	O8.5 V	4	5.27±0.15	3,5	<5.39×10^{-8}	<31.54	<–7.01±0.27	···	···	···

Table S1. (continued)

RA h m s	Dec deg m s	R	Sk	BI	Mk	VFTS	MH	HSH	SMB	P	ST	CCE	BAT	Spect. Type	Ref	log $L_{\rm Bol}$ $L_\odot$	Ref	Photon Flux cm^{-2} s^{-1}	log $L_{\rm X}^{t}$ erg s^{-1}	log $L_{\rm X}^{tc}/L_{\rm Bol}$	Nature	Ref	PSC source‡
05 38 32.28	–69 05 44.6	···	···	···	···	382	···	···	226	···	···	2901	···	O4–5 V((fc))z	4	5.31±0.13	3,5	<7.48×10^{-8}	<31.68	<–6.90±0.26	···	···	···
05 38 32.54	–69 04 32.0	···	···	···	58b	386	···	···	···	294	···	···	···	O9 V(n)+B1 V:	4,37	5.41±0.3:	6	<7.96×10^{-8}	<31.71	<–6.98±0.38	SB2	4,37	···
05 38 32.67	–69 04 32.6	···	···	···	58	389	···	···	···	304	···	···	···	O9.5 IV	4	5.23±0.10	3	<7.96×10^{-8}	<31.71	<–6.80±0.25	···	···	···
05 38 32.78	–69 03 19.5	···	···	···	···	390	···	···	···	316	···	···	···	O5.5 V:+O9.7: V:	4,37	5.25±0.3:	6	<6.77×10^{-8}	<31.64	<–6.89±0.38	SB2	4,37	···
05 38 32.83	–69 05 44.6	···	···	···	···	392	···	···	268	···	···	3007	···	O6–7 V((f))z	4	5.11±0.23	3,5	<7.48×10^{-8}	<31.68	<–6.70±0.33	···	···	···
05 38 33.39	–69 04 38.3	···	···	···	59	398	···	···	···	341	···	···	···	O6–7 V((f))z	4	5.47±0.17	3,5	<6.22×10^{-8}	<31.60	<–7.14±0.28	SB	4	c5306
05 38 34.58	–69 06 52.8	···	···	···	···	409	···	···	228	404	···	538	···	O3.5: V:+B:	4,37	5.75±0.3:	6	<5.76×10^{-8}	<31.57	<–7.46±0.38	SB2:	4,37	···
05 38 35.74	–69 08 19.7	···	···	···	···	418	···	···	···	473	···	···	···	O5 V((n))((fc))z	4	5.24±0.18	3,5	<9.22×10^{-8}	<31.77	<–6.74±0.29	SB?	4	···
05 38 35.92	–69 05 34.9	···	···	···	···	419	···	···	158	485	···	2897	···	O9: V(n)	4	5.07±0.24	3,5	<7.98×10^{-8}	<31.71	<–6.64±0.33	···	···	···
05 38 36.00	–69 06 16.9	···	···	···	···	422	···	···	140	···	···	1373	···	O4 III(f)	4	5.59±0.05	13	<6.06×10^{-8}	<31.59	<–7.27±0.24	SB1	4	···
05 38 36.05	–69 06 46.5	···	···	···	52	423	···	···	48	493	···	660	···	B1 Ia: Nwk	1	5.72±0.10	2,3	<6.37×10^{-8}	<31.61	<–7.38±0.25	···	···	···
05 38 36.13	–69 05 58.0	138	···	···	···	424	···	···	4	499	···	···	···	B9 I^{+}p	1	5.87±0.10	3	<7.73×10^{-8}	<31.70	<–7.45±0.25	···	···	···
05 38 36.86	–69 04 58.3	···	···	···	57	429	···	···	79	541	···	···	···	O7 V:+B1 V:	4,37	5.09±0.3:	6	<8.95×10^{-8}	<31.76	<–6.61±0.38	SB2	4,37	···
05 38 36.86	–69 06 46.2	···	···	···	···	430	···	···	181	538	···	647	···	B0.5 Ia^{+}((n)) Nwk	1	5.56±0.10	2	<6.37×10^{-8}	<31.61	<–7.22±0.25	SB1	21	···
05 38 36.96	–69 05 07.9	137	···	···	···	431	···	···	5	548	···	2889	···	B1.5 Ia Nstr	1	5.79±0.10	2,3	<8.95×10^{-8}	<31.76	<–7.31±0.25	···	···	···
05 38 37.04	–69 06 50.7	···	···	···	···	432	···	···	214	547	···	466	···	O8–9 V(n)((f))	4	5.18±0.05	22	<6.37×10^{-8}	<31.61	<–6.84±0.24	SB2?	4	···
05 38 37.22	–69 07 05.7	···	···	···	···	435	···	···	···	566	···	···	···	O7–8 V	4	5.15±0.13	3,5	<6.45×10^{-8}	<31.62	<–6.81±0.26	···	···	···
05 38 37.68	–69 05 42.0	···	···	···	···	···	···	···	123	600	···	2946	···	O3–5 V	23	5.49±0.05	22	<9.31×10^{-8}	<31.78	<–6.99±0.24	···	···	···
05 38 37.74	–69 05 21.0	···	···	···	47	440	···	···	29	607	···	2417	···	O6 V:+O8 V	4,37	5.63±0.03	9	<7.79×10^{-8}	<31.70	<–7.21±0.23	SB2	4,37	···
05 38 37.99	–69 06 15.2	···	···	···	···	443	···	···	208	615	···	1557	···	O7: V(n):+O7: V(n):	4	5.13±0.3:	6	<7.96×10^{-8}	<31.71	<–6.70±0.38	SB2	4	···
05 38 38.01	–69 06 09.7	···	···	···	···	···	···	···	327	618	···	1651	···	O6:	22	5.12±0.08	22	<7.69×10^{-8}	<31.70	<–6.70±0.24	···	···	···
05 38 38.26	–69 06 17.3	···	···	···	···	446	···	···	194	···	···	1339	···	Onn(f)	4	5.51±0.04	9	<7.38×10^{-8}	<31.68	<–7.11±0.23	···	···	···
05 38 38.52	–69 06 29.9	···	···	···	···	451	···	···	346	···	···	1124	···	O(n)	4	5.56±0.06	9	<7.71×10^{-8}	<31.70	<–7.14±0.24	···	···	···
05 38 38.83	–69 05 25.5	···	···	···	···	456	···	···	172	···	···	2385	···	Onn	4	5.17±0.1	3,9	<7.97×10^{-8}	<31.71	<–6.74±0.25	EB	12	···
05 38 38.86	–69 08 14.6	···	···	···	B	458	···	···	···	662	···	···	···	B5 Ia^{+}p	1	5.64±0.20	2,3	<8.68×10^{-8}	<31.75	<–7.17±0.30	···	···	···
05 38 39.13	–69 06 25.1	···	···	···	···	···	···	···	225	687	···	1177	···	O8:	23	5.17±0.05	23	<7.34×10^{-8}	<31.68	<–6.77±0.24	···	···	···
05 38 39.28	–69 07 53.0	···	···	···	···	466	···	···	···	696	···	···	···	O9 III	4	5.22±0.1	3,9	<7.05×10^{-8}	<31.66	<–6.84±0.25	···	···	···
05 38 39.48	–69 05 10.3	···	···	···	···	···	···	···	72	713	···	2245	···	O5 V	22	5.31±0.3:	6	<8.05×10^{-8}	<31.72	<–6.87±0.38	Single	24	···
05 38 39.56	–69 07 05.4	···	···	···	···	472	···	···	···	712	···	···	···	O6 Vz	4	5.01±0.15	3,5	<7.00×10^{-8}	<31.66	<–6.63±0.27	···	···	···
05 38 39.65	–69 05 26.3	···	···	···	···	···	···	···	92	723	···	2570	···	O5:	23	5.16±0.04	23	<8.67×10^{-8}	<31.75	<–6.69±0.23	···	···	···
05 38 39.75	–69 05 39.2	···	···	···	···	476	···	···	206	···	···	2789	···	O((n))	4	5.15±0.1	3,9	<7.44×10^{-8}	<31.68	<–6.75±0.25	···	···	···
05 38 39.82	–69 03 41.1	···	···	···	···	479	···	···	···	747	···	···	···	O4.5 V((fc))z+B:	4,37	5.15±0.3:	6	<6.15×10^{-8}	<31.60	<–6.83±0.38	SB2	4,37	···
05 38 39.86	–69 06 07.9	···	···	···	···	···	33	···	159	740	···	1537	···	O6:	23	5.38±0.3:	6	<7.28×10^{-8}	<31.67	<–6.99±0.38	···	···	···
05 38 40.18	–69 01 12.4	···	···	···	···	481	···	···	···	9017	···	···	···	O8.5 V+O9.7: V:	4,37	5.25±0.3:	6	<1.16×10^{-7}	<31.87	<–6.65±0.38	SB2	4,37	···
05 38 40.37	–69 05 43.7	···	···	···	···	484	···	···	124	···	···	3081	···	O6–7 V((n))	4	5.41±0.14	3,5	<6.75×10^{-8}	<31.64	<–7.05±0.26	···	···	cc4730
05 38 40.54	–69 05 53.5	···	···	···	···	···	66	72	113	781	···	1974	···	O6:	23	5.13±0.05	23	<8.63×10^{-8}	<31.75	<–6.66±0.24	···	···	···
05 38 40.60	–69 04 56.0	···	···	···	···	486	···	···	164	···	···	···	···	B1–2ne+	1	5.11±0.10	3	<7.93×10^{-8}	<31.71	<–6.68±0.25	···	···	···
05 38 40.70	–69 05 31.2	···	···	···	···	···	···	···	185	796	···	2565	···	O6:	23	5.15±0.05	23	<1.09×10^{-7}	<31.85	<–6.58±0.24	···	···	···
05 38 40.72	–69 08 24.9	···	···	···	···	488	···	···	···	791	···	···	···	O6 V((f))z	4	5.33±0.25	3	<7.26×10^{-8}	<31.67	<–6.94±0.34	···	···	···
05 38 40.85	–69 06 12.2	···	···	···	···	···	92	199	304	···	···	1439	···	O7:	23	5.04±0.05	23	<8.57×10^{-8}	<31.74	<–6.57±0.24	···	···	···

Table S1. (continued)

RA h m s	Dec deg m s	R	Sk	BI	Mk	VFTS	MH	HSH	SMB	P	ST	CCE	BAT	Spect. Type	Ref	log $L_{\rm Bol}$ $L_\odot$	Ref	Photon Flux cm^{-2} s^{-1}	log $L_{\rm X}^t$ erg s^{-1}	log $L_{\rm X}^{tc}/L_{\rm Bol}$	Nature	Ref	PSC source‡
05 38 40.85	–69 06 57.5	···	···	···	···	491	···	···	213	803	···	276	···	O6 V((fc))	4	5.43±0.16	3,5	<8.66×10^{-8}	<31.75	<–6.96±0.27	SB?	4	···
05 38 41.04	–69 04 24.8	···	···	···	21	492	···	···	···	830	···	···	···	O8 V+O9.5: V	4	5.28±0.3:	6	<7.68×10^{-8}	<31.70	<–6.86±0.38	SB2	4	···
05 38 41.04	–69 06 16.7	···	···	···	···	493	···	···	432	···	···	1297	···	O9 V	4	5.06±0.16	3	<9.05×10^{-8}	<31.77	<–6.57±0.27	···	···	···
05 38 41.04	–69 06 59.9	···	···	···	···	494	···	···	822	···	···	195	···	O8 V(n)	4	5.03±0.20	3,5	<8.66×10^{-8}	<31.75	<–6.56±0.30	SB2?	4	···
05 38 41.07	–69 06 15.2	···	···	···	···	1006	127	···	257	823	···	1409	···	O6.5 V–III	26	5.25±0.05	23	<9.05×10^{-8}	<31.77	<–6.76±0.25	Single	25	c6563
05 38 41.08	–69 06 01.7	···	···	···	···	1007	129	60	95	827	···	1763	···	O6.5 V–III	26	5.38±0.08	23	<1.14×10^{-7}	<31.87	<–6.79±0.24	Single	25	···
05 38 41.11	–69 05 58.3	···	···	···	···	1008	134	96	163	···	1852	···	···	ON6.5 II–I	26	5.08±0.3:	6	<1.06×10^{-7}	<31.84	<–6.52±0.38	Single	26	···
05 38 41.13	–69 05 13.1	140d	···	···	···	497	···	···	81	···	···	2231	···	O3.5 V((f))z+OB	4	5.48±0.10	3	<3.22×10^{-7}	<32.32	<–6.44±0.25	···	···	···
05 38 41.16	–69 06 02.8	···	···	···	···	1009	141	88	165	···	···	1732	···	O6.5 V–III	26	5.12±0.3:	6	<1.14×10^{-7}	<31.87	<–6.53±0.38	Single	26	···
05 38 41.23	–69 05 52.1	···	···	···	···	···	152	98	157	841	···	2016	···	O4–6(n)(f)p	33	5.16±0.05	23	<8.71×10^{-8}	<31.75	<–6.69±0.24	···	···	···
05 38 41.27	–69 06 16.9	···	···	···	···	1010	···	103	189	···	···	1346	···	O7 V–III	26	5.39±0.05	23	<9.05×10^{-8}	<31.77	<–6.90±0.24	Single	26	···
05 38 41.28	–69 05 32.3	···	···	···	27W	502	···	···	38	850	···	2653	···	O9.7 II	4	5.55±0.03	9	<1.09×10^{-7}	<31.85	<–6.98±0.23	SB	4	···
05 38 41.36	–69 06 14.0	···	···	···	···	1011	···	···	177	853	···	1447	···	O5 V	27	5.63±0.05	23	<9.05×10^{-8}	<31.77	<–7.14±0.24	···	···	···
05 38 41.38	–69 05 32.5	···	···	···	27E	503	···	···	100	858	···	···	···	O9 III	4	5.08±0.10	3,9	<1.06×10^{-7}	<31.84	<–6.52±0.25	SB1	4	···
05 38 41.39	–69 03 00.9	···	···	···	···	504	···	···	···	861	···	···	···	B0.7 V	1	5.06±0.10	28	<7.75×10^{-8}	<31.70	<–6.64±0.25	···	···	···
05 38 41.45	–69 05 57.8	···	···	···	···	···	168	67	96	852	···	1857	···	O5–7 V	31	5.32±0.05	23	<1.34×10^{-7}	<31.94	<–6.66±0.24	···	···	···
05 38 41.64	–69 06 00.7	···	···	···	···	···	249	84	145	···	···	1956	···	O5:	23	5.81±0.23	23	<1.55×10^{-7}	<32.00	<–7.09±0.33	···	···	···
05 38 41.73	–69 06 28.1	···	···	···	···	511	···	···	143	884	···	1008	···	O5 V((n))((fc))z	4	5.46±0.15	3,5	<7.55×10^{-8}	<31.69	<–7.05±0.27	SB1	4	···
05 38 41.77	–69 06 19.0	···	···	···	···	1016	···	85	154	887	···	1371	···	O8 V	22	5.63±0.05	23	<8.93×10^{-8}	<31.76	<–7.15±0.24	SB2	26	···
05 38 41.89	–69 06 12.4	···	···	···	···	1018	290	37	77	900	···	1459	···	O3 III(f*)	29	5.75±0.05	23	<9.75×10^{-8}	<31.80	<–7.23±0.24	Single	26	···
05 38 41.92	–69 04 38.8	···	···	···	29	517	···	···	···	909	···	···	···	O9.5 V–III((n))	4	5.09±0.10	3,5	<8.80×10^{-8}	<31.75	<–6.61±0.25	···	···	···
05 38 41.94	–69 06 29.6	···	···	···	···	518	···	···	138	901	···	1068	···	O3.5 III(f*)	4	5.67±0.02	9	<7.55×10^{-8}	<31.69	<–7.26±0.23	SB	4	···
05 38 41.94	–69 05 13.0	140c	···	···	···	519	···	···	55	908	···	3112	···	O3–4((f))	4	5.54±0.1	3,9	<3.22×10^{-7}	<32.32	<–6.50±0.25	SB1	4	···
05 38 41.99	–69 07 04.9	···	···	···	···	521	···	···	···	905	···	···	···	O9 V(n)	4	5.21±0.12	5	<7.81×10^{-8}	<31.70	<–6.78±0.26	···	···	···
05 38 42.02	–69 06 16.7	···	···	···	···	1020	314	101	178	···	···	1401	···	O3–4	26	5.40±0.15	23	<1.03×10^{-7}	<31.82	<–6.85±0.27	Single	26	···
05 38 42.06	–69 06 04.7	···	···	···	···	···	338	123	···	···	···	···	···	O6 V	30	5.01±0.22	30	<2.02×10^{-7}	<32.12	<–6.17±0.32	···	···	···
05 38 42.12	–69 06 00.7	···	···	···	···	···	372	33	60	923	···	1793	···	O3 V	29	5.91±0.3:	6	<1.92×10^{-7}	<32.09	<–7.09±0.38	···	···	···
05 38 42.24	–69 06 25.9	···	···	···	38	525	···	···	45	930	···	1184	···	B0 Ia	4	5.48±0.2	2	<7.55×10^{-8}	<31.69	<–7.07±0.30	SB	4	···
05 38 42.26	–69 06 12.2	···	···	···	···	···	422	113	190	···	···	1503	···	O7:	23	5.24±0.05	23	<1.12×10^{-7}	<31.86	<–6.66±0.24	···	···	···
05 38 42.46	–69 06 09.4	···	···	···	···	···	525	99	167	···	···	1527	···	O7:	23	5.16±0.16	23	<1.58×10^{-7}	<32.01	<–6.43±0.28	···	···	···
05 38 42.63	–69 06 10.9	···	···	···	···	1023	591	83	142	···	···	1580	···	O6 V	29	5.18±0.06	23	<1.30×10^{-7}	<31.92	<–6.53±0.24	Single	26	···
05 38 42.64	–69 06 01.1	···	···	···	···	···	603	64	···	···	···	···	···	O4–5 V	30	5.69±0.18	30	<3.05×10^{-7}	<32.29	<–6.67±0.29	···	···	···
05 38 42.65	–69 05 38.6	···	···	···	···	···	···	···	139	977	···	2893	···	O6: V	22	5.22±0.3:	6	<1.28×10^{-7}	<31.92	<–6.58±0.38	···	···	···
05 38 42.73	–69 05 52.7	···	···	···	···	···	638	160	258	982	···	2044	···	O4: V((f))	31	5.02±0.07	23	<1.14×10^{-7}	<31.87	<–6.43±0.24	···	···	···
05 38 42.74	–69 06 03.9	136b	···	···	···	···	637	9	18	985	···	···	111	O4 If/WN8	32	6.35±0.15	30	<5.19×10^{-7}	<32.53	<–7.10±0.27	···	···	···
05 38 42.74	–69 05 42.6	142	···	···	···	533	···	1	3	987	···	2912	···	B1.5 Ia$^+$p Nwk	1	5.88±0.10	2,3	<8.75×10^{-8}	<31.75	<–7.41±0.25	···	···	···
05 38 42.79	–69 06 03.4	···	···	···	···	···	657	65	···	···	···	···	···	O4 V	32	5.74±0.17	30	<2.62×10^{-7}	<32.23	<–6.79±0.28	···	···	···
05 38 42.82	–69 06 32.4	···	···	···	···	536	···	···	295	988	···	955	···	O6 Vz	4	5.19±0.17	3,5	<7.21×10^{-8}	<31.67	<–6.80±0.28	···	···	···
05 38 42.83	–69 06 03.4	···	···	···	···	···	666	45	···	···	···	···	···	O4: Vz	30	5.84±0.17	30	<4.98×10^{-7}	<32.51	<–6.61±0.28	···	···	···
05 38 42.86	–69 05 59.3	···	···	···	···	···	674	193	360	···	···	1781	···	O6:	23	5.06±0.16	23	<1.51×10^{-7}	<31.99	<–6.35±0.28	···	···	···

Table S1. (continued)

RA h m s	Dec deg m s	R	Sk	BI	Mk	VFTS	MH	HSH	SMB	P	ST	CCE	BAT	Spect. Type	Ref	log $L_{\rm Bol}$ $L_\odot$	Ref	Photon Flux cm^{-2} s^{-1}	log $L_{\rm X}^t$ erg s^{-1}	log $L_{\rm X}^{tc}/L_{\rm Bol}$	Nature	Ref	PSC source‡
05 38 42.96	–69 06 05.2	···	···	···	···	···	695	57	···	···	···	···	···	O3 III(f*)	29	5.71±0.3:	6	<3.97×10^{-7}	<32.41	<–6.58±0.38	···	···	···
05 38 43.04	–69 03 44.9	···	···	···	···	537	···	···	···	1022	···	···	···	O5 V((fc))z	4	5.19±0.13	3,5	<5.91×10^{-8}	<31.58	<–6.89±0.26	···	···	···
05 38 43.05	–69 05 40.3	···	···	···	···	···	···	···	41	1014	···	3062	···	O8:	23	5.60±0.05	23	<9.71×10^{-8}	<31.80	<–7.07±0.24	···	···	···
05 38 43.07	–69 04 13.1	···	···	···	22	538	···	···	···	1024	···	···	···	O8.5 III:+O9.5 III:	10	5.47±0.06	19	<5.87×10^{-8}	<31.58	<–7.17±0.24	SB2	4,10	···
05 38 43.08	–69 01 32.6	···	···	···	···	541	···	···	···	9024	···	···	···	B0.5 Ia Nwk	1	5.57±0.10	2,3	<1.38×10^{-7}	<31.95	<–6.90±0.25	···	···	···
05 38 43.17	–69 06 03.7	···	···	···	···	···	740	59	99	1023	···	1703	···	O3 III(f*)	29	6.00±0.3:	6	<4.98×10^{-7}	<32.51	<–6.77±0.38	···	···	···
05 38 43.18	–69 04 41.4	···	···	···	···	···	···	···	···	1035	···	···	···	O3–6 V	33	5.38±0.4	6	<8.80×10^{-8}	<31.75	<–6.90±0.46	SB?	24	···
05 38 43.27	–69 05 42.4	···	···	···	···	1027	748	61	85	1034	···	2987	···	O5 V	27	5.44±0.21	23	<9.54×10^{-8}	<31.79	<–6.93±0.31	···	···	···
05 38 43.59	–69 07 51.9	···	···	···	···	549	···	···	···	1063	···	···	···	O6.5 Vz	4	5.09±0.15	3,5	<7.98×10^{-8}	<31.71	<–6.66±0.27	SB?	4	···
05 38 43.60	–69 04 42.5	···	···	···	···	550	···	···	···	1077	···	···	···	O5 V((fc))z	4	5.20±0.13	3,5	<6.97×10^{-8}	<31.65	<–6.82±0.26	SB?	4	···
05 38 43.75	–69 05 55.6	···	···	···	···	···	820	148	250	1085	···	1929	···	O5:	23	5.11±0.14	23	<1.21×10^{-7}	<31.89	<–6.49±0.26	···	···	···
05 38 44.06	–69 05 55.7	···	···	···	33Sb	···	859	34	···	1111	···	···	115	WC5	29	5.90±0.3:	6	<1.21×10^{-7}	<31.89	<–7.28±0.38	Single	19	···
05 38 44.09	–69 05 44.5	···	···	···	···	1032	863	53	78	1113	···	2977	···	O8 III	27	5.31±0.05	23	<9.26×10^{-8}	<31.78	<–6.81±0.24	···	···	p1_988
05 38.44.18	–69 05 42.0	···	···	···	···	1033	872	···	74	1123	···	2913	···	O7 III	27	5.37±0.05	23	<9.07×10^{-8}	<31.77	<–6.88±0.24	EB,SB2	12,26	···
05 38 44.19	–69 05 46.6	···	···	···	···	···	886	74	121	···	···	···	·	O6 V	29	5.39±0.3:	6	<9.55×10^{-8}	<31.79	<–6.88±0.38	···	···	···
05 38 44.47	–69 05 55.6	···	···	···	33Nb	···	900	32	66	1152	···	1896	···	O6.5 V	29	5.42±0.06	23	<1.12×10^{-7}	<31.86	<–6.84±0.24	···	···	···
05 38 44.69	–69 05 45.2	···	···	···	···	570	916	···	179	···	···	3134	···	O9.5ne+	4	5.17±0.3:	4	<9.26×10^{-8}	<31.78	<–6.67±0.38	SB2	4	···
05 38 44.94	–69 15 11.4	···	···	···	···	576	···	···	···	···	···	···	···	B1 Ia Nwk	1	5.31±0.20	2	Variable background (survey field edge)			SB1	21	···
05 38 44.94	–69 07 04.6	···	···	···	···	577	···	···	···	1189	···	···	···	O6 V((fc))z	4	5.08±0.24	5	<7.16×10^{-8}	<31.66	<–6.69±0.34	···	···	···
05 38 44.96	–69 08 06.8	···	···	···	···	578	···	···	···	1184	···	···	···	B1.5 Ia Nwk	1	5.35±0.20	2,3	<7.14×10^{-8}	<31.66	<–6.96±0.30	···	···	···
05 38 44.96	–69 05 38.6	···	···	···	···	···	930	···	130	1196	···	2763	···	O6:	23	5.19±0.05	23	<8.39×10^{-8}	<31.73	<–6.73±0.24	EB	12	cc5386
05 38 45.05	–69 04 47.1	···	···	···	···	···	···	···	205	1209	···	···	···	O9–B0 V	22	5.24±0.3:	6	<6.97×10^{-8}	<31.65	<–6.86±0.38	···	···	···
05 38 45.07	–69 04 15.6	···	···	···	···	581	···	···	···	1218	···	···	···	O4–5 V((fc))	4	5.42±0.13	3,5	<5.62×10^{-8}	<31.56	<–7.14±0.26	···	···	···
05 38 45.22	–69 05 48.5	···	···	···	···	583	939	···	106	1225	···	2107	···	O8 V+O8.5 V	4	5.20±0.3:	6	<8.77×10^{-8}	<31.75	<–6.72±0.38	SB2	4	···
05 38 45.39	–69 02 51.5	···	···	···	···	586	···	···	···	···	···	···	···	O4 V((n))((fc))z	4	5.42±0.13	3,5	<9.69×10^{-8}	<31.80	<–6.90±0.26	SB?	4	c8111
05 38 45.50	–69 05 43.9	···	···	···	···	···	955	···	112	1248	···	3034	···	O6:	23	5.25±0.06	23	<7.68×10^{-8}	<31.70	<–6.83±0.24	···	···	···
05 38 45.59	–69 05 47.7	141	···	···	···	590	959	···	9	1253	···	2190	···	B0.7 Iab	1	5.87±0.10	2,3	<8.77×10^{-8}	<31.75	<–7.39±0.25	···	···	···
05 38 45.69	–69 05 38.9	···	···	···	24	···	963	···	47	1260	···	2760	···	O3 V	33	5.74±0.04	23	<8.13×10^{-8}	<31.72	<–7.30±0.23	···	···	···
05 38 45.79	–69 05 40.9	···	···	···	···	···	965	···	90	1267	···	2911	···	O7: V	31	5.33±0.05	23	<7.68×10^{-8}	<31.70	<–6.91±0.24	···	···	···
05 38 45.84	–69 06 20.9	···	···	···	···	···	···	···	59	1273	···	1223	···	O7:	23	5.43±0.05	23	<7.34×10^{-8}	<31.68	<–7.03±0.24	···	···	···
05 38 46.07	–69 06 15.5	···	···	···	···	596	···	···	137	1295	···	1325	···	O7–8 V((n))	4	5.22±0.05	23	<7.98×10^{-8}	<31.71	<–6.79±0.24	SB1	4	···
05 38 46.12	–69 05 54.4	···	···	···	15Sa	···	983	···	117	1306	···	2053	···	O8 III	33	5.26±0.3:	6	<7.28×10^{-8}	<31.67	<–6.87±0.38	···	···	···
05 38 46.15	–69 05 51.3	···	···	···	15	···	984	···	43	1312	···	2165	···	O7 V	33	5.50±0.3:	6	<8.39×10^{-8}	<31.73	<–7.04±0.38	···	···	···
05 38 46.54	–69 05 44.2	···	···	···	···	···	···	···	153	1337	···	2876	···	O8:	23	5.08±0.04	23	<7.68×10^{-8}	<31.70	<–6.66±0.23	···	···	···
05 38 46.58	–69 05 37.1	···	···	···	···	604	···	···	110	1340	···	2884	···	O8.5 V	4	5.04±0.05	23	<8.13×10^{-8}	<31.72	<–6.60±0.24	SB2?	23	···
05 38 48.20	–69 08 10.9	···	···	···	···	626	···	···	···	1423	···	···	···	O5–6n(f)p	4	5.55±0.1	3,9	<7.75×10^{-8}	<31.70	<–7.13±0.25	SB?	4	···
05 38 49.72	–69 06 43.1	···	···	···	11	641	···	···	15	1500	···	762	···	B0.5: I	1	5.66±0.04	23	<7.60×10^{-8}	<31.69	<–7.25±0.23	···	···	···
05 38 48.90	–69 10 42.9	···	···	···	···	642	···	···	···	···	···	···	···	O5.5 V+O9 V	10	5.22±0.15	19	<1.45×10^{-7}	<31.97	<–6.53±0.27	SB2	4,10	···
05 38 51.04	–69 05 54.7	···	···	···	7	651	···	···	94	1553	···	2057	···	O7 V(n)z	4	5.24±0.05	23	<6.67×10^{-8}	<31.63	<–6.88±0.24	SB1	4	···
05 38 51.04	–69 06 20.5	···	···	···	5	652	···	···	54	1552	···	1405	···	B2 Ip+O9 III:	4	5.49±0.05	10	<7.93×10^{-8}	<31.71	<–7.06±0.24	SB2	4,10	···

Table S1. (continued)

RA h m s	Dec deg m s	R	Sk	BI	Mk	VFTS	MH	HSH	SMB	P	ST	CCE	BAT	Spect. Type	Ref	$\log L_{\rm Bol}$ $L_\odot$	Ref	Photon Flux cm^{-2} s^{-1}	$\log L_{\rm X}^{t}$ erg s^{-1}	$\log L_{\rm X}^{tc}/L_{\rm Bol}$	Nature	Ref	PSC source‡
05 38 51.20	–69 05 59.4	···	···	···	6	656	···	···	61	1563	···	1979	···	O7.5 III(n)(((f))p	4	5.34±0.05	23	<7.62×10^{-8}	<31.69	<–6.93±0.24	SB1	4	···
05 38 51.31	–69 04 08.5	···	···	···	···	657	···	···	···	1573	···	···	···	O7 II:(f)+OB:	4,37	5.48±0.3:	6	<5.14×10^{-8}	<31.52	<–7.24±0.38	SB2:	4,37	···
05 38 51.62	–69 08 07.3	143	···	···	···	···	···	···	···	1575	···	···	···	B9 Ip	33	5.8 ±0.2	34	<9.34×10^{-8}	<31.78	<–7.30±0.30	···	···	···
05 38 52.05	–69 05 33.9	···	···	···	···	661	···	···	125	1594	···	2691	···	O6.5 V(n)+O9.7: V:	4	5.08±0.03	10	<7.43×10^{-8}	<31.68	<–6.68±0.23	EB, SB2	4,12	···
05 38 52.83	–69 06 12.1	···	···	···	···	667	···	···	118	1614	···	1699	···	O6 V((f))	4	5.21±0.10	3	<6.64×10^{-8}	<31.63	<–6.86±0.25	SB?	4	···
05 38 52.97	–69 07 45.4	···	···	···	···	669	···	···	···	1619	···	···	···	O8 Ib(f)	4	5.51±0.10	3,9	<7.62×10^{-8}	<31.69	<–7.10±0.25	SB1	4	···
05 38 53.65	–69 08 11.3	···	···	···	···	···	···	···	···	1643	···	···	···	O5 V	26	5.29±0.3:	h	<8.61×10^{-8}	<31.75	<–6.82±0.38	···	···	···
05 38 54.09	–69 08 07.7	···	···	···	···	672	···	···	···	1661	···	···	···	B0.7 II Nwk?	1	5.23±0.10	2,3	<8.61×10^{-8}	<31.75	<–6.76±0.25	···	···	···
05 38 54.43	–69 08 00.5	···	···	···	···	675	···	···	···	1674	···	···	···	B1 Iab Nwk	1	5.16±0.20	2	<8.61×10^{-8}	<31.75	<–6.69±0.30	···	···	···
05 38 54.75	–69 03 48.8	···	···	···	···	677	···	···	···	1696	···	···	···	O9.5 V	4	5.03±0.18	5	<5.33×10^{-8}	<31.54	<–6.77±0.29	·	···	···
05 38 54.78	–69 08 44.4	···	···	···	···	···	···	···	···	1685	···	···	···	B0.5 Ia	33	5.28±0.3:	6	<8.86×10^{-8}	<31.76	<–6.80±0.38	···	···	···
05 38 57.17	–68 56 53.2	···	–68° 140	···	···	696	···	···	···	···	···	···	···	B0.7Ib-Iab	1	5.64±0.10	2,3	<4.58×10^{-7}	<32.47	<–6.45±0.25	···	···	···
05 38 57.31	–69 07 09.8	···	···	···	2	698	···	···	···	1797	···	···	···	early B + late B	35	5.41±0.3:	35	<5.91×10^{-8}	<31.58	<–7.11±0.38	SB2	35	···
05 38 58.39	–69 04 35.2	···	···	···	···	702	···	···	···	1829	···	···	···	O8 V(n)+OB+OB+OB	4,37	5.01±0.3:	6	<5.82×10^{-8}	<31.57	<–6.71±0.38	EB, SB2	4,37	···
05 38 58.77	–69 05 23.9	···	···	···	···	706	···	···	···	1838	···	···	···	O6–7 Vnnz	4	5.02±0.26	3,5	<8.27×10^{-8}	<31.73	<–6.57±0.35	···	···	···
05 39 00.75	–69 07 12.9	···	···	···	···	717	···	···	···	1892	···	···	···	O9 IV	4	5.09±0.12	3,5	<6.20×10^{-8}	<31.60	<–6.77±0.26	SB?	4	···
05 39 02.95	–69 15 00.1	···	···	···	···	724	···	···	···	···	···	···	···	O7 Vnnz	4	5.01±0.47	3,5	Variable background (survey field edge)			···	···	···
05 39 03.59	–69 07 16.9	···	···	···	···	729	···	···	···	1969	···	···	···	B0.2 III	1	5.30±0.10	3	<6.85×10^{-8}	<31.65	<–6.93±0.25	···	···	···
05 39 03.78	–69 03 46.6	···	···	···	···	731	···	···	···	1974	···	···	121	WC4	17	5.40±0.2	6	<5.46×10^{-8}	<31.55	<–7.13±0.30	···	···	···
05 39 04.77	–69 04 10.0	···	···	256	1	732	···	···	···	1987	···	···	···	B1.5 Iap Nwk	1	5.61±0.20	2,3	<6.19×10^{-8}	<31.60	<–7.29±0.30	···	···	···
05 39 04.87	–69 05 40.5	···	···	···	···	733	···	···	···	1988	···	···	···	O7,5 V+B1 II	4,37	5.34±0.20	2	<6.69×10^{-8}	<31.64	<–6.98±0.30	SB2	4,37	···
05 39 05.39	–69 04 31.2	···	···	···	···	737	···	···	···	2000	···	···	···	O9 Vz	4	5.11±0.12	3,5	<6.40×10^{-8}	<31.62	<–6.77±0.26	···	···	···
05 39 05.93	–69 16 26.8	···	–69° 250	···	···	739	···	···	···	···	···	···	···	A0 Ip	1	5.19±0.32	3	Variable background (survey field edge)			···	···	···
05 39 09.00	–69 01 29.3	···	···	···	···	751	···	···	···	···	···	···	···	O7–8 Vnnz	4	5.01±0.31	3,5	<1.17×10^{-7}	<31.88	<–6.41±0.39	···	···	···
05 39 14.52	–69 16 42.5	···	–69° 252	···	···	764	···	···	···	···	···	···	···	O9.7 Ia Nstr	4	5.39±0.1	3,9	Variable background (survey field edge)			SB1	4	···
05 39 19.89	–69 01 12.9	···	···	···	···	777	···	···	···	···	···	···	···	O9.2 II	4	5.30±0.1	3,9	<1.43×10^{-7}	<31.97	<–6.61±0.25	SB?	4	···
05 39 23.80	–69 10 54.5	···	···	···	···	782	···	···	···	···	···	···	···	O8.5 III	4	5.20±0.1	3,9	<1.39×10^{-7}	<31.95	<–6.52±0.25	···	···	···
05 39 30.64	–69 09 26.4	···	···	···	···	797	···	···	···	···	···	···	···	O3.5 V((n))(((fc))z	4	5.60±0.13	3,5	<1.32×10^{-7}	<31.93	<–6.93±0.26	SB?	4	···
05 39 32.58	–69 00 02.6	···	···	258	···	802	···	···	···	···	···	···	···	O7,V:+O8: V	4,37	5.21±0.3:	6	<1.65×10^{-7}	<32.03	<–6.47±0.38	SB2	4,37	···
05 39 34.87	–68 59 48.6	···	···	259	···	806	···	···	···	···	···	···	···	O5.5 V((fc)):z+O7 Vz:	4	5.39±0.04	10	<2.19×10^{-7}	<32.15	<–6.52±0.23	SB2	4	···
05 39 36.12	–69 04 59.1	···	···	···	···	812	···	···	···	2246	···	···	···	O4 V((fc))	4,37	5.45±0.3:	6	<1.05×10^{-7}	<31.83	<–6.90±0.38	SB2	4,37	···
05 39 39.27	–69 11 44.2	···	···	···	···	827	···	···	···	···	···	···	···	B1.5 III	1,37	5.03±0.20	2	<2.30×10^{-7}	<32.17	<–6.14±0.30	SB1:	1,37	···
05 39 39.87	–69 12 04.3	···	···	···	···	831	···	···	···	···	···	···	···	B5 Ia	1	5.10±0.20	2,3	<2.30×10^{-7}	<32.17	<–6.21±0.30	···	···	···
05 39 42.25	–69 13 28.4	···	···	···	···	841	···	···	···	···	···	···	···	B2.5 Ia	1	5.10±0.20	2,3	Variable background (survey field edge)			···	···	···
05 39 47.37	–68 59 22.0	···	···	···	···	849	···	···	···	···	···	···	···	O7 Vz	4	5.02±0.13	3,5	Variable background (survey field edge)			···	···	···

1: Evans et al. (2015) 2: McEvoy et al. (2015) 3 :Schneider et al. (2018) 4: Walborn et al. (2014) 5: Sabín-Sanjulián et al. (2017) 6: Doran et al. (2013) 7: Hainich et al. (2014) 8: Foellmi et al. (2003) 9: Ramírez-Agudelo et al. (2017) 10: Mahy et al. (2020) 11: Schild & Testor (1992) 12: Graczyk et al. (2011) 13: Crowther & Smith (1997) 14: Bestenlehner et al. (2014) 15: Schnurr et al. (2008) 16: Pawlak et al. (2016) 17: Smith et al. (1990) 18: Crowther et al. (2002a) 19: Bartzakos et al. (2001) 20: Evans et al. (2011) 21 :Villaseñor et al. (2021) 22: Castro et al. (2021) 23: Bosch et al. (1999) 24: Bosch et al. (2009) 25: Massey et al. (2012) 26: Hénault-Brunet et al. (2012) 27: D.J. Lennon (priv. comm.); 28: Dufton et al. (2018) 29: Massey & Hunter (1998) 30: Bestenlehner et al. (2020) 31: Parker (1993) 32: Crowther et al. (2016) 33: Walborn & Blades (1997) 34: Smith et al. (1998) 35: Dunstall et al. (2012) 36: Shenar et al. (2022) 37. T. Shenar et al. submitted

This paper has been typeset from a TEX/LATEX file prepared by the author.